

Max-Planck Institut für Kolloid- und Grenzflächenforschung
Theorie und Bio-Systeme

Phase Separation in Giant Vesicles

Dissertation
zur Erlangung des akademischen Grades
"doctor rerum naturalium"
(Dr. rer. nat.)
in der Wissenschaftsdisziplin "Weiche Materie"

eingereicht an der
Mathematisch-Naturwissenschaftlichen Fakultät
der Universität Potsdam

von
Yanhong Li

Potsdam, im November 2008

Published online at the
Institutional Repository of the University of Potsdam:
<http://opus.kobv.de/ubp/volltexte/2009/2913/>
<urn:nbn:de:kobv:517-opus-29138>
[<http://nbn-resolving.de/urn:nbn:de:kobv:517-opus-29138>]

Abstract

Giant vesicles may contain several spatial compartments formed by phase separation within their enclosed aqueous solution. This phenomenon might be related to molecular crowding, fractionation and protein sorting in cells. To elucidate this process we used two chemically dissimilar polymers, polyethylene glycol (PEG) and dextran, encapsulated in giant vesicles. The dynamics of the phase separation of this polymer solution enclosed in vesicles is studied by concentration quench, i.e. exposing the vesicles to hypertonic solutions. The excess membrane area, produced by dehydration, can either form tubular structures (also known as tethers) or be utilized to perform morphological changes of the vesicle, depending on the interfacial tension between the coexisting phases and those between the membrane and the two phases. Membrane tube formation is coupled to the phase separation process. Apparently, the energy released from the phase separation is utilized to overcome the energy barrier for tube formation. The tubes may be absorbed at the interface to form a 2-dimensional structure. The membrane stored in the form of tubes can be retracted under small tension perturbation.

Furthermore, a wetting transition, which has been reported only in a few experimental systems, was discovered in this system. By increasing the polymer concentration, the PEG-rich phase changed from complete wetting to partial wetting of the membrane. If sufficient excess membrane area is available in the vesicle where both phases wet the membrane, one of the phases will bud off from the vesicle body, which leads to the separation of the two phases. This wetting-induced budding is governed by the surface energy and modulated by the membrane tension. This was demonstrated by micropipette aspiration experiments on vesicles encapsulating two phases. The budding of one phase can significantly decrease the surface energy by decreasing the contact area between the coexisting phases. The elasticity of the membrane allows it to adjust its tension automatically to balance the pulling force exerted by the interfacial tension of the two liquid phases at the three-phase contact line. The budding of the phase enriched with one polymer may be relevant to the selective protein transportation among lumens by means of vesicle in cells.

Contents

Chapter 1. Introduction	1
1.1. Molecular crowding in cells	1
1.2. Phase separation in bulk polymer solutions	4
1.3. Lipids, lipid membranes and vesicles	7
1.4. Vesicles containing aqueous two-phase system	12
1.5. Transitions from partial to complete wetting	16
Chapter 2. Materials and experimental techniques	21
2.1. Materials	21
2.2. Bulk polymer solutions characterization	21
2.2.1. Phase diagram	22
2.2.2. Interfacial tension measurement	24
2.3. Vesicle preparation	26
- Spontaneous swelling	28
- Electroformation	29
2.4. Vesicle observation	30
2.4.1. Vesicle deflation	30
2.4.2. Optical microscopy	32
- Phase contrast and differential interference contrast microscopy ..	32
- Fluorescence and confocal microscopy	34
2.5. Micropipette manipulation	36
Chapter 3. Phase behaviour of polymer solutions	39
3.1. Characterization of PEG and dextran aqueous solution in bulk	39
3.2. Phase separation of polymer solution in giant vesicles	43
- Dynamics of phase separation in giant vesicles	44
- Effect of polymer composition	48
- Effect of membrane composition	50
Chapter 4. Membrane tube formation coupled to phase separation	53
4.1. Vesicle trajectories in phase diagram	53
4.2. Formation of membrane tubes	56
- Microscopy observations of tube formation	56

- The evolution of areas in deflated vesicles	61
- Discussion	63
4.3. Retraction of membrane tubes	66
4.4. Possible implications for biological system	71
4.5. Summary	74
Chapter 5. Morphologies of vesicles with internal phase separation	75
5.1. Classification of vesicle morphology	75
5.2. Wetting transition in membrane compartment	78
5.3. Wetting-induced budding	82
- Budding transition	83
- Force balance at three-phase contact line	89
- Vesicle aspiration	92
- Discussion	95
Chapter 6. Conclusion and outlook	97
List of abbreviations	101
List of symbols	103
List of figures	105
List of tables	108
Bibliography	109
Acknowledgements	117

Chapter 1

Introduction

1.1 Molecular crowding in cells

The interior of living cells is a crowded milieu of organelles. It's full of both macromolecules and small molecules. In a bacterial cell, there are approximately 26% macromolecules, 4% small molecules (inorganic ions, sugars, amino acids, fatty acids and their precursors, other small molecules), and 70% water of total cell weight [Alberts 1994]. The cytoplasm contains a variety of macromolecules, such as proteins, nucleic acids, and polysaccharide. None of them may be present at high concentration if we consider them individually. However, they do occupy a substantial volume fraction of the medium collectively. For example, the macromolecule concentration in the cytoplasm of *Escherichia coli* is estimated to be ≈ 0.3 to 0.4 g/ml depending on the growth phase [Zimmerman 1991]. Figure 1.1.1 illustrates this degree of crowding for the cytoplasm of an eukaryote and a prokaryote.

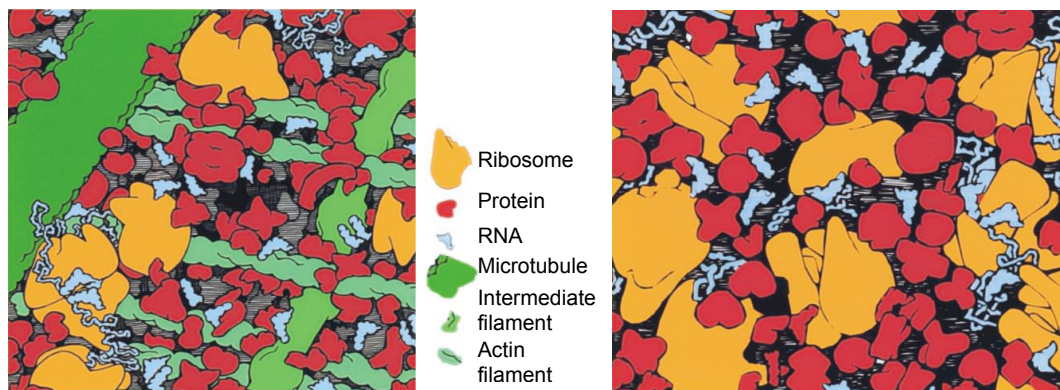


Figure 1.1.1 The crowded state of the cytoplasm in eukaryotic (left) and *E. coli* (right) cells. Each square illustrates the face of a cube of cytoplasm with an edge 100 nm in length. The sizes, shapes and numbers of macromolecules are approximately correct. Small molecules are not shown. [Ellis 2001a]

The term macromolecular crowding, as applied to biological systems, describes the fact that the total concentration of macromolecules inside cells is so high that a significant portion of the volume is physically occupied and, hence, unavailable to other molecules. Molecular crowding is more precisely termed as the excluded volume effect. In liquid state theory, excluded volume is the volume which is not accessible to other molecules when it is already occupied by one molecule. Likewise, in polymer physics,

excluded volume implies that one part of a polymer chain cannot occupy the place that is already occupied by another part of the same molecule (in lattice models, two monomers are not allowed to be on the same site). This is equivalent to a self avoiding walk. The excluded volume effect is a purely physical, nonspecific effect originating from steric repulsion.

The rather high concentration of macromolecules in cells can have a dominant effect on the effective concentration or thermodynamic activity of cellular components. The thermodynamic activity of each macromolecular species inside cells is greater than its actual concentration. And this difference has kinetic and thermodynamic consequences for the properties of that macromolecule. On the one hand, it can alter the diffusion processes. In fact, the diffusion coefficient can be reduced by orders of magnitude, see [Ellis 2001a]. This reduction applies to both small molecules and macromolecules. The rate of any process which is diffusion controlled will be limited. However, the diffusion of larger molecules will be impeded more strongly than that of the small molecules. On the other hand, it may promote protein association [Minton 1981]. The crowding effect is largely restricted to macromolecules. Both the reaction rates and the equilibria are highly non-linear with respect to the sizes and concentrations of the interacting species [Ellis 2001b].

Macromolecular crowding is ubiquitously occurring in the interiors of both prokaryotic and eukaryotic cells, as shown in Fig. 1.1.1. Molecular crowding occurs even at the cell surface [Ryan 1988]. Proteins on the surface of living cells do not behave as ideal solutes in the lipid membrane. Strong steric interactions among proteins were revealed even at typical cell receptor concentrations. Polysaccharides also contribute to crowding, especially in the glycocalyx on the outer membrane surface. Thus, crowding occurs outside, inside, as well as on the surface of the cells.

The cytoplasm of cells was once considered as a more or less homogeneous solution with many proteins, metabolites of all kinds and inorganic ions, in which different organelles are suspended. However, this concept cannot explain the fact that the solvent viscosity of cytoplasm is not substantially different from that of water. This phenomenon can possibly be explained with intracellular structural heterogeneity: The intrinsic macromolecular density is relatively low within the interstitial voids in the cell because many soluble enzymes are apparently integral parts of the insoluble cytomatrix

and are not distributed homogeneously [Ovádi 2004]. The idea of compartmentation was introduced in order to explain important physiological phenomena. The reference phase technique was developed to measure the regional concentrations and the amounts of diffusive and nondiffusive forms of individual proteins within the full-grown oocyte of *Xenopus laevis* [Paine 1984]. The results suggest that a large fraction of the cytoplasmic proteins form a highly organized system.

It is plausible that macromolecular crowding may lead to local composition differences even in cytoplasmic regions that are not separated by lipid membranes. This phenomenon is called microcompartmentation. Microcompartmentation is functionally an isolation of the molecules from those in the rest of the cell resulting in high local concentration of molecules [Al-Habori 1995]. It is thought to have profound implications for cell functions.

Mixtures of structurally distinct macromolecules tend to phase separate when the concentration is above a few weight percent. The phases formed are generally solutions, which differ in concentration and physical properties. The cytoplasm contains high concentrations of macromolecules, and their effective concentrations are significantly elevated due to macromolecular crowding. Thus, phase separation might occur and lead to the local concentration differences in cells.

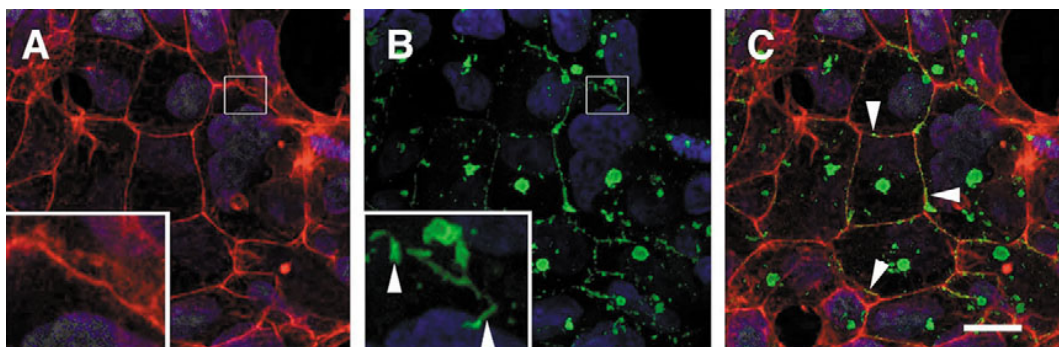


Figure 1.1.2 Colocalisation of F-actin and HA-Dvl-2-ER protein in single-copy cell line. Nuclei were stained with ToPro III (blue). F-actin is in red (A) and HA-Dvl-2-ER in green (B). Arrowheads in inset image indicate patches of HA staining projecting from the juxtamembrane region into cell interior. Arrowheads in the merged image (C) indicate examples of areas of colocalisation at the cell membrane which appears yellow. Scale bar = 10 μm . [Smalley 2005]

Phase separation occurs in the aqueous solution of lens γ -crystalins, a family of lens-specific monomeric proteins [Liu 1996]. They have been implicated in cataract formation. Another example is shown in Fig. 1.1.2. Dishevelled protein (Dvl, labelled in green) interacts strongly with itself. It forms different domains in cells; Fig. 1.1.2 B, C.

The green puncta are regions with high Dvl concentration, coexisting with low Dvl concentration in the rest of the cytosol. Each cell has one large punctum which is located at the microtubule-organising centre. A number of puncta are situated at the peripheries of the cells. They are essential to trigger the Wnt signalling [Sear 2007]. Wnt signalling is a highly conserved cell-cell signalling event during embryogenesis. Wnt signals are pleiotropic, with effects that include mitogenic stimulation, cell fate specification, and differentiation. [Logan 2004]

1.2 Phase separation in bulk polymer solutions

A polymer molecule is defined by IUPC (International Union of Pure and Applied Chemistry) as “a molecule of high relative molecular mass, the structure of which essentially comprises the multiple repetitions of units derived, actually or conceptually, from molecules of low relative molecular mass”. Polymers have a large molecular weight ($>10^4$ g/mol). In contrast to small molecules with a specific molecular weight, the molecule weight of synthetic polymers exhibits a broad distribution. Note that this is different for synthetic and biological polymers such as proteins. Biological polymers are monodisperse. When polymers are mixed with a solvent, phase separation may occur under certain conditions. A typical phase diagram of polymer solution is shown in Fig. 1.2.1. It shows the phase behavior of the mixture.

There are three regions in the phase diagram, which are stable, metastable and unstable. In the stable region, there is only one phase. The polymer solution is homogeneous, as indicated in the insets A and D of Fig. 1.2.1. The boundary of the stable region is the so-called binodal. The binodal curve defines the locations in the phase diagram at which a transition occurs from miscibility of the components to conditions where single-phase mixtures are metastable or unstable.

Encompassed by the binodal is the two-phase region. It can be further divided into the metastable and the unstable regions. They are separated by the spinodal curve. Under the spinodal curve, the solution spontaneously separates into two continuous phases, a polymer-rich phase and a solvent-rich phase. The compositions of the two phases can be read out from the binodal. Between the binodal and the spinodal is the metastable region. Tiny polymer-rich (B in Fig. 1.2.1) or solvent-rich (E in Fig. 1.2.1)

droplets form in this domain. The solution must overcome an energy barrier before it can phase separate. In the absence of external disturbances such a solution will remain stable.

When a stable solution with a certain concentration is cooled down, as the vertical magenta arrow indicates in Fig. 1.2.1, it starts to phase separate after it reaches the binodal. But the solution is kinetically stable. The solution just becomes turbid. Within the metastable regime, a solution may remain homogeneous for a very long time, despite the possibility to reduce the Gibbs energy upon phase separation. Under these conditions the demixing process takes place via nucleation and growth mechanism. The individual droplets of the minor phase formed in the early state of the process grow slowly. They are dispersed in the matrix of the corresponding coexisting phase and can become rather large. The driving force for this process is the minimization of the interface (contributing to high values of the Gibbs energy). As the temperature decreases further, it passes through the metastable region and reaches the spinodal. The solution now arrives in the unstable region. The coexisting phases are separated macroscopically and form two continuous phases, a polymer-rich phase and a solvent-rich phase. The compositions of the two phases can be read out from the binodal. The line which connects these two points is called tie line.

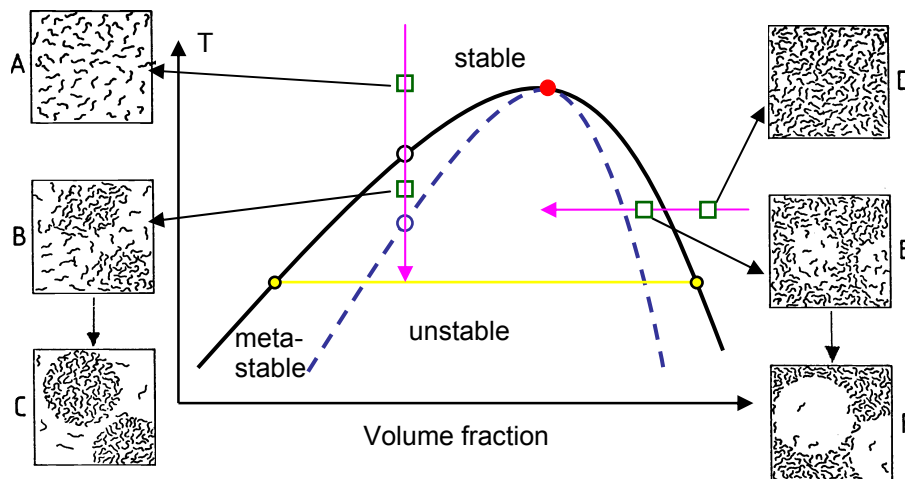


Figure 1.2.1 Typical phase diagram of temperature versus volume fraction. The black line presents the binodal. The dashed blue line presents the spinodal. The red dot is the critical point. The yellow line is the tie line. The magenta arrows are trajectories of phase separation. A, D: stable domain; B, E: metastable domains; C: segregation of polymer-rich phase; F: segregation of solvent-rich phase. [modified after Galina 1982]

The phase behavior of polymer solution does not only depend on temperature but also the polymer volume fraction. At a fixed temperature below the critical temperature, the concentrated polymer solution undergoes phase separation when its concentration

decreases as indicated by the magenta horizontal arrow in Fig. 1.2.1. In principle, the volume fraction can not be determined experimentally. It is usually calculated from the weights and the specific volumes of the solvent and polymer. In the framework of the lattice theory, the solvent molecules are equivalent to the segments of polymer chains with the same mass. Then the composition variable is equal to the weight fraction. Since the specific volume of the solvent and polymer does not differ too much, namely their ratio is not far from unity, the volume fraction becomes equal to the weight fraction. Perhaps the weight fraction is the most suitable measure of concentration in polymer solution, at least the most popular one in practice. It has the advantage to be independent of temperature.

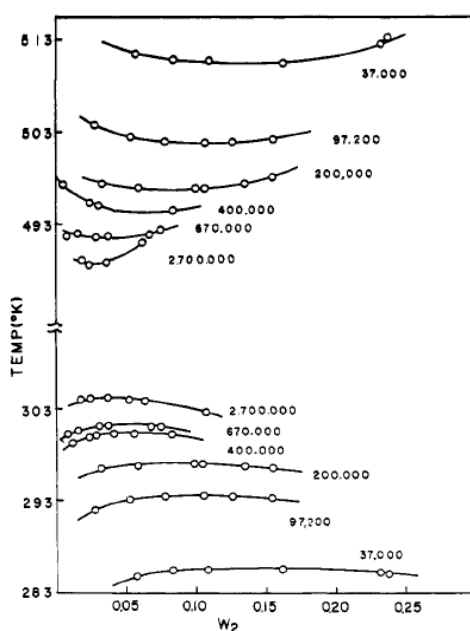


Figure 1.2.2 The (temperature versus weight fraction of polymer w_2) phase diagram for the polystyrene-cyclohexane system for samples of indicated molecular weight. [Saeki 1973]

Figure 1.2.1 shows schematically the behavior of a system exhibiting a so-called upper critical solution temperature (UCST, phase separation upon cooling). Phase separation might occur upon heating. Then we say that the system exhibiting a lower critical solution temperature (LCST). Differing from the phase diagrams of small molecules, the binodal and the spinodal of polymer solution are asymmetric due to the significant difference between the molecular weights of the solvent and the polymer. The effect of the molecular weight is similar as the effect of pressure on the phase diagram. Figure 1.2.2 shows one example. The polystyrene-cyclohexane system exhibits both UCST and LCST. As the molecular weight increases, the UCST is raised and the LCST is lowered.

Polymer chains may have different molecular weights even though they are synthesized under the same condition, even in the same batch. The polymer solution is not a strict binary system any more due to the polydispersity. It is actually a multicomponent system. This makes the phase behavior of the polymer solution much more complex.

The binodal and the spinodal curves touch at the critical point (CP), also called consolute point. The determination of its position is a problem for two-phase systems including binary, ternary and multi-component mixtures. The binodal of a binary mixture is usually very flat in the neighborhood of the CP. It is easy to determine the critical temperature, but not the critical concentration. Theoretically one can measure the spinodal and binodal curves independently and find out their touch-point to obtain the CP. Practically there is always a gap or overlay between these two curves when they are determined using different techniques. A more practical way to determine the CP is the phase volume ratio method [Koningsveld 2001].

The phase volume ratio method assumes that the locus of the mean of the tie lines passes through the CP upon linear extrapolation. This implies that, if the volume fraction is used as the concentration variable, the volume ratio of the vanishing phases at the CP should be equal to unity [Koningsveld 1968]. This does not indicate that the mean of the tie lines passing through the CP is linear. This method is not only valid for binary systems but also for systems consisting of more than two components. A necessary and sufficient criterion for determining the critical concentration is the equality of the phase volumes as measured at a temperature very close to the cloud-point (one point on the binodal) of that concentration.

1.3 Lipids, lipid membranes and vesicles

Life became possible when the nature discovered the trick with membrane. Membranes allow the separation of living entities from the lifeless environment. Biomembranes are constituted of lipids and proteins. Besides water, proteins, nucleic acids and carbohydrates, lipids are essential biomolecules in cells. The membrane lipids are extremely diverse. The major role of the membrane lipids is to form a bilayer matrix in which proteins embed.

Lipids are amphiphilic molecules which contain hydrophilic head groups and hydrophobic tails. The head groups can be charged (positive or negative), zwitterionic, or non-charged polyhydroxylated moieties. The hydrophobic part contains normally one or two fatty acid chains. Figure 1.3.1 shows one lipid with two acyl chains.

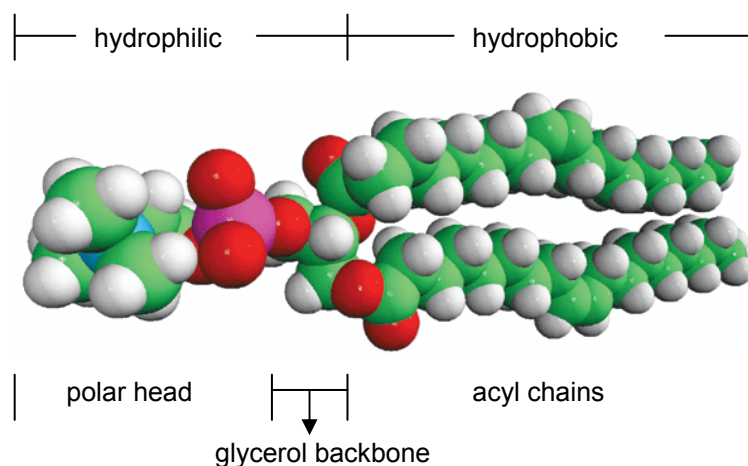


Figure 1.3.1 The molecular structure of 1,2-dioleoyl-*sn*-glycero-3-phosphocholine (DOPC). DOPC is a phospholipid which consists of hydrophilic, phosphate-bearing head attached by a glycerol backbone to two hydrophobic hydrocarbon chains. The white beads present hydrogen, the green ones present carbon, the red ones present oxygen, and the pink bead presents phosphate. [The structure is from www.avantilipids.com]

According to their geometry, the amphiphilic molecules can pack into differently shaped aggregates. A crude but useful parameter to predict the aggregate shape is the so-called packing parameter, which is defined as $p=V/(AL)$, where V is the volume of the molecule, A is the area of the hydrophilic head group and L is the length of the hydrophobic chain(s). Figure 1.3.2 shows the structure of amphiphilic aggregates formed with different molecules. This packing model is also valid in many cases of different mixtures where a number average packing parameter is used.

When the packing parameter is around one, arising either from one type amphiphiles or a mixture of several types, the amphiphiles can pack into lamellar structures, such as disk-like micelles, large vesicles and lamellae, as shown in the second and last row in Fig. 1.3.2. In the lamellar structures, lipids pack into a bilayer or a stack of bilayers. The hydrophobic tails of one monolayer face the hydrophobic tails of the other monolayer and the hydrophilic head groups face the aqueous surroundings in lipid bilayers. This structure is of particular interest since it is the structure of cell membranes. In connection with cell membranes, as well as liposomes, the building blocks are polar lipids and sterols, predominantly cholesterol.

One special property of lipid membranes is their permeability. The membrane structure changes including disorder during membrane permeation. The membrane permeability is different for anions, cations, and neutral species. For some uncharged molecules, the permeability is proportional to the solubility of the compounds in nonpolar environment similar in nature to the hydrophobic core of the membrane. In some cases, the diffusion through the bilayer can be enhanced by the chain kink mechanism: *trans*-gauge conformational sequence, for example, kink, travelling along the chain. Apart from water and some other small molecules which permeate either through holes created by statistical lateral diffusion and clustering of molecules, or in the cavity of down-the-chain-travelling-kink, some molecules may form short-lived complexes with the polar heads, and cross the bilayer via flip-flop.


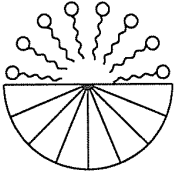
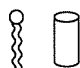
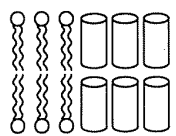

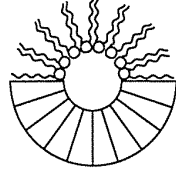

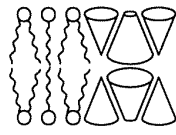
Lipids	Shape	Organization	Phase
Soaps Detergents Lysophospholipids	 Inverted cone $p < \frac{1}{3} - \frac{2}{3}$	 Micelles	Isotropic hexagonal I
Phosphatidyl- choline - serine - inositol Sphingomyelin Dicetylphosphate DODAC	 Cylinder $p \sim 1$	 Bilayer	Lamellar (Cubic)
Phosphatidyl- ethanolamine Phosphatidic acid Cholesterol Cardiolipin Lipid A	 $p > 1$	 Reverse micelles hexagonal II	
Mixtures Lysophosphatidyl- choline and Phosphatidyl- ethanolamine	 $p \sim 1$	 Lamellar	

Figure 1.3.2 Structure of amphiphilic aggregates. The colloidal aggregates of various amphiphiles are described by the model of geometrical packing. p is the packing parameter. [Lasic 1993]

The permeability coefficient describes how fast a molecule diffuses across a bilayer. In general, the bilayer is less permeable to ions than neutral molecules due to the reduced solubility in the nonpolar phase. The water permeability coefficient through lecithin membranes is of the order of 10^{-3} - 10^{-4} cm/s, for anions this value is about 10^{-11} - 10^{-12} cm/s and up to 10^{-15} cm/s for some large multivalent inorganic anions, and cations have permeability coefficient ranging between 10^{-12} and 10^{-14} cm/s. In practice this means that 3000 - 4000 water molecules cross the lipid bilayer per second per area of polar head (70 \AA^2) while it takes about 70 h for one sodium atom to cross the membrane [Lasic 1993]. For macromolecules it is also very difficult to pass through the membrane. The permeability coefficient of dextran through egg PC is 10^{-13} cm/s. [Lasic 1993] One can assume that the lipid membrane is permeable to water but not to ions, some small molecules and macromolecules due to the significant difference in their permeabilities.

Vesicles are membrane ‘bubbles’ formed by bending and closing up a lipid bilayer. Giant vesicles are vesicles with several tens of microns in size. They are big enough to be observed and manipulated under optical microscopy. They have long been recognized as models for the cell membrane. [Dimova 2006]

The membrane of a closed vesicle divides the space into interior and exterior compartments. Both compartments may contain different particle species. In dilute solution, the osmotic pressure difference across the membrane is proportional to the number density difference of the particles. It is balanced by the bending rigidity of the bilayer membrane. However, in giant vesicles, which have large volumes, the osmotic pressure difference is approximately equal to zero. In other words, we can consider that the osmotic pressures in and out of the vesicle are equal. Thus, one can control the vesicle volume by changing the exterior number densities or concentrations.

Lipid bilayers respond elastically to mechanical deformations including bending, shearing, and stretching or compressing of the membrane. It is very hard to stretch a membrane, but easy to bend it. The flexibility of the membrane makes it possible for the vesicle to have different morphologies [Käs 1995]. Three types of models have been developed to describe the behaviours of vesicles [Lipowsky 1991].

In the theoretical models, the vesicle shapes depend on the geometric parameters such as vesicle volume and membrane area, as well as on the material parameters such as spontaneous curvature and bending rigidity. The vesicle shapes are constrained by the

coupling model. The shape of the individual fluid bilayer vesicles is the one that minimizes the bending energy at given geometrical parameters. A cartoon of the correspondence between shape parameters and vesicle shapes is shown in Fig. 1.3.3.

There are mainly two pathways in the vesicle morphology deviation from a sphere with equilibrium differential area equal to one. When the equilibrium differential area of the two monolayers is higher than one, the vesicle is a prolate and may bud outwards. When it is smaller than one, the vesicle is an oblate and may bud inwards. Budding means the developing of one or more daughter vesicles from the vesicle body.

In experiment, the area-to-volume ratio can be manipulated through osmotic pressure. Another method to adjust the area-to-volume is via temperature, which introduced the temperature trajectories into the morphology diagram [Berndl 1990].

According to the flexibility of the hydrophobic tails, the bilayer has two states: liquid ordered phase (gel phase) and liquid disordered phase. The phase transition temperature is influenced by the headgroup, the length of the tails, the number of unsaturated bonds and their positions. When a bilayer contains lipids at the liquid ordered and disordered phases, phase separation may occur depending on the composition and the temperature, and domains form. The composition of the domains differs from the membrane matrix. This difference in composition usually leads to a difference in spontaneous curvature. It may induce the budding of domains. At the same time, the line tension is decreased. [Lipowsky 2002]

1.4 Vesicles containing aqueous two-phase system

As it was discussed in chapter 1.1, the interior of living cells is a crowded milieu of macromolecules, such as proteins, RNAs, DNAs. This results in the local composition difference even in the cytoplasm regime which is not bounded by lipid membrane. This phenomenon is referred as microcompartmentation, which is thought to have profound implications for cell function. Phase separation is a possible mechanism of the microcompartmentation. However, the real system is too complex to be characterized. Mixtures of aqueous solutions of structurally distinct macromolecules undergo phase separation above certain concentrations in bulk. This phenomenon can be applied to mimic the microcompartmentation in the cell. The simplest model of the cell as a container is giant vesicles containing aqueous two-phase system (ATPS) consisting of

polymer solutions. The first group which initiated the work in this field is Keating's group. This part is mainly a review of her group's work.

Keating's group reported the preparation of giant vesicles with ATPS for the first time in 2002 [Helfrich 2002]. The vesicles were prepared by "gentle swelling" method, namely a dried lipid film was hydrated in a warm homogeneous aqueous solution containing polyethylene glycol (PEG) and dextran. The concentrations of both polymers were carefully chosen according to their phase diagram. They were in the one-phase regime at the preparation temperature and in the two-phase regime at the observation temperature. Vesicles containing two phases can be obtained by simply decreasing the temperature. The ATPS-giant vesicles observed from above appeared as two concentric circles, as shown in Fig. 1.4.1A. The phase separation process induced by temperature is reversible.

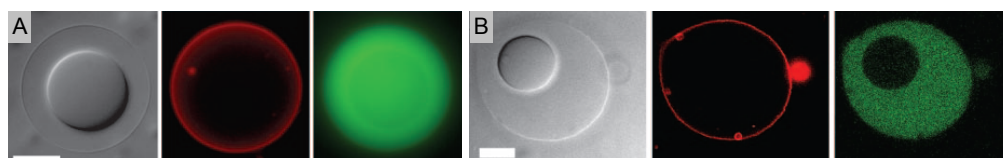


Figure 1.4.1 Optical microscope images of giant vesicles (horizontal cross section). The three images in each panel are transmitted light (DIC) (left), rhodamine-tagged lipid fluorescence (centre), and Alexa Fluor 488-tagged PEG in (A) or fluorescein-tagged streptavidin in (B) (right). (A) Encapsulation of ATPS. The vesicles were formed at 55 °C in a bulk aqueous solution with 3.24% dextran 511 kDa and 4.17% PEG 8 kDa, and imaged at 21 °C. (B) Protein partitioning. The vesicles were formed at 37 °C in a bulk aqueous solution with 9.375% PEG 4.6 kDa and 9.375% dextran 10 kDa, 5 mM phosphate buffer (pH 7.0). 0.004 wt% of the PEG has been biotinylated. Images were acquired on a confocal microscope at 4 °C. Lipid composition was 44.3:1 mol ratio DOPC/DOPE-PEG 2,000. The scale bars are 10 μm . [Long 2005]

The two phases in the vesicles have different compositions and constitute separated microcompartments. One phase is the PEG-rich phase and the other one is the dextran-rich phase. They have also different affinities to the same protein. Figure 1.4.1B shows the location of fluorescently tagged streptavidin in a vesicle containing biotinylated PEG. The protein preferably stays in the PEG-rich phase. Partitioning within these microvolumes was quantified using confocal fluorescence microscopy images. Microcompartmentation within living cells is not static. The distribution of intracellular components changes throughout the cell cycle and in response to stimuli. This model cytoplasm based on aqueous phase separation can provide dynamic alterations in local concentrations. When the synthetic cells are heated, their interiors can convert to a single phase in which the polymers are homogeneously distributed, and so do the proteins.

The phase separation of the aqueous polymer solution within a vesicle can be induced not only by changing the temperature but also by changing the concentration. The polymer concentration inside the vesicles can be adjusted through the osmolarity of the external medium because the lipid membrane is only permeable to water but not to the polymer molecules. In order to achieve the osmotic pressure balance in the interior and the exterior of the vesicles, water molecules are forced to diffuse across the membrane in react to the osmotic stimuli.

Three classes of ATPS vesicle morphologies upon osmotic dehydration were observed in the literature [Long 2008]: (A) spherical vesicles with the PEG-rich phase contacting the lipid membrane; (B) nonspherical vesicles in which one or more buds protrude from the central sphere, such that the buds contain one of the aqueous phases (e.g., dextran-rich) and the body of the vesicle contained the other (PEG-rich) aqueous phase; and (C) spherical vesicles with the dextran-rich phase contacting the lipid membrane. For the ATPS compositions used in this paper, the dextran-rich phase is generally smaller, such that when the two phases cease to be concentric, the dextran-rich phase appears as a “bud” on the larger PEG-rich phase. Which of these structures was observed in a given experiment depended on the degree of hypertonicity, the ATPS polymer composition, and the lipid membrane composition.

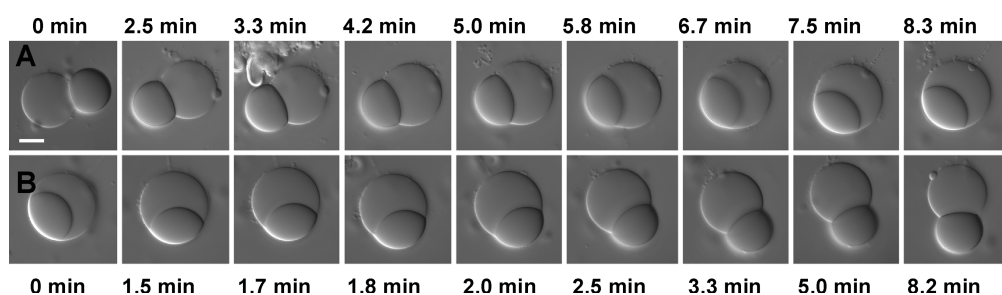


Figure 1.4.2 DIC images of dynamic aqueous phase budding within an ATPS giant vesicle (horizontal cross section). The dense part is the dextran-rich phase and the light part is the PEG-rich phase. This vesicle (44:1 mol ratio DOPC/DOPE-PEG2000) was originally imaged in a hypertonic sucrose/buffer solution. The minutes above (below) each frame indicate the time at which the images were acquired. (A) Transition induced by adding deionized water. (B) Transition induced by adding hypertonic sucrose. T is 3 °C. The scale bar is 10 μm . [Long 2008]

By exposing an ATPS vesicle firstly to hypotonic and then to hypertonic external solutions, the vesicle morphology may change from (A) to (C) [Long 2005]. More frequently encountered case is the transition between (A) and (B). Figure 1.4.2 shows one such example. This transition is a reversible process when the membrane elasticity permits. When a budded vesicle was exposed to a hypotonic medium by adding

deionized water into the chamber, the bud moved back into the vesicle body, returning the vesicle to a spherical morphology, case (A). A subsequent increase of the external medium osmolarity resulted in the reappearance of the bud. Importantly, budding in the ATPS vesicles induced asymmetric distribution not only of the aqueous phases but also of the proteins preferentially partitioned to one of the aqueous phases.

The interactions between the lipid membrane and the two phases are different. The head groups of the lipids are the key factor to the interaction because they are in direct contact with the interior solution, but not the tails. This interaction may influence the lipid distribution in multicomponent membranes, e.g. in vesicles with lipids phase separated into two phases, the liquid ordered and liquid disordered phases, each of them having different lipid compositions. There are four interactions between the two lipid domains and the two polymer phases. In the equilibrium state, the domains are located at one specific phase of budded vesicles in response to the local internal composition.

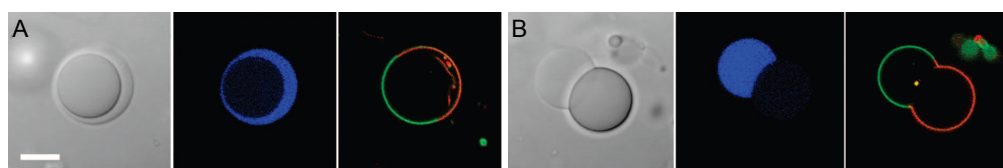


Figure 1.4.3 ATPS-containing giant vesicle before (A) and after (B) budding was induced by osmotic stress. Fluorescence images have been false colored: blue indicates Alexa647, red indicates rhodamine, green indicates CF. Images: transmitted light DIC (left), Alexa 647-labeled PEG 5 kDa fluorescence (center), overlay of DOPE-rhod and DSPE-PEG-CF fluorescence images (right). The lipid composition is 1:1 DOPC/DPPC + 30% cholesterol. $T = 4\text{ }^{\circ}\text{C}$. Please check the abbreviation list for the full names of the chemicals. The scale bar is 10 μm . [Cans 2008]

In a spherical ATPS vesicle, see Fig. 1.4.3A, only the PEG-rich phase (blue) is in contact with the membranes. There is no preference of the two domains in the membrane. Once the dextran-rich phase protruded out of the PEG-rich phase, the domains have their preferred locations; Fig. 1.4.3B. The PEGylated lipid DSPE-PEG-CF prefers the DPPC-rich liquid ordered domain (green) to the DOPC-rich disordered domain (red). The liquid ordered domain with more PEGylated lipids has a lower interaction with the PEG-rich phase than the dextran-rich phase. Therefore it encloses the PEG-rich droplet and the liquid disordered domain encloses the dextran-rich droplet. The overall shape of the ATPS vesicles is governed primarily by the internal aqueous phases rather than the reduction of line tension in the case of the domains induced budding. [Lipowsky 1998] This can be proven by the vesicle shown in Fig. 1.4.2B. The kink in the membrane is located at the interface of the two phases, but not at the boundary of the two domains.

There is one problem in this system, namely the heterogeneity of the vesicles. The polymer concentrations (PEG and dextran) differ in different vesicles. As a result, the volume ratio of the two phases significantly differs from vesicle to vesicle, even if they are from the same batch. [Long 2005] In addition, the polymers are also polydisperse. The concentration heterogeneity of the dextran molecules is stronger than that of the PEG molecules. [Dominak 2007]

To summarize, vesicles with ATPS have different shapes. The overall shape can be influenced by the volume ratio of these two phases, the vesicle area, especially the excess area (the difference between the actual area and the area required to form a sphere of the same volume), the membrane and the interfacial tensions. These factors also influence the contact zone of the two phases within the vesicles. The volume ratio of the two phases can be varied by changing the osmolarity of the external medium, the temperature and the concentration of the polymers in the vesicle preparation. The excess area and the membrane tension can be controlled externally, for example by using micropipette aspiration.

1.5 Transitions from partial to complete wetting

Wetting and dewetting of surfaces are ubiquitous phenomena. It is quite common to encounter such phenomena in our everyday life. The spreading of ink on paper provides a familiar example of wetting. The formation of water droplets sitting on a plant leaf is an example of dewetting. Wetting and dewetting are important processes for many applications, including adhesion, lubrication, painting, printing, and protective coating. For most applications, dewetting is an unwanted process because it destroys the applied thin film. In ATPS vesicles, there are two aqueous phases, the PEG-rich phase and the dextran-rich phase, and the membrane which serves as a substrate. Wetting and dewetting of the membrane by one of the two phases may occur in such vesicles.

Let us consider a liquid drop on a solid substrate as depicted in Fig. 1.5.1b. The edge of the droplet can be characterized by a certain angle θ , which is called contact angle. Since there are three different phases denoted by α , β , and γ , see Fig. 1.5.1c, there are three interfacial (or surface) tensions that need to be considered: $\Sigma_{\beta\gamma}$ (liquid-solid), $\Sigma_{\alpha\beta}$ (vapour-liquid) and $\Sigma_{\alpha\gamma}$ (vapour-solid). The relation between the three tensions and

the cosine of the contact angle, which is also called wettability, is given by Young's equation

$$\cos(\theta) = (\Sigma_{\alpha\gamma} - \Sigma_{\beta\gamma}) / \Sigma_{\alpha\beta} \quad (1.5.1)$$

As shown in Fig. 1.5.1b, this equation can be also interpreted as a force balance at the three-phase contact line. The unit of the interfacial tension (J/m^2) allows one to consider each of the three tensions as a force per unit length (N/m), acting on the three-phase line. The direction of the three forces is then defined in such a way that they are tangential to the interfaces and perpendicular to the three-phase contact line. Note that this discussion is somewhat imprecise since the quantities $\Sigma_{\beta\gamma}$, $\Sigma_{\alpha\beta}$ and $\Sigma_{\alpha\gamma}$ in Eq. 1.5.1 are scalar quantities, whereas the forces shown in Fig. 1.5.1 and Fig. 1.5.2 are vectors. Young's equation then simply expresses the mechanical equilibrium at this contact line. Therefore, the thermodynamic expression of the interfacial tension is equivalent to the mechanical expression.

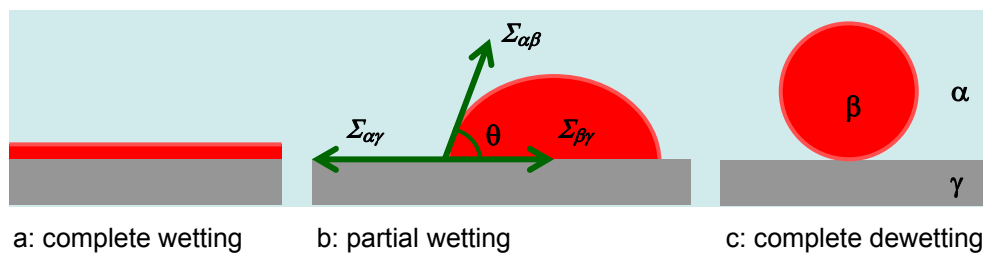


Figure 1.5.1 Wetting of a liquid drop (β , red) on a solid substrate (γ , gray): (a) complete wetting; (b) partial wetting, and the force balance at the three-phase contact line; (c) complete dewetting.

Three morphologies of a droplet sitting on a substrate can be distinguished as a direct consequence of Young's equation (1.5.1). The situation in Fig. 1.5.1b is commonly called partial wetting, since the surface is only partially covered by the liquid. If we now change some thermodynamic variable, say the temperature, the three interfacial tensions will change gradually in different ways and, consequently, the contact angle will also change. At a certain point, the sum of interfacial tensions $\Sigma_{\beta\gamma}$ and $\Sigma_{\alpha\beta}$ may become equal to $\Sigma_{\alpha\gamma}$. The contact angle will then be zero and the system will be in equilibrium when a uniform film covers the whole solid surface, see Fig. 1.5.1a. This is called complete wetting. Analogously, the situation might be reversed. When the contact angle reaches 180° , the liquid does not wet the solid at all. It remains separated from the solid by a film of vapour in equilibrium. This situation is called complete dewetting. It is depicted in Fig. 1.5.1c.

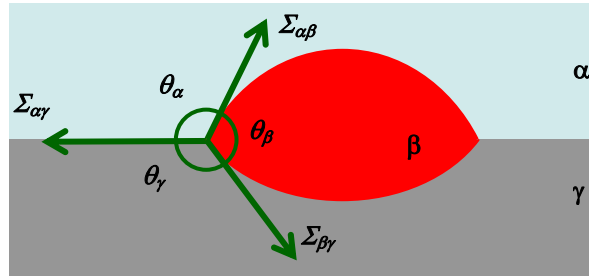


Figure 1.5.2 Wetting of a liquid drop (red) on a soft interface.

Young's equation describes wetting of rigid substrates. The droplet morphology is only influenced by the tangential component of the interfacial tension, but not by the normal component because it is counterbalanced by the rigid substrate which is not deformable. What will happen if the substrate became soft and deformable, e.g. for a system in which the phase γ is a liquid instead of a solid? The β - γ interface becomes curved, and a lens-shaped droplet forms, as illustrated in Fig. 1.5.2. This situation corresponds to mechanical equilibrium of both the tangential and the normal components of interfacial tensions. Young's equation is not valid any more in this case. The relation among the three contact angles and the three interfacial tensions at equilibrium is then described by Neumann's equations [Rowlinson 2002] as given by

$$\begin{aligned}\Sigma_{\alpha\beta} + \Sigma_{\beta\gamma} \cos\theta_{\beta} + \Sigma_{\alpha\gamma} \cos\theta_{\alpha} &= 0, \\ \Sigma_{\alpha\beta} \cos\theta_{\beta} + \Sigma_{\beta\gamma} + \Sigma_{\alpha\gamma} \cos\theta_{\gamma} &= 0, \text{ and} \\ \Sigma_{\alpha\beta} \cos\theta_{\alpha} + \Sigma_{\beta\gamma} \cos\theta_{\gamma} + \Sigma_{\alpha\gamma} &= 0.\end{aligned}\quad (1.5.2)$$

These three equations are not independent. The dependence arises from the constraint that the sum of the contact angles must be equal to 2π . Because of the force balance, the three tensions form the sides of a triangle, the so-called Neumann triangle. The largest tension of the three must be smaller than the sum of the other two. Under this condition, the three phases meet at a common contact line. When the Neumann triangle collapses to a line, which means that the largest interfacial tension becomes equal to the sum of the other two, one of these phases spreads and completely covers the high tension interface corresponding to complete wetting. This state is analogous to the case shown in Fig. 1.5.1a. Complete dewetting can also occur when one of the three interfacial tensions is smaller than the other two. Young's equation can be considered as a simplified Neumann's equations with the contact angle θ_{γ} , see in Fig. 1.5.2, equal to π .

Transitions can occur from partial wetting to complete wetting or from complete dewetting to partial dewetting. Complete dewetting is in fact analogous to complete wetting if one interchanges the two phases α or β . In the following text, we are going to discuss the wetting transition from partial to complete wetting.

Partial-to-complete wetting transitions were first predicted by Cahn (1977) and Ebner and Saam (1977) independently. In any two-phase mixture of fluids near its critical point, phase contact angles against any third phase became zero in that one of the critical phases completely wetted the third phase and excluded contact with the other critical phase. [Cahn 1977] In Cahn's model, the liquid/solid interface is described by a continuum theory, where the liquid number density varies smoothly as a function of the distance from the solid surface, and the forces between the solid and liquid are short-ranged. In addition, the fluid surface is treated by mean-field theory. Another approach to elucidate the critical properties at the wetting transition is the effective solid-on-solid model [Kroll 1983]. Effective interface models were introduced to study this problem in three dimensions in [Lipowsky 1983]. In this model, the attention is focused on the interface fluctuation, which is underestimated within the mean-field approximation. Furthermore, renormalization-group methods were used to study wetting phenomena [Lipowsky 1987]. These methods yield a unified description of the transition in the mean-field, weak-fluctuation and strong-fluctuation scaling regimes.

Partial-to-complete wetting transitions can be first-order transitions or second-order. The order of the transition can be determined from the hysteresis in the thickness of the absorbed wetting film or the contact angle [Durian 1987]. The wetting transition is generally first order (discontinuous), implying a discontinuity in the first derivative of the surface free energy. In this case, a discontinuous jump in film thickness occurs from a microscopically thin to a thick film at the wetting transition [Ross 1996]. Second-order transitions are probably rather rare, for which a discontinuity in a higher derivative of the surface free energy occurs. This consequently leads to a continuous divergence of the film thickness [Ross 2001]. Two different types of continuous or critical wetting transition have been reported. The first type is the so-called long-range critical wetting transition [Lipowsky 1984b], which is due to the long-range van der Waals forces. The second type is the short range critical wetting transition [Ross 1999], for which the layer thickness diverges continuously from a very thin to a macroscopically thick film.

In contrast to the large amount of theoretical studies concerning wetting transitions [Lipowsky 1984a, de Gennes 1985], there are not many experimental studies in this direction. The experimental evidence is far more lagging behind the theoretical predictions. There are a few experimental examples of the wetting transition [Daniel 2001]. Much of the recent progress has occurred along these two fronts: low-temperature liquid/vapor/substrate systems [Klier 1995] and binary liquid mixture. In the former system, the wetting transition of cryogenic liquids on the surface of alkali metals is studied. Most experiments involved helium [Rolley 1997, Rutledge 1998], but H₂ [Ross 1998] and Ne have also been investigated. The latter system has the advantage of exhibiting homogeneous interfaces, and the experiments can be performed at room temperature. The contact angles of suspended liquid drops under the liquid-vapour interfaces were measured in the work of Moldover (1980) and Ross (1999) in order to characterize the wetting transition. Interestingly, the images in both papers showed that the droplets formed spherical caps instead of the lens-shaped droplets. It seems that it is not necessary to use Neumann's equations to characterize these two systems, although all interfaces are deformable.

Chapter 2

Materials and Experimental Techniques

2.1 Materials

Poly(ethylene glycol) (PEG, average molecular weight 8 kg/mol, lot.: 05723EO-124) and dextran from *Leuconostoc mesenteroides* (molecular weight between 400 kg/mol and 500 kg/mol, batch: 076K0702) were purchased from Sigma-Aldrich. Fluorescein isothiocyanate-dextran (dextran-FITC, average molecular weight 500 kg/mol) was purchased from Sigma. Sucrose was purchased from Fluka. Water is deionized to a resistance of 18 M Ω (USF Seral, Pure Lab).

Lipids including 1,2-dioleoyl-*sn*-glycero-3-phosphocholine (DOPC), 1,2-dioleoyl-*sn*-glycero-3-phosphoethanolamine-N-[methoxy(polyethylene glycol)-2000] (DOPE-PEG2000), 1,2-dioleoyl-*sn*-glycero-3-[phospho-L-serine] (sodium salt) (DOPS), and 1,2-dipalmitoyl-*sn*-glycero-3-phosphoethanolamine-N-(lissamine rhodamine B sulfonyl) (DPPE-rhod) as chloroform solutions and galbeta1-3galnacbeta1-4(neuacalpha2-3)galbeta1-4glcbeta1-1'-cer (G_{M1} ganglioside) as powder were purchased from Avanti Polar Lipids. The powder was dissolved in chloroform/methanol = 80:20 (volume ratio) before use. Chloroform and methanol were purchased from Merck KGaA.

2.2 Bulk polymer solution characterization

An aqueous solution of two chemically dissimilar polymers will typically phase separate at the weight concentration above a few percentages. The most widely studied aqueous two-phase systems are derived from mixtures of two polymers, particularly PEG and dextran [Edmond 1968, Cesi 1996, Raemsch 1999, Wu 1999, Hopkinson 2002]. The structures of PEG and dextran are shown in Fig. 2.2.1. Poly(ethylene glycol) (PEG) is also known as poly(ethylene oxide) (PEO) or polyoxyethylene (POE). It is a linear molecule, soluble in water, non-toxic. It is a very important polyether. Dextran is a kind of polyglucose. It is composed of approximately 95% alpha-D-(1-6) linked glucose units. The rest of the inter-glucose bonds are (1-3) links, which account for the branching of dextran. Dextran is characterized by their high molecular weight, good water solubility, low toxicity, and relative inertness.

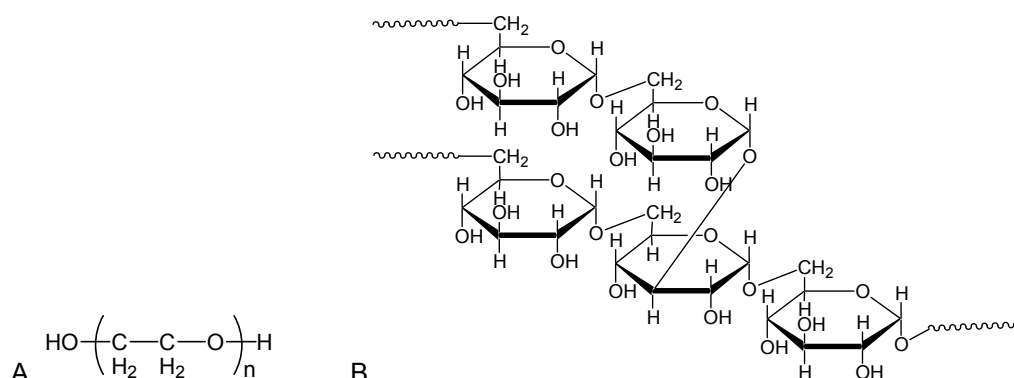


Figure 2.2.1 Structures of PEG (A) and dextran (B). For the PEG molecules used in this work, n corresponds to 181 and the molecular weight is 8 kg/mol. The dextran used in this work is composed of about 3080 glucose units and the molecular weight is 500 kg/mol. The schematic presentation in (B) illustrates three (1-6) links and one (1-3) link, the latter being responsible for the branching of the polymer.

The PEG and dextran aqueous solutions, used to prepare ATPS vesicles, are homogeneous at room temperature. One important property of synthesized polymers is the polydispersity. It can affect the phase behaviour of the polymer solution and other properties, e.g., the interfacial tension. The molecular weight and the polydispersity may differ in different batches. They were measured using gel permeation chromatography (GPC), which is also called size exclusion chromatography.

Before performing each experiment described below, PEG stock solutions and dextran stock solutions were prepared at first. The concentration ranges from 10% to 20% depending on the specific experiments. It may take hours to dissolve them in water, especially dextran because of the high molecular weight.

2.2.1 Phase diagram

The binodal of the PEG and dextran aqueous solution was determined by cloud-point titration at 23 °C, 40 °C and 60 °C, respectively. The solution is clear and transparent in the one-phase region. It starts to become turbid at certain concentration, which is the so-called cloud point. At this point, the second phase starts to appear. This point is at the binodal, namely the boundary between the one-phase region and the two-phase region. Either of both stock solutions can serve as the titrator. Here, PEG stock solution was used because it had much lower viscosity than the dextran stock solution.

The mass of a small well sealed vial was measured with a balance (Mettler AT261 DeltaRange). A certain amount (several millilitres) of dextran stock solution and water was injected into the vial through a syringe, and the added masses were measured.

Then PEG stock solution was injected drop wise into the vial through a syringe until the solution in the vial became turbid. The vial was shaken by hand between the consecutive injections to ensure the homogeneity of the solution. The mass of the added PEG solution was measured with the balance.

The same vial was put into a water bath at 40 °C for at least 1 hour. The solution was titrated again to determine the cloud-point at this temperature. Depending on the concentration combination of PEG and dextran, the titrator can be either water (in case of turbid solution) or PEG stock solution (in case of clear solution). The same procedure was repeated to determine the cloud-point at 60 °C.

The forgoing procedures were carried out for more than ten samples with different initial dextran concentration. The binodal curves could be constructed by connecting these cloud points. One should note that the molecular weight and the polydispersity of the polymers can influence the binodal. The binodal has to be measured for each polymer batch.

Cloud-point titration is a fast method to determine the binodal. It can be done routinely in the lab. However, the binodal curve is not the coexistence curve. One can not construct the tie lines using this method. In order to obtain the tie lines, the PEG and dextran concentrations in each phase have to be measured, e.g. with GPC. These points are also the cloud points. The curve connecting these points is the coexistence curve.

Certain amount of PEG stock solution, dextran stock solution and water were added into a 50 ml separatory funnel, respectively. The mass of each component was measured with a balance. This included around 60 g solution in the funnel. Then the solution was shaken by hand to make the polymers mix well. It was left at 24.2 °C (room temperature with small fluctuations ± 0.5 °C) for 4 to 5 days. Afterwards, the two phases were separated. The dextran-rich phase was taken out through the lower outlet, and the PEG-rich phase through the upper outlet.

Each phase was diluted to a total polymer concentration around 1.5 g/L with 0.1 mol/l NaNO₃ aqueous solution. Their densities at 25 °C were measured using a density meter (DMA5000, Anton Paar). The PEG and dextran concentrations (g/L) were determined using GPC at 25 °C. In the end, the weight concentrations of the polymers were calculated for each phases. In this way, one tie line can be constructed.

Six samples with different concentrations were measured. The coexistence curve was constructed at 24.2 °C. The weight ratio of PEG and dextran was fixed in all samples. The osmolarity of each phase was also measured using an osmometer (Gonotec Osmomat 030).

The volume ratio of the dextran-rich and the PEG-rich phase were measured at room temperature by diluting a concentrated solution in a volumetric cylinder. The concentration changed after each dilution but the PEG/dextran weight ratio was fixed. Circa 5 ml concentrated PEG and dextran aqueous solution were prepared in a 10 ml volumetric cylinder. It was left to phase separate at room temperature for 2 or 3 days. The volume of each phase was recorded. The solution was diluted by adding circa 1 ml water into the cylinder. The volume ratios were recorded after the phase separation was completed. The dilution and phase separation were repeated several times until the solution arrived at the cloud point. The more dilute the solution was, more time needed for the phase separation. The volume ratios of several samples with different PEG/dextran weight ratios were determined in this way.

2.2.2 Interfacial tension measurement

The interfacial tensions of the coexisting phases were measured at 24.2 °C using a spinning drop tensiometer (SITE100SQ, Krüss). The polymer solutions were the same ones used in the coexistence curve determination. The density differences of the coexisting phases were needed for this method. They were measured at 24.2 °C with a density meter (DMA5000, Anton Paar).

The spinning drop technique is suitable to measure low tensions, typically below 1 mN/m, and down to ultra low values ($\mu\text{N/m}$ or less), which is the case for the polymer solutions used in this work. In order to measure the interfacial tension of the coexisting PEG-rich phase and the dextran-rich phase, $\sim 4 \mu\text{l}$ PEG-rich phase is injected into a glass capillary filled with the denser dextran-rich phase. The capillary with the solution and the drop rotated around the horizontal axis with a certain angular velocity ω .

The drop's geometry is illustrated in Fig. 2.2.2. The x axis is the rotational axis. The y axis denotes the distance from the rotational axis. The drop shape is symmetric around the x axis. The gravity effect is negligible. The centrifugal acceleration is $\omega^2 y$ and it increases with the distance from the x axis. Hence the influence of the density difference between the two fluids increases with the distance from the x axis and

produces a pull force applied to the interface toward the x axis. This leads to the elongation of the drop along the x axis, which is opposed by the interfacial tension that tends to minimize the surface area, i.e. to make the drop shape more spherical.

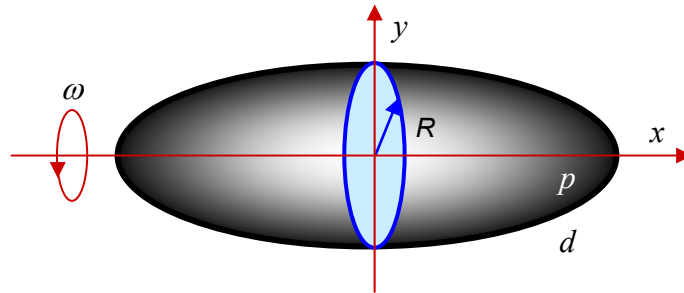


Figure 2.2.2 Geometry of a spinning drop of a light PEG-rich phase p in the dense dextran-rich phase d .

When the central part of such an elongated drop is essentially cylindrical (which is approximately valid for aspect ratios larger than 4), the interfacial tension Σ_{pd} can be described by the Vonnegut's equation:

$$\Sigma_{pd} = (\rho_d - \rho_p)\omega^2 R^3 / 4 \quad (2.2.1)$$

where ρ_d and ρ_p are the density of the dextran-rich phase and the PEG-rich phase, respectively. R is the radius of the drop at the equator as indicated in Fig. 2.2.2.

This formula is valid within 0.1% when the length of the drop is at least 4 times its diameter, which is roughly the case of the drop shown in Fig. 2.2.2. In practice, a much more elongated drop is usually used which looks like a cylinder in its central part ($x = 0$). It is worth noting that the radius of the cross section perpendicular to the y axis is different in the rotating drop. It is smaller at the tip than at the equator, as shown in Fig. 2.2.2. This is due to the non-constant centrifugal acceleration. Therefore, it is very important to assure that the measured radius is the one at the equator, especially for a very long drop whose centre is difficult to be determined in the experiment. Vonnegut's equation (Eq. 2.2.1) indicates that low tension will be associated with small radius R , i.e., an elongated drop and slow rotational velocity, whereas high tension will require a high rotational velocity and the drop might not be elongated enough to fall into the Vonnegut's formula case.

The spinning tube is often a capillary of internal diameter equal or less than 1 mm. This tube produces a lens effect which blows up the drop size. The lens effect is influenced by the reflective index of the denser phase and the thickness of the glass

capillary. The correction has to be applied to estimate the real radius of the drop. The easiest way is to measure the diameter of the stiff cylindrical stick inserted in the capillary filled with the denser phase. The correct factor is estimated from the comparison with the real diameter measured outside the capillary, e.g., with a micro ruler. This method is used by the SITE100SQ spinning drop tensiometer.

2.3 Vesicle preparation

Corresponding to the structures of PEG and dextran as shown in Fig. 2.2.1, mainly two kinds of membrane compositions were chosen to prepare vesicles: PEG-membrane and sugar-membrane. The former contains DOPE-PEG2000 whose headgroup contains ethylene oxide units, and the latter contains G_{M1} ganglioside whose headgroup contains glucose units. Their compositions are listed in Table 2.3.1. The majority is DOPC and the fluorescent label is DPPE-rhod in both membranes. The key part is the third component from which the names arise. Most of the experimental results shown in the following chapters are from the vesicles with PEG-membrane and sugar-membranes. DOPS-membranes shown in Table 2.3.1 are only used in chapter 4.

Table 2.3.1 The membrane compositions

type	lipids mole fraction		
PEG-membrane	DOPE-PEG2000 4.00%	DOPC 95.93%	DPPE-rhod 0.07%
sugar-membrane	G_{M1} ganglioside 4.00%	DOPC 95.93%	DPPE-rhod 0.07%
DOPS-membrane	DOPS 27.94%	DOPC 71.98%	DPPE-rhod 0.07%

In DOPE-PEG2000, a linear PEG chain with molecular weight 2 kg/mol corresponding to 45 ethylene oxide units is attached to the headgroup of DOPE. The molecular structure is shown in Fig. 2.3.1. The headgroup of DOPE-PEG2000 (the green part) has the same repeat unit as the PEG molecule used in the polymer solution, but different end groups and chain length.

According to the configuration of the polymer chains anchored on the membrane, there are two regimes in the membrane behaviour, the mushroom regime and the brush regime. The mushroom regime holds for low concentrations of grafted lipids. The polymer headgroups do not interact. The polymer chain assumes a random configuration, like that of the polymer free in solution. The brush regime pertains to higher concentrations. In the brush regime, the polymer chains are more densely packed,

mutually interact, and extend out from the membrane surface forming a polymer layer. The transition between the mushroom and brush regimes occurs at the concentration of grafted lipid, for which the surface-associated polymer chains first begin to overlap.

In fluid-phase membranes, the mushroom to brush regime transition is at molar ratio 1.4% for PEGylated lipids with molecular weight 2000 g/mol [Marsh 2003]. There is 4% DOPE-PEG2000 in the PEG-membrane. The PEG chains form a densely packed layer on the surface of the lipid membrane with a thickness larger than 3.8nm, which is the Flory radius of PEG2000 in aqueous solution [Marsh 2003]. It implies that the enclosed aqueous solution will only interact with the grafted PEG chains, but not with the rest of the membrane. It is straight forward that the PEG-membrane favours the PEG-rich phase, but not the dextran-rich phase.

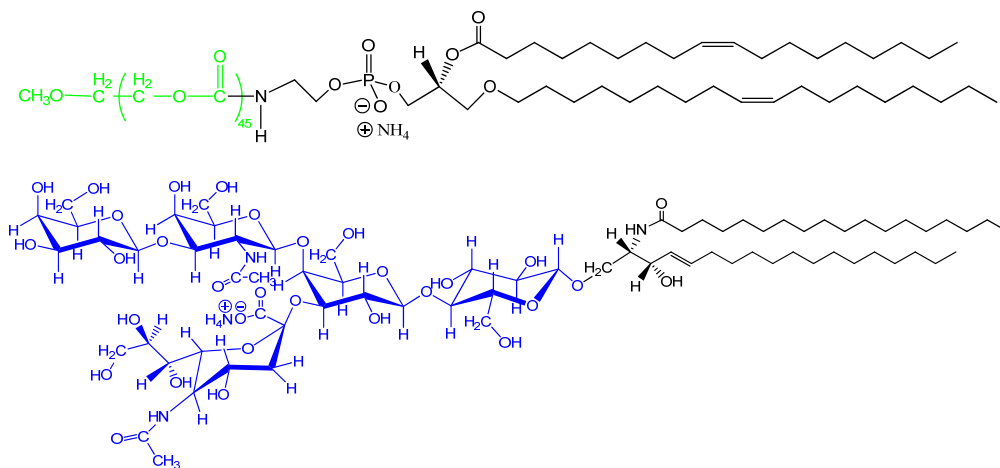


Figure 2.3.1 The molecular structures of DOPE-PEG2000 (top) and G_{M1} ganglioside (bottom).

In the sugar-membranes, 4% G_{M1} ganglioside is used instead of DOPE-PEG2000. The structure of G_{M1} ganglioside is shown in Fig. 2.3.1. Its headgroup (the blue part), containing glucose and galactose moieties, is similar to the structure of dextran which is in fact a kind of polyglucose. The sugar-membrane favours the dextran-rich phase of the polymer solution compared to the PEG-membrane. The sugar headgroup can decrease the interfacial tension between the membrane and the dextran-rich phase.

Two kinds of polymer solutions (PS) were used to prepare vesicles, namely PS1 and PS2. Their concentrations are listed in Table 2.3.2. Both solutions are homogeneous at room temperature. There is more PEG than dextran in PS1. When it is converted to the two-phase region through dehydration (with a fixed dextran/PEG weight ratio), the PEG-rich phase has a bigger volume than the dextran-rich phase, and vice versa in PS2 as

demonstrated in chapter 3 (see Fig. 3.1.4). A small amount of dextran-FTIC was used to label PS1 in some experiments (see chapter 5.2). The vesicles were diluted in an isotonic external solution (IS) and deflated by the addition of a hypertonic solution (HS) into the observation chamber. Their compositions are also listed in Table 2.3.2. Note that “isotonic solution” and ‘hypertonic solution’ appearing in the latter chapters always refer to the solutions with the compositions shown in Table 2.3.2.

Table 2.3.2 Polymer weight concentrations and weight ratio in the solutions enclosed into vesicles

solution	PEG	dextran	sucrose	dextran/PEG (wt/wt)
PS1	4.05%	2.22%	0	0.55
PS2	2.10%	7.44%	0	3.55
IS	4.41%	1.45%	0	0.33
HS	3.92%	2.14%	3.27%	0.55

Either PS1 or PS2 was firstly prepared at room temperature ($\sim 23^{\circ}\text{C}$) depending on the experiments which would be done. Around 100 g solutions were prepared each time. They were separated into several portions ($\sim 10\text{ml}$ each) and stored in the fridge to avoid bacteria. In several cases, the volume ratio of the PEG-rich and dextran-rich phase at 4°C was measured using 10ml volumetric cylinders. The equilibrium time is 2-4 days.

Spontaneous swelling

Certain microlitres of several lipid solutions and 100 μl chloroform were added into a 5ml round-bottomed flask which was wrapped with aluminium foil. The lipid compositions depended on the specific experiment. Chloroform was used to ensure the homogeneity of the solution. The lipid solution was dried under a gentle flow of nitrogen while rapidly rotating the flask by hand. The lipid film within the flask was desiccated under vacuum in dark for at least 4 hours to remove the remaining solvent.

The dried lipid film was prehydrated in a water bath at 40°C for 4 hours in the oven. At the same time, the polymer solution, the syringe and filters were preheated at 40°C . Then circa 10 ml preheated polymer solution were filtered with a $0.22\ \mu\text{m}$ filter and carefully added into the vial. The vial should be almost fully filled with polymer solution and well closed in order to avoid the concentration change induced by the water evaporation and condensation on the vial walls during the vesicle incubation. The vial

was sealed with parafilm and well wrapped by aluminum foil. Then it stayed in the oven at 40 °C for vesicle self-assembly for 1 – 2 days.

When enough vesicles formed, pink clouds can be observed in the solution. They were vesicle aggregates together with some lipids and/or micelles. The pink colour was due to the fluorescence labelled lipids. Then the flask was taken out of the oven. The prepared vesicles were stored at room temperature for use. The vesicles were prepared at 40 °C to ensure the homogeneity of the polymer solution.

Vesicles made of DOPS-membrane were prepared in this way and used in some of the tether formation experiments in chapter 4.

Electroformation

Lipid stock solutions were prepared by simply mixing several concentrated lipid solutions with chloroform. The lipid concentration of the stock solutions was 7.1mg/ml. The concentrated lipid solutions were diluted again with chloroform to 2 mg/ml for electroformation.

A small amount (25~30 μ l) of the lipid stock solution (2 mg/ml) was spread on glass substrates coated with indium tin oxide (ITO). The lipid films were dried in a vacuum desiccator for at least 3 hours or in a vacuum oven at 60 °C. A rectangular Teflon frame of thickness 1.6 mm served as a spacer between two opposing glass substrates. The chamber was sealed with silicon grease. The coated ITO surfaces acted as electrodes. Circa 2 ml preheated polymer solution was injected into the chamber through a 0.22 μ m filter. The chamber was placed in an oven at 60 °C afterwards an AC field of 1.5V (peak-to-peak) and 10 Hz was applied using a function generator (Agilent 33220A 20MHz function/arbitrary waveform generator). The electroformation continued for 2 or 3 hours. The chamber was taken out of the oven and cooled to room temperature (~23 °C). Then the polymer solution with vesicles was transferred into a small tube and stored at room temperature.

Note that the temperature of electroformation can be either 60 °C or room temperature according to the concentrations of the polymer solutions. The applied voltage was adjusted according to the conductivity of the ITO glass.

The vesicles were rinsed in the IS several times to get rid of the lipid aggregates and small vesicles formed during the preparation. Note that all of the polymer

concentrations were weight concentrations. This vesicle external medium had the same osmolarity as the polymer solution used for vesicle formation (internal medium), but a lower density. The osmolarity was measured with an osmometer (Gonotec Osmomat 030). To rinse the vesicles, circa 300 μl vesicle solution was diluted in about 1.5 ml IS in a 2 ml cylindrical tube. After several hours, most of the vesicles sedimented at the bottom of the tube. The upper solution (circa 1.6 ml) was carefully removed through a pipette.

Vesicles made of PEG-membrane and sugar-membrane were prepared in this way and used in most of the experiments in chapters 3 – 5.

2.4 Vesicle Observation

2.4.1 Vesicle deflation

The vesicles were firstly diluted in the isotonic aqueous solution. Phase separation of the polymer solution in vesicles was induced by deflation, namely by injecting the HS into the chamber. The latter was prepared by dissolving 0.1 mole sucrose in 1 L polymer solution containing 2.22% dextran and 4.05% PEG, namely PS1. Its osmolarity was 0.146 Osmol/kg. The deflation was done stepwise. The osmolarity of the external medium was increased 10~20% each time by the addition of small volumes of HS to the vesicle solution. The behaviour of the vesicles after deflating was observed using inverted microscopes: the Axiovert 135 microscope (Zeiss, Germany, adjusted for side-view observation) and the TCS SP5 confocal microscope (Leica, Germany).

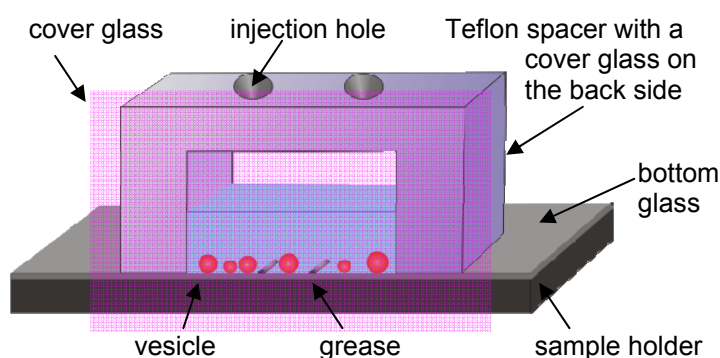


Figure 2.4.1 Schematic illustration of the chamber used for the side-view microscope filled with the external medium (blue) and vesicles (red). The vesicles are enlarged.

The Zeiss microscope was specifically adapted for side-view observation with home-made stages. The microscope is horizontally aligned. The chamber used for this microscope is shown in Fig. 2.4.1. It was assembled with high viscous grease which served as glue. The front of the chamber, where the cover glass is located, faced the

objective of the microscope. After the chamber was assembled, certain amount of the external medium (0.5 - 1 ml) was injected through one of the holes on the top of the chamber, followed by the addition of the vesicle solution, and in the end $\sim 20 \mu\text{l}$ decane. The decane, which does not mix with the aqueous solution, was added to reduce the water evaporation, although the open area was very small for this chamber. The lower diameter of the two holes is 1.5 mm. The chamber was left titled at $\sim 45^\circ$ with the front facing down for 0.5 – 1 hour. In this way, most of the vesicles settled close to the cover glass. In other words, they were located closest to the objective, which ensured the best image quality. The total number of the vesicles was crucial in these experiments. If there were too few vesicles, no ideal vesicle will be found (only $\sim 5\%$ were ideal, i.e., without internal defects, large enough ($\sim 70 \mu\text{m}$), and located close to the objective) in the chamber. If there were too many, the front part of the chamber would be full of vesicles, which led to interference, and thus, bad image quality. Even worse, one could not follow the observed vesicle or distinguished it from other vesicles after the injection of HS.

The injection of HS introduces strong convections in the chamber. The vesicles could abruptly displace and float around in the chamber. This makes it difficult to follow the same vesicle. One easy and effective way to reduce the vesicle movement is to put a short thread(s) (1-2mm) of grease on the bottom glass, as indicated in Fig. 2.4.1. The HS is injected through the hole further away from the observed vesicles. Another issue one should pay attention is the smoothness of the bottom glass edge facing the front cover glass. There is always a tiny slot formed between the cover glass and the bottom glass. The moving vesicles can fall into it to ruin the experiment. The solution of this problem is to make the slot as thin as possible by carefully choosing the bottom glass. The edge facing the cover glass should be straight, and as smooth as possible.

The chamber used for the confocal microscope is shown in Fig. 2.4.2. The chamber assembling and the experimental procedures are similar with the ones for the side-view microscope. One difference is that the chamber had to be removed from the microscope stage when HS is injected. In order to find the same vesicle, the surface of the cover glass was separated into ~ 10 small parts with grease. The height of the grease threads is $\sim 0.5 \text{ mm}$. These barriers helps making the vesicle of interest in confinement.

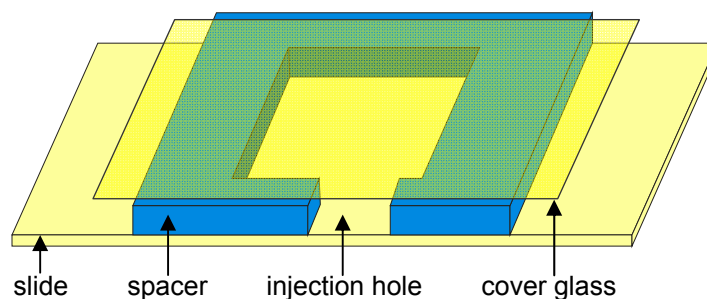


Figure 2.4.2 Schematic illustration of the chamber used for confocal microscope.

The vesicles were imaged under different conditions using the optical microscopes. The techniques for imaging the vesicles were phase contrast, differential interference contrast (DIC), fluorescence, as well as confocal microscopy.

2.4.2 Optical microscopy

The application of optical microscopy has witnessed an enormous growth during the past decades in a wide variety of disciplines. The advanced contrast enhancing techniques make it possible to observe the details of unstained specimens which do not absorb the light. The rapid development of fluorescent labels has accelerated the expansion of fluorescence microscopy in laboratory applications and studies. Confocal optical systems make it possible to image very thin sections of the subject at different depth. All of these developments result in a burst in the number of applications of optical microscopy in life sciences. Optical microscope is ideal for imaging cells, which are usually in the micrometer scale. Furthermore, living cells can be even imaged in their natural environment.

Phase contrast and differential interference contrast microscopy

Unstained specimens that do not absorb light are called phase objects. They slightly alter the phase of the light diffracted by the specimen, usually by retarding such light approximately $1/4$ wavelength. However, the direct light passes through or around the specimen undeviated. The diffracted light is slowed down by the specimen because of the specimen's refractive index or/and thickness. It arrives at the image plane out of phase and interferes with the undeviated light. The interference does not change the intensity significantly to be distinguishable by eye.

Phase contrast microscopy, which was invented by the Dutch physicist F. Zernike, makes phase objects yield contrast images as if they were amplitude objects, which show

excellent contrast when the diffracted and direct light are out of phase by $1/2$ wavelength. Zernike's method consists of speeding up the undeviated light by $1/4$ wavelength so that the difference in wavelength between the deviated and undeviated light would now be $1/2$ wavelength. The two are able to produce destructive interference at the image level of the eyepiece. The basic phase contrast microscope configuration is schematically illustrated in the left cartoon of Fig. 2.4.3.

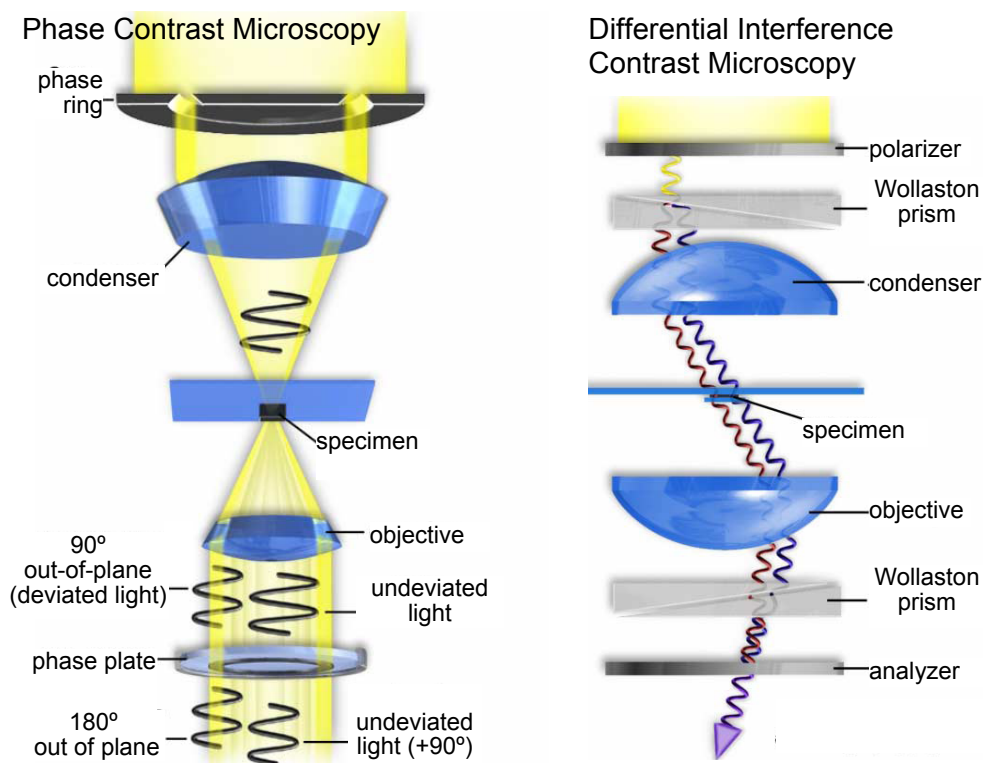


Figure 2.4.3 Schematic configurations of phase contrast microscopy (left) and differential interference contrast microscopy (right) in an inverted microscope. [Davidson]

Phase contrast involves the separation of the undeviated light from the diffracted light at the rear focal plane of the objective. To do this, a phase ring is placed above the lower lens of the condenser (for inverted microscopes). Light passing through the phase ring is first concentrated onto the specimen by the condenser. The hollow cone of light passes through the specimen undeviated, it enters the objective in the shape of a ring and is advanced $1/4$ wavelength by a ring shaped phase shifter attached to the phase plate at the rear focal plane of the objective. The weaker light diffracted by the specimen spread over the rear focal plane of the objective. When the direct undeviated light and the diffracted light proceed to the image plane, they are $1/2$ wavelength out of phase with each other. The diffracted and direct light can now interfere destructively so that the details of the specimen appear dark against a lighter background. This is called dark or

positive phase contrast. If the phase shifter ring is made thicker than the rest of the phase plate, the undeviated light may be slowed down by $1/4$ wavelength. In this case, the image of the specimen appears brighter on a darker background. This type is called bright or negative phase contrast.

Another very often encountered contrast enhancing technique is DIC. DIC improves the detecting of the optical gradients in specimens and converts them into intensity difference. In transmitted light DIC, light from the lamp is passed through a polarizer located above the substage condenser (for inverted microscopes), see the right cartoon in Fig. 2.4.3. The polarized light is split into two rays vibrating perpendicular to each other by a modified Wollaston prism. They travel together but in slightly different directions. The rays intersect at the front focal plane of the condenser. The split beams enter and pass through the specimen where their wave paths are altered in accordance with the specimen's varying thickness, slopes, and refractive indices. When the parallel beams enter the objective, they are focused above the rear focal plane where they enter a second modified Wollaston prism that combines them. The combined light passes another polarizer (the analyzer), where it interferes both constructively and destructively. The light then proceeds toward the eyepiece where it can be observed as differences in intensity and colour. One side of the specimen appears bright (or possibly in colour) while the other side appears darker (or another color). This shadow effect leads to a pseudo three-dimensional appearance to the specimen.

Fluorescence and confocal microscopy

Fluorescent molecules absorb light with certain wavelengths and emit light with longer wavelengths. The specimen may fluoresce either in its natural form or by treated with chemicals capable of fluorescing. Taking the advantage of rapidly developed fluorescent dyes, fluorescence microscopy becomes one of the fastest growing areas of investigation using microscopes. It is an excellent tool for studying samples due to the high sensitivity, selectivity and versatility of the fluorescence. The configuration of a fluorescence microscope is schematically illustrated in Fig. 2.4.4. Light emitted from a mercury lamp is concentrated by the collector lens, then directed to pass through the aperture and field diaphragms and arrives at the exciter filter. Only the desired excitation wavelengths are allowed to pass through the exciter filter. The passed light is reflected down through the objective to illuminate the specimen by the dichroic mirror. The

dichroic mirror is a mirror, which transmits one wavelength and reflects another wavelength. The fluorescence emitted by the specimen passes back through the objective and dichroic mirror then finally being filtered by the emission filter which only allows the passing of desired wavelength.

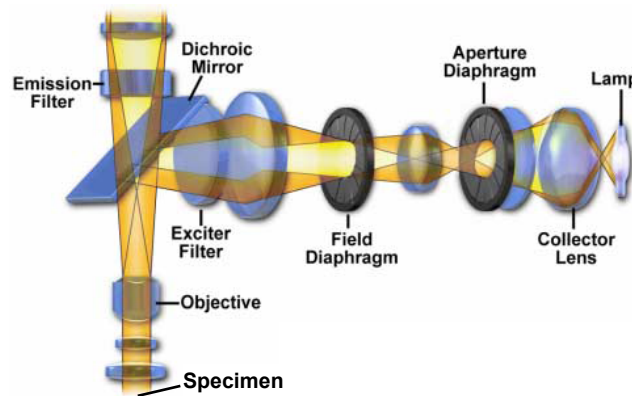


Figure 2.4.4 Schematic configuration of fluorescence microscopy. [Davidson].

A recent development of the optical microscope is the confocal microscope. "Confocal" is defined as "having the same focus". The great idea of a confocal microscope is to illuminate and image a sample just one spot at a time. The resulting image is then a slice of the specimen. Using the stacks of slices at different depths, it is possible to build a 3D image of the specimen. But the 3D image is distorted in the z direction due to spherical aberration arising from the different refractive index of the specimen, the medium and the cover slide.

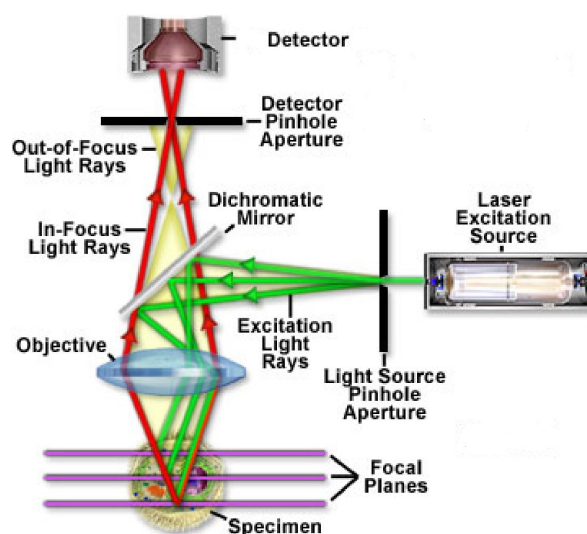


Figure 2.4.5 Schematic configuration of a simple confocal microscope setup. (From <http://www.microscopyu.com>)

When an object is imaged in the normal fluorescence microscope, the signal produced is normally from the full thickness of the specimen. The confocal microscope eliminates this out-of-focus information by means of a confocal "pinhole" situated in front of the image plane which acts as a spatial filter and allows only the in-focus portion of the light to pass through. Light from above and below the focal plane of the specimen is largely blocked by the pinhole. The confocal principle is illustrated in Fig. 2.4.5.

Similar to normal fluorescence microscopy, the light coming from the laser passes a pinhole and is reflected by a dichroic mirror and focused by a microscope objective to a small spot on the sample. When the sample is excited, it starts to emit light in a random direction. A fraction of the emitted photons is collected by the microscope objective. The collected light passes through a pinhole and images onto the detector. The pinhole only allows the fluorescence generated on the focal plane passing through. The position of this pinhole is such that it is in a plane conjugate with both the plane of focus of the microscope objective and the point of the excitation of the laser, which is defined by the excitation pinhole. The size of the pinhole, of course, determines how much background reduction can be realized.

2.5 Micropipette Manipulation

Micropipette aspiration was used to pressurize vesicles, and thus manipulate the mechanical tension on the membrane of the pre-deflated vesicles. The newly formed vesicles were diluted in the IS. The osmolarity of the external medium was increased stepwise by mixing with the HS (hypertonic solution). The increment of the osmolarity was about 6.5% for each step, and the time interval between consecutive concentration steps is at least 15 minutes in order to avoid vesicle budding during deflation. If the osmolarity change was too small, it took lots of time to prepare the sample. The system was left at room temperature over night to equilibrate. Afterwards, the vesicles were carefully transferred into the microscope chamber together with the external solution where they were deflated.

The system setup is schematically illustrated in Fig. 2.5.1 for horizontally aligned microscope. The opening was covered by high viscous grease to stop the evaporation of water. High viscous grease was used here because it is viscous enough to stay where it is placed, but at the same time, the micropipette can move freely through it. The micropipette was pre-covered with the same lipids as the vesicles to eliminate adhesion

of the membrane to the inner wall of the glass pipette. This was done by simply breaking some vesicles and sucking them into the pipette. The micropipette was prefilled with the same external solution as the solution in the chamber to eliminate the osmotic pressure difference of the solutions in and out of the micropipette.

The images taken by the camera are actually the projection of the vesicle and the micropipette tip on the focal plane, which is indicated by the dashed blue line in Fig. 2.5.1. The micropipette has to be exactly parallel to the focal plane in order to have both the micropipette and the vesicle on focus simultaneously. This is very important for the calculation of the membrane area expansion, as well as the vesicle volume. The diameter of the micropipette is not uniform, with the upper diameter equal to 1 mm, and the lower diameter 20-50 μm , as schematically illustrated in Fig. 2.5.1. In order to bring the vesicle close enough to the objective to have good image quality and to have the micropipette parallel to the focal plane at the same time, the cover glass was set to have a small angle to the focal plane, as indicated in Fig. 2.5.1.

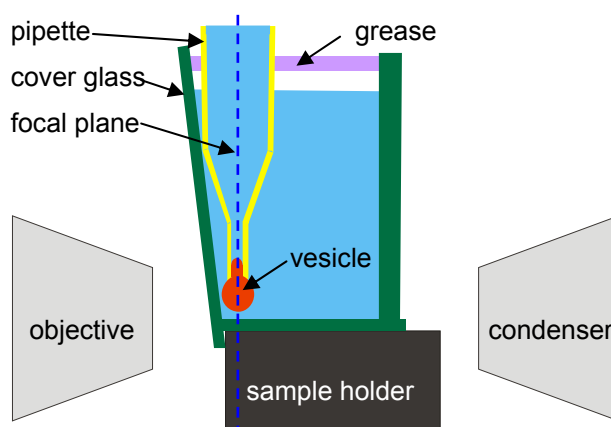


Figure 2.5.1 The vertical cross section of the micropipette system setup.

The upper outlet of the micropipette was connected to a water reservoir, which was located on a vertically placed position stage (Physik Instrumente, Germany). The aspirating pressure was controlled through moving the water reservoir upwards or downwards. The aspirating pressure P , namely the pressure difference between the internal and the external solutions at the plane of the micropipette entrance, was calculated through the equation below:

$$P = \rho_w g(h - h_0) \quad (2.5.1)$$

where ρ_w is the density of water, g (9.80665 m/s^2) is the gravitational acceleration, h is the position of the water reservoir, and h_0 is the initial position where the pressure

difference is zero. h_0 was predetermined slightly above the vesicle by observing the movement of a small vesicle or dirt close to the entrance (in the pipette). When it did not move for ~ 10 minutes, the corresponding position of the reservoir was considered as h_0 . Afterwards, one should not change the pipette location, as well as the stage of the microscope. In case anything had to be adjusted, h_0 had to be determined again.

After applying a pressure on the vesicle, it was aspirated into the micropipette as shown in Fig. 2.5.1. The aspirating pressure applied to a fluid membrane produces a uniform membrane tension σ_e over the entire surface (except in the sharp bend at the pipette entrance) at mechanical equilibrium [Kwok 1981, Evans 1990]. The tension is simply proportional to the suction pressure:

$$\sigma_e = \frac{PR_m}{2(1 - R_m/R_v)} \quad (2.5.2)$$

Where R_v and R_m is the radius of the vesicle and micropipette at the entrance, respectively.

The fluorescent and phase contrast images of the vesicle were taken under different pressures. In all cases, the vesicle adopted an axisymmetric shape. This shape is a combination of spherical caps plus the cylindrical part inside the pipette. To measure the apparent area of the vesicle, the vesicle volume and the contact angles of the phases under different pressures, we superimpose circles and straight lines on top of the digitized images. To ease this procedure and enhance accuracy, Rubèn Serral Gracià developed a software that computes the intersections between the user given circles and lines. The program uses libtiff to read the images (<http://www.libtiff.org>), and Qt4 to display and treat them (<http://trolltech.com>). The rest is done in C++ and compiled with GNU tools for either windows (using mingw: <http://www.mingw.org/>) or linux.

Chapter 3

Phase Behaviour of Polymer Solutions

3.1 Characterization of PEG and dextran aqueous solution in bulk

There are an abundant number of studies on the phase behaviour of PEG and dextran aqueous solutions [Croll 2003, Edelman 2003]. Although both polymers are water soluble, PEG is more hydrophobic compared to dextran. Their aqueous solution undergoes phase separation when the weight concentration is above several percent. It separates into a PEG-rich phase and a dextran-rich phase. The interfacial tension of the coexisting phases is extremely low. Different techniques were developed to measure it [Ryden 1971, Schürch 1981, Boyce 1984]. Both the phase behaviour and the interfacial tension depend on the molecular weights and their distribution. [Diamond 1989, Forciniti 1990] They have to be determined routinely in the lab.

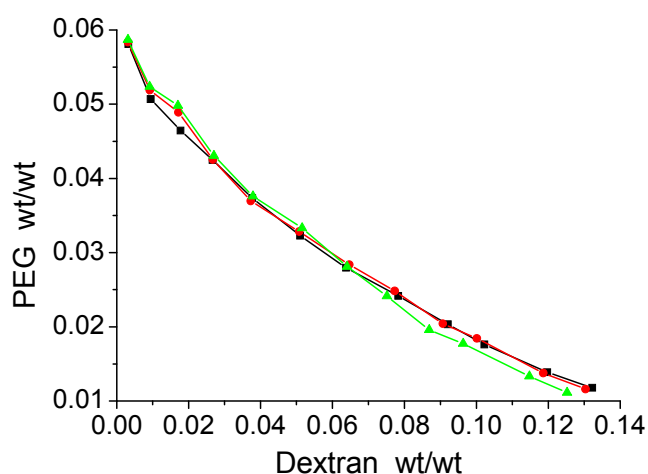


Figure 3.1.1 Binodals of dextran (500 kg/mol) and PEG (8 kg/mol) aqueous solution at 23 °C (black squares), 40 °C (red dots) and 60 °C (green triangles). The lines just guide the eyes.

It is important to know the binodal, which is the boundary between the one-phase region and the two-phase region, in order to investigate the phase separation in giant vesicles. The binodal of PEG and dextran aqueous solution was determined using cloud-point titration. This kind of binodal is also called cloud-point curve. The results are shown in Fig. 3.1.1. When the polymer solution is located below the binodal for the specific temperature, it is in the one-phase region. The solution is stable and homogeneous. When the solution is located above the binodal, it is in the unstable region.

It will spontaneously separate into two phases. The binodal is a function of temperature. The binodals determined at different temperatures are very close to each other as shown in Fig. 3.1.1. They intersect at the point with dextran concentration ~ 0.062 . It implies that the solutions may have both low critical solution temperature (LCST) and upper critical solution temperature (UCST). It has LCST with dextran concentration less than 0.062. It has UCST with dextran concentration more than 0.062. When the solution moves across the binodal either by changing the temperature or the concentration, phase transition will occur. Temperature dependent phase transition is easy to control in the experiment, but it has much less versatility than the concentration dependent phase transition, especially in giant vesicles. For example, the temperature range is limited by the property of the solvent.

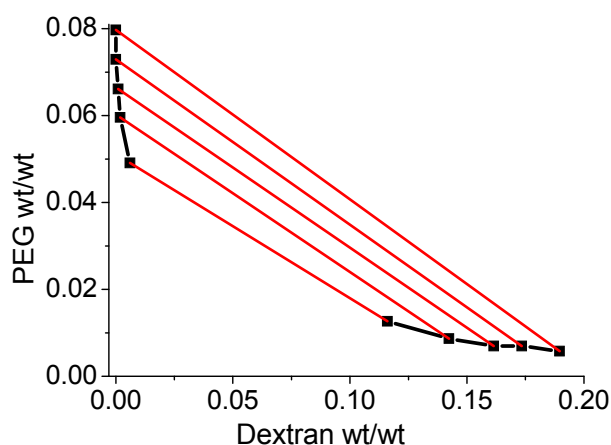


Figure 3.1.2 Coexistence curve and tie lines of dextran (500 kg/mol) and PEG (8 kg/mol) aqueous solution at 23 °C. The black squares present two branches of the coexistence phases. The black lines just guide the eyes. The red lines are the tie lines.

The thermodynamic properties of the coexisting phases, e.g. density and interfacial tension, depend on the concentrations of the two coexisting phases. At a specific temperature, no matter what the overall polymer concentration is, the composition of each coexisting phase is always the same if the systems are located on the same tie line. It is necessary to know the coexistence curve to have a better understanding of the experimental results. However, the cloud-point curve only presents the temperature-concentration pairs at which phase separation sets in. It does not give information about the tie lines. To know this, the concentrations of the coexisting phases have to be analyzed. One of the methods to measure the polymer concentrations is gel permeation chromatography (GPC). The binodal constructed in this way is called coexistence curve. Figure 3.1.2 shows the coexistence curve of the polymer solution at

23 °C together with the tie lines. When the volume of one phase becomes very small, it is difficult to measure its compositions, even difficult to separate it from the bulk phase. Therefore, Fig. 3.1.2 only shows two branches of the coexistence curve. The binodal between the branches can be determined through cloud-point titration, see Fig. 3.1.1.

As the name indicates, there is more PEG than dextran in the PEG-rich phase. The PEG concentration increases in the PEG-rich phase as the overall concentration increases, and so does the dextran concentration in the dextran-rich phase. The concentration difference between the coexisting phases is related to the length of the tie line. In the PEG-rich phase, the dextran concentration is very low, even no dextran molecules are detected by GPC in the PEG-rich phases (> 0.07 wt/wt PEG) formed from very concentrated solutions. In contrast, there is about 1% PEG in the dextran-rich phases in all measured solutions; see Fig. 3.1.2.

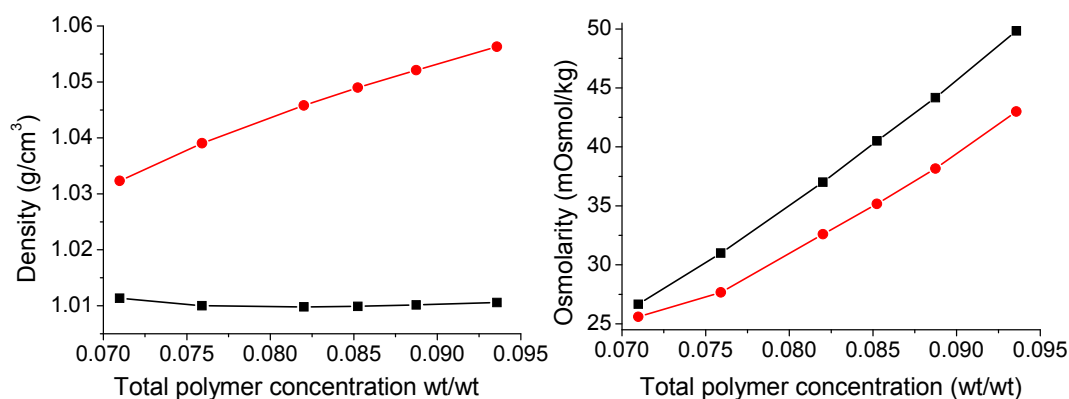


Figure 3.1.3 The density (left) and the osmolarity (right) at 24.2 °C of the coexisting phases at different overall concentrations. The dextran/PEG weight ratio was fixed to 0.55 in all cases. The red dots present the dextran-rich phase and the black squares present the PEG-rich phase in both graphs. The phase separation was carried out at 24.2 °C. The lines guide the eyes.

There is always a top phase and a bottom phase in bulk phase separated solutions due to their density difference, which arises from the concentration difference. In the PEG and dextran aqueous system, the PEG-rich phase is the top phase. The densities of the coexisting phases are shown in Fig. 3.1.3 left. The density of the dextran-rich phase increases with increasing total concentration. However, the density of the PEG-rich changes insignificantly with concentration. Their difference increases with increasing concentration. The concentration difference also leads to osmolarity difference of the coexisting phases; see Fig. 3.1.3 right. The osmolarities of the coexisting phases increase with the total concentration, as well as the difference between them. Note that the osmolarity of the PEG-rich phase is always higher than that of the dextran-rich phase due

to the smaller molecular weight of PEG molecules although it has a lower density and lower weight concentration.

Another important characteristic is the volume ratio of the coexisting phases. It is a function of the concentration and the dextran/PEG weight ratio at a constant temperature. This characteristic is very important because it is the only one which can be directly compared between the bulk solution and the solution enclosed in giant vesicles and, thus, used to estimate the concentration of the encapsulated polymers. Figure 3.1.4 shows the volume fraction of the dextran-rich phase. There is always a smaller dextran-rich phase in the solutions with dextran/PEG weight ratio equal to 0.55. In the rest of the cases, the volume fraction of the dextran-rich phase increases with decreasing concentration.

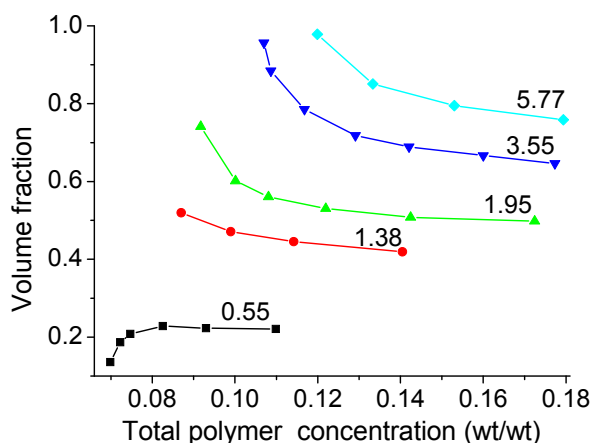


Figure 3.1.4 Volume fraction of the dextran-rich phase at different total polymer concentrations at 23 °C. The numbers are the weight ratios of the dextran and PEG. The lines just guide the eyes.

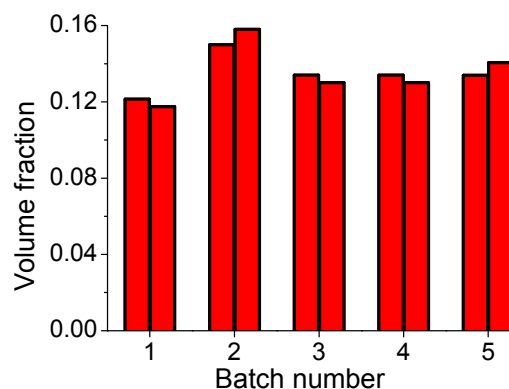


Figure 3.1.5 Volume fraction of the dextran-rich phase in bulk polymer solution at 4 °C. The total polymer concentration is 0.0625 with dextran/PEG weight ratio equal to 0.55. The paired columns present two parallel measurements for each batch.

The heterogeneity of the volume fraction of the dextran-rich phase in giant vesicles was addressed in the literature [Long 2005]. This heterogeneity does not only exist in the solution enclosed in vesicles, but also in bulk solution; see Fig. 3.1.5. The stock solutions were prepared at room temperature (~ 23 °C). The cloud-point at this temperature is 0.0669, which indicates that the solution is homogeneous. However, the volume fraction of dextran-rich phase is not constant, even in the solutions from the same stock solution; see the paired columns in Fig. 3.1.5. It varies between 0.117 and 0.158. The difference of the volume fraction in the same batch is smaller than the difference among batches. The variations of the volume fractions imply the heterogeneity of the stock solution at room temperature. The reason is not clear.

3.2 Phase separation of polymer solution in giant vesicles

Phase separation takes place when a system is brought into the two-phase region. The study of the dynamics of the polymer solutions follows a long tradition and remains of fundamental importance. Most of the experiment involves a “homogeneous” quench, often of temperature. Little scientific attention was paid on solvent quench, which is inhomogeneous and results in concentration variations of the solvent and polymers [Hopkinson 2002]. Recently, the coarsening of a colloidal-polymer solution was investigated using horizontally aligned confocal microscope in real space and thermal capillary waves were observed during coalescence of colloid liquid droplets with the bulk liquid phase [Aaarts 2004, 2005].

Depending on the initial instability, the phase separation may occur through “nucleation and growth” or “spinodal decomposition”. When the system slowly enters the two-phase region through the binodal or the critical point, the phase separation often occurs through nucleation. Nucleation is the onset of the phase separation. It normally occurs at nucleation sites. The creation of the nucleus implies the formation of an interface at the boundaries of the new phase. If the nucleus is too small, the energy released by forming its volume is too small to compensate the energy consumed by forming the interface. The nucleation does not proceed spontaneously. The growth of the new phase is limited by the nucleation. When the nucleus is big enough, the addition of new molecules to the new phase will release energy. The phase separation occurs spontaneously. The growth of the new phase is not limited by the nucleation any more, but by, for instance, diffusion.

When the phase separation is delayed until the system enters the two-phase region, a small perturbation in composition leads to a decrease in energy and thus spontaneous growth of the perturbation. The phase separation through unstable growth is known as spinodal decomposition. Different from the nucleation, the spinodal decomposition occurs everywhere in the system. To observe spinodal decomposition, the system has to be quenched from the stable region to the unstable region. The quench can be either a fast change of temperature or concentration. The spinodal decomposition may be governed by Cahn-Hilliard equation.

In this section, we report the dynamics of phase separation taking place in the giant vesicles containing polymer aqueous solution. This system is more complicated

than the bulk system because the interactions between the membrane and the phases may affect the dynamics.

Dynamics of phase separation in giant vesicles

According to the phase diagram of the dextran and PEG aqueous solution (see Fig. 3.1.1), the phase separation in a vesicle can be induced by dehydration, namely by increasing the polymer concentration inside the vesicle. The polymer concentration inside the vesicles can be adjusted through the osmolarity of the external medium because the lipid membrane is only permeable to water but not to polymers. Water molecules diffuse across the membrane under osmotic stress in order to keep the osmotic pressure balance.

The phase separation process in the polymer solution encapsulated in vesicles is observed with microscopy during vesicle deflation. The vesicles are firstly diluted in the IS (see Table 2.3.2) in a specimen chamber; Fig. 2.4.1. Then the medium's osmolarity is increased by injecting a certain volume of the HS (see Table 2.3.2) into the chamber. In order to keep the osmolarity balance, water molecules diffuse out of the vesicle, which results in the increment of the polymer concentrations. In this way, the polymer solution is quenched from the stable one-phase region to the unstable two-phase region. The quenching velocity depends on the diffusion of the water molecules and the osmotic pressure gradient across the membrane. Figure 3.2.1 shows the time evolution of one giant vesicle after the injection of the HS.

The vesicle initially enclosed the homogeneous PS1 as shown in Fig. 3.2.1A. It was sitting on the surface of the bottom glass of the chamber (the black region in Fig. 3.2.1A). When the HS was carefully injected into the chamber, a flow was created. This flow made the vesicle suddenly displace and move further away from the injection place. The bottom glass could not be captured in the images until at time 13.3 min after the injection; see the corresponding images in Fig. 3.2.1.

The created flow changes the local refractive index gradually. It could be observed with the digital camera about 30 seconds after initiating the injection. Shortly after that, the vesicle started to move away from the place of injection. It implied that the vesicle sensed the osmotic stress soon after the injection. Due to the loss of water, the vesicle became smaller and the polymer concentration increased. Once the concentration

crossed the binodal, phase separation occurred. At time 1.45 min, the solution became turbid which indicated the starting of the phase separation; Fig. 3.2.1B.

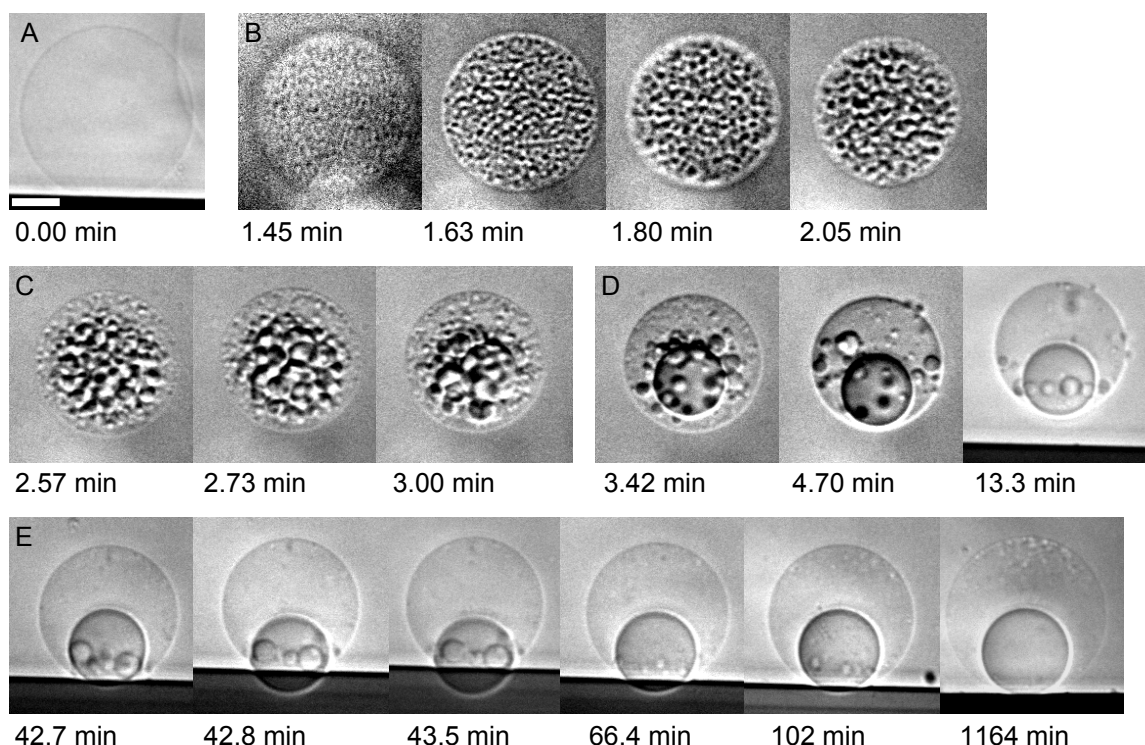


Figure 3.2.1 DIC images of the phase separating process induced by dehydration. These images present the side view observation of a vesicle sitting or close to the chamber bottom. The minutes below each frame indicate the time after the HS was injected. (A): The vesicle before the deflation; (B): Coarsening of the new phase; (C): Gravity-driven growing; (D): Formation of mesoscopic interface; (E): Vesicle inflation process with a partial budding event. In (B)-(E), the dense part(s) is the dextran-rich phase and the light part is the PEG-rich phase. The dark zone at the lower part of some of the images is a shadow from the glass which is not exactly parallel to the direction of observation. The osmolarity of the external medium was increased 24%. The vesicle made of PEG-membrane was prepared in PS1. The scale bar is 20 μm .

The whole interior of the vesicle was turbid, which meant the phase separation occurred homogeneously in the polymer solution. Both phases were continuous. The detailed structure is shown in Fig. 3.2.2. The bicontinuous structure indicated that the system separated through spinodal decomposition. Sharp interfaces formed around the new dextran-rich phase. Many tiny dextran-rich droplets appeared in the vesicle interior. They interconnected with each other to form a spinodal network. The network was coarsening with time. The coarsening took place through the coalescence of the tiny droplets, driven by the release of surface energy. The interfacial area decreased by the fusion of the droplets. The coarsening velocity was determined by the diffusion of the polymer molecules in this stage. The coarsening was a fast process. It finished within one

minute. Gravity did not play a roll in this stage due to the small size of the droplets. The dextran-rich phase was homogeneously distributed in the interior of the vesicle.

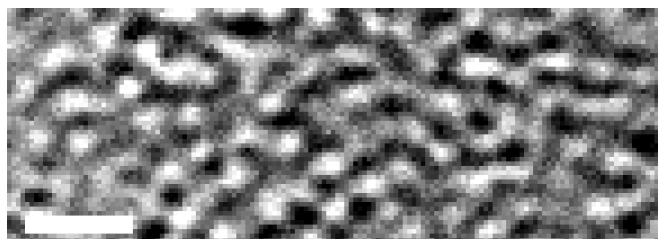


Figure 3.2.2 The bicontinuous structure in the phase separating solution in the vesicle interior. This is an enlarged section of the image at time 1.63 min in Fig. 3.2.1. The black holes present the dextran-rich phase. The scale bar is 10 μm .

As the size of the dextran-rich droplets increased, the phase separation process became gravity-driven. The density difference between the two phases led to the directional flow of the spinodal network (formed in the first stage) towards the bottom of the vesicle. It accelerated the growing of the new phase. At the same time, the membrane expelled the dextran-rich phase into the centre of the vesicle due to their higher interaction. This gravity-driven stage is shown in Fig. 3.2.1C. The dextran-rich phase accumulated in the lower centre part of the vesicle. Only some very small droplets could be seen in the upper part and in the vicinity of the membrane. The dextran-rich droplets were growing by fusing with each other during the sedimentation. The bicontinuous network was destroyed. The dextran-rich phase existed as individual droplets. The gravity-modulated stage was also a fast process. It lasted less than one minute.

The last stage of the phase separation process was the formation of the mesoscopic interface. At the end of the gravity-driven flow, the dextran-rich droplets coalesced into a big droplet with other small droplets around it. A clear mesoscopic interface formed; see Fig. 3.2.1D. The big droplet sedimented towards the bottom of the vesicle, as well as other small ones. They fused into one big droplet in the end. This droplet was surrounded by the PEG-rich phase. There was only one interface between the coexisting phases. It took hours to let all droplets to fuse into one.

By carefully observing the vesicle images in Fig. 3.2.1, one can find that the vesicle volume did not keep constant all the time. There were two regimes in the vesicle deflation process according to the size evolution. In the first regime, the volume of the vesicle became smaller with time, i.e. a deflation regime. This was corresponding to the time range from 0.0 min to 4.70 min in Fig. 3.2.1. This process was easy to be

understood. When the vesicle was under osmotic stress, there was a net water flux out of the vesicle. The loss of water resulted in a smaller volume. It took some time for the vesicle to reach the osmotic balance. Interestingly, the vesicle became bigger with increasing time after the vesicle size reached the minimum. This second regime is thus an inflation regime. It corresponded to the time range from 13.3 min to the end of the experiment; see Fig. 3.2.1E. One has to consider the detailed deflation process in order to understand the existence of the inflation regime.

After the HS was injected into the chamber from the top, a flow was created towards the bottom of the chamber. This convection could be directly seen. Because the HS had a relative higher density than the external medium, it crept towards the chamber bottom due to gravity. It reached the vesicle before the solution in the chamber became homogeneously mixed by diffusion. This resulted in overshooting in the osmolarity (higher than the average osmolarity in the chamber but lower than the osmolarity of the HS) in the vicinity of the vesicle, namely at the bottom of the chamber. The response to the high local osmolarity led to fast dehydration. After the local osmolarity became the same as the rest part of the solution, the vesicle had been over-deflated. Since then, deflation changed to inflation, which resulted in the increasing of the vesicle size. Accompanying the vesicle swelling, membrane tension could be built up in the inflation regime. The chamber equilibration needed up to a few hours to reach completion. The inflation regime is a kinetic one, and is affected by the osmolarity of the HS, the injection volume, and the distance between the observed vesicle and the place of the injection.

One interesting phenomenon was observed in the vesicle inflation regime. The big dextran-rich droplet protruded out of the body of the vesicle suggesting wetting of the membrane. This occurred at time 42.8 min; see Fig. 3.2.1E. The protrusion is a fast event. It reached its maximum within 2 minutes, namely at time 43.5 min. This protrusion indicated a quick increment of the membrane area. A possible explanation was temporal local concentration gradient or the fusion of a small budded vesicle with the big one. The small vesicle might form during the phase separation process, but it was difficult to be observed. As the vesicle became bigger and bigger with time, the increased membrane tension forced the protruded dextran-rich phase back into the vesicle body to have a spherical shape vesicle; see the image at 102 min in Fig. 3.2.1. This process lasted for about 50 minutes.

Effect of polymer composition

The polymer composition, here mainly referring to the dextran/PEG weight ratio, may affect the phase separation process. There is more PEG than dextran in PS1. This results in a big PEG-rich phase in the deflated vesicle. The small dextran-rich phase arose from the bulk PEG-rich solution during phase separation. When the polymer solution has more dextran than PEG, e.g. PS2, the small PEG-rich phase will appear in the big dextran-rich solution. It may lead to a different phase separation process. Fig. 3.2.3 shows one example.

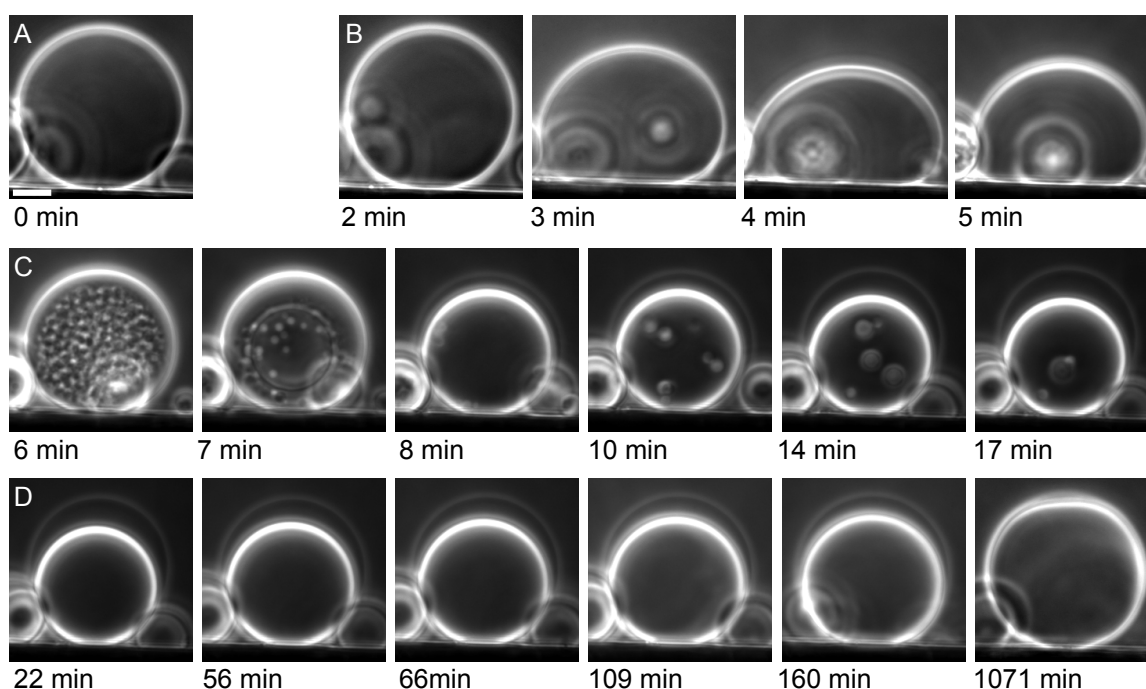


Figure 3.2.3 The effect of the polymer composition on the phase separating process induced by dehydration. These phase contrast images present the side view observation of a vesicle sitting on the chamber bottom. The minutes below each frame indicate the time after the HS was injected. (A): The vesicle before the deflation; (B): Sessile-shaped vesicle; (C): The phase separation process; (D): Vesicle inflation. In (C)-(D), the dense part is the dextran-rich phase and the light part(s) is the PEG-rich phase. The osmolarity of the external medium was increased 28%. The vesicle was made of PEG-membrane and prepared in PS2. The scale bar is 20 μm .

The vesicle was prepared in PS2 and diluted in the IS. Initially there is only one phase in the enclosed polymer solution, and the vesicle was spherical; see Fig. 3.2.3A. After the injection of the HS, the vesicle shape changed from spherical to sessile-shaped, but the enclosed solution was still homogeneous; see Fig. 3.2.3B. The osmotic deflation led to a smaller vesicle volume, higher density difference, and more excess area if the membrane area remained constant. The gravity, arising from the density difference, tend to pull the solution in the vesicle towards the bottom of the chamber. Meanwhile, the

membrane tension tends to keep the vesicle spherical. The balance of the two forces leads to the sessile-shaped vesicle when the membrane tension could not overcome the gravity. As time went on, the vesicle became flatter and flatter. After 5 min, the vesicle began to become more spherical, which indicated the increasing of the membrane tension. The sessile-shaped vesicle was not observed during the phase separating process in the vesicles enclosing PS1. This might be due to the smaller density difference between PS1 and the external medium.

Phase separation was observed in the vesicle after 6 min; see Fig. 3.2.3C. At the same time, the vesicle became spherical again, which indicated an increase in the membrane tension. The latter was high enough to overcome gravity and dominate the vesicle shape. In addition, the vesicle apparent area decreased. The excess membrane area formed many tethers, which led to the increase of the membrane tension. The formation of the tubular structure and the phase separation occurred simultaneously. The details about the tubular membrane structure are going to be discussed in chapter 4.

The dynamics of the phase separation was similar to the one introduced before. The formation of the bicontinuous structure indicated that the solution separated through spinodal decomposition. The PEG-rich droplets grew with time. They coalesced with each other and formed a big droplet in the middle of the vesicle. The big PEG-rich phase moved upward due to its smaller density, spreading along the membrane and enclosing the big dextran-rich phase; see the third image in Fig. 3.2.3C. The spreading of the small PEG-rich phase is due to the lower interaction between the membrane and the PEG-rich phase. At this moment, there were still several small PEG-rich droplets in the dextran-rich phase. They grew bigger, moved upwards and fused with the big PEG-rich phase with time. After 22 min, there was only one PEG-rich phase in the vesicle. The formation of mesoscopic interface took much less time than in the case of PS1 because the contact area between the two phases was bigger in the vesicle formed in PS2 than the one formed in PS1. The images showed that the vesicle was slightly elongated at time equal to 17 min and 22 min. This might be due to buoyancy because the PEG-rich phase had a lower density than the external medium.

The vesicle was deflated at first, and then inflated similarly to the vesicle enclosing PS1. In the deflation regime, the volume fraction of the PEG-rich phase increased with time. After it reached the maximum, which is also the minimum of the

vesicle volume, the volume fraction of the dextran-rich phase began to increase with time, as well as the vesicle volume; see Fig. 3.2.3D. In the end, there was only an extremely small PEG-rich phase left, and the interface was slightly bended (kinks located on the top of the dextran-rich phase); see the last image in Fig. 3.2.3.

Effect of membrane composition

The interactions between the membrane and the coexisting phases are different due to the different polymer concentration in the two phases. These interactions played an important role on the final morphology of the two phases. The PEG-rich phase prefers to be in contact with the PEG-membrane as shown in the foregoing experiments. We cannot conclude that lipid sorting has occurred in the membrane, whereby PEG-lipids redistribute so that they are preferably in contact with the PEG-rich phase. This might be energetically unfavourable as this would lead to making a denser polymer brush. Instead of forming an upper and lower phase as in bulk, the dextran-rich droplet, no matter big or small, was always surrounded by the PEG-rich phase. In this way, the contact area between the membrane and the dextran-rich phase is minimized. The interactions may also influence the dynamics of the phase separation. They can be adjusted through the lipids composition. Figure 3.2.4 shows the phase separation of PS2 loaded in a vesicle made of sugar-membrane.

As the foregoing vesicles, the phase separation process was started with a spherical vesicle loaded with homogeneous PS2; see Fig. 3.2.4A. After the injection of the HS, the vesicle became smaller and sessile-shaped as in the deflated vesicle with PEG-membrane; see Fig. 3.2.4B. As the phase separation started, the vesicle became spherical again; see Fig. 3.2.4C. The PEG-rich phase started forming in the middle of the vesicle, but not in the whole interior. This suggested that the phase separation occurred through nucleation. That is because the polymer concentration increased slowly due to the small increment (17%) of the osmolarity in the external medium. With time, more and more PEG-rich droplets appeared and grew through coalescence. This process is relatively slow compared to the coarsening in spinodal decomposition. It took several minutes.

The PEG-rich droplets located in the vicinity of the membrane protruded out of the big dextran-rich phase and wetted the membrane. Small PEG-rich buds formed. These buds resulted in deflections in the surface of the dextran-rich phase. After 12.7 min, small kinks could already be observed; see Fig. 3.2.4C.

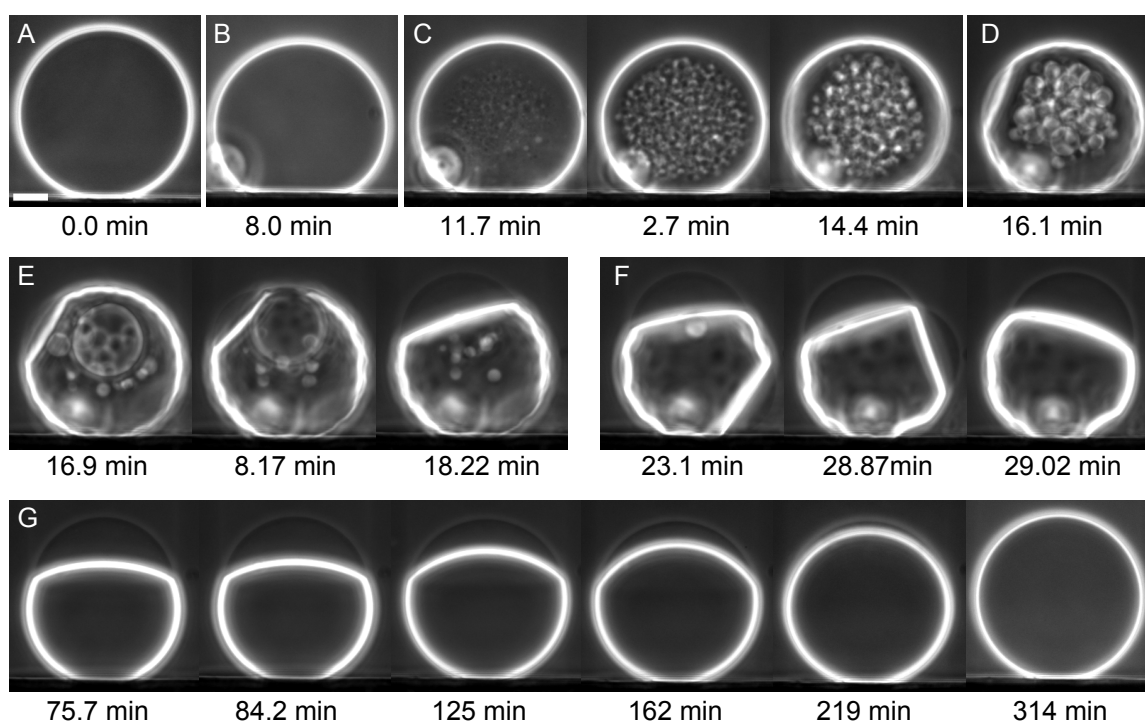


Figure 3.2.4 The effect of membrane composition on the phase separating process induced by dehydration. These phase contrast images present the side view observation of a vesicle sitting on the chamber bottom. The minutes below each frame indicate the time after the HS was injected into the observation chamber. (A): The vesicle before deflation; (B): The sessile-shaped vesicle; (C): Nucleation and growth; (D): Kinks on the surface of the dextran-rich phase; (E): The fusion of a bud with a big droplet; (F): The fusion of two buds; (G): Vesicle inflation. In (C)-(G), the dense part is the dextran-rich phase and the light part(s) is the PEG-rich phase. The osmolarity of the external medium was increased 17%. The vesicle made of sugar-membrane was prepared in PS2. The scale bar is 20 μm .

When the PEG-rich droplets became bigger enough, they creamed upwards due to buoyancy. Thus, all droplets located in the upper part of the vesicle; see Fig. 3.2.4D. At the same time, the small buds moved up along the surface of the dextran-rich phase and fused to bigger ones. Figure 3.2.4D also shows the first big bud. The buoyancy-driven growing occurred both within the vesicle and at the membrane, which has also been observed in the deflated vesicles using confocal microscope.

After the formation of the PEG-rich buds, the process of formation of the final mesoscopic interface could take two pathways. One pathway is via the fusion of the PEG-rich droplets in the middle of the vesicle with the PEG-rich buds at the membrane. Figure 3.2.4E shows such an event. The big PEG-rich droplet formed within the vesicle volume moved upwards. When it reached the top of the vesicle, it pushed away the dextran-rich liquid and got in contact with the membrane. Then it fused with the small PEG-rich bud nearby. The newly formed bud protruded out of the vesicle body. The flexibility of the membrane made the protrusion possible. The fusion of the droplets with

the buds leads to the growth of the buds and the decrease of the interface area between the PEG-rich and dextran-rich phases. The other pathway is the growing of the buds through bud fusion: see Fig. 3.2.4F. The small PEG-rich bud at the bottom moved upwards along the surface of the dextran-rich phase. It collected all other even smaller buds on the way up and became bigger. When it was very close to the big bud on the top, a nearly 90° kink formed in the dextran-rich phase. This structure was very unstable. The two buds fused within a few seconds in order to decrease the interfacial energy.

In general, the buds moved more slowly than the droplets. It took more time in the formation of mesoscopic interface in vesicles made of sugar-membrane than in vesicles made of PEG-membrane. After 75.7 min, all PEG-rich droplets and buds fused into a big one on the top of the dextran-rich phase with a single interface between them; see Fig. 3.2.4G. The PEG-rich phase did not engulf the dextran-rich phase as the one in the vesicles with PEG-membrane because the sugar-membrane favoured the dextran-rich phase more than the PEG-membrane. Kinks could be observed both in the membrane and the dextran-rich phase. Since the vesicle was over-deflated, its volume increased with time in the late stage; see Fig. 3.2.4G. This led to the decrease of the polymer concentration with time, and thus the decrease of the interfacial tension. As a result, the area of the interface increased and became more curved. After 125 min, the vesicle became spherical again. The volume fraction of the dextran-rich phase increased with decreasing concentration. This is consistent with the situation in bulk; see Fig 3.1.4. In the end, the polymer solution became homogeneous as in the beginning, but with higher polymer concentrations.

The phase separation of the polymer solution in the vesicle interior leads to several consequences on the vesicle morphology. At first, the phase separation leads to the formation of tethers. This will be discussed in Chapter 4. Secondly, the PEG-rich phase may enclose the dextran-rich phase (Fig. 3.2.1) or sit on top of it (Fig. 3.2.4) depending on the membrane composition. This is related a transition from partial to complete wetting and will be discussed in Chapter 5.2. Thirdly, Vesicles containing two liquid phases may be with spherical shape or with a bud formed from the protrusion of the smaller phase. The budding event will be discussed in Chapter 5.3.

Chapter 4

Membrane Tube Formation Coupled to Phase Separation

In last chapter, the dynamics of phase separation in giant vesicles was discussed in details. This chapter considers one of the consequences of phase separation, namely membrane tube formation. Section 4.1 describes the change of the polymer concentration in the vesicles by deflation. Section 4.2 describes the experimental discovery that phase separation in the vesicles leads to membrane tube formation. The retraction of the membrane tubes via vesicle aspiration is discussed in the last section.

4.1 Vesicle trajectories in phase diagram

According to the phase diagram (see Fig. 3.1.1), we developed several systems with different PEG/dextran/water weight concentrations for encapsulation in vesicles consisting of different membrane compositions. The details of these systems are shown in Table 4.1.1. The polymer concentrations in PS1 and PS2 are listed in Table 2.3.2. These two solutions are homogeneous solutions with the same osmolarity. Their locations in the phase diagram are indicated as red (PS1) and green (PS2) stars under the binodal in Fig. 4.1.1. Vesicles made of PEG-membrane or sugar-membrane were prepared in these two solutions.

Table 4.1.1 The systems used in membrane tube formation*

	membrane type	initial polymer solution
Sys I	sugar-membrane	PS1
Sys II	PEG-membrane	PS1
Sys III	sugar-membrane	PS2
Sys IV	PEG-membrane	PS2

*see also Table 2.3.1 on page 26 for the membrane composition and Table 2.3.2 on page 28 for the compositions of the polymer solutions and the hypertonic solution used in vesicle deflation.

In order to obtain vesicles containing both phases, the polymer concentration is raised above the binodal by deflation, i.e., by exposing the vesicles to a hypertonic medium. In order to balance the resulting osmotic pressure, water is forced out of the vesicle. As a result, the polymer concentration increases and phase separation occurs. To make the vesicles sediment to the bottom of the chamber, they were first diluted in the

isotonic solution (its composition is shown in Table 2.3.2). The initial osmolarity P_0 of the solutions in the vesicle interior and exterior was 22 mOsmol/kg. The osmolarity P of the medium was then increased stepwise (in 10 – 20 % osmotic increments) by injecting the hypertonic solution into the working chamber. The osmolarity ratio r is defined as P/P_0 . The system was left to equilibrate for at least 2 hours in Sys I and II or 4 hours in Sys III and IV after each consecutive injection.

Once the polymer concentration is located above the binodal, the polymer solution undergoes phase separation, resulting in the formation of droplets inside the vesicle. The deflating trajectories of vesicles are indicated as red and green dashed lines in Fig. 4.1.1. According to the weight ratio of PEG and dextran, there may be a bigger PEG-rich phase in Sys I and II, or a bigger dextran-rich phase in Sys III and IV; see the insets in Fig. 4.1.1.

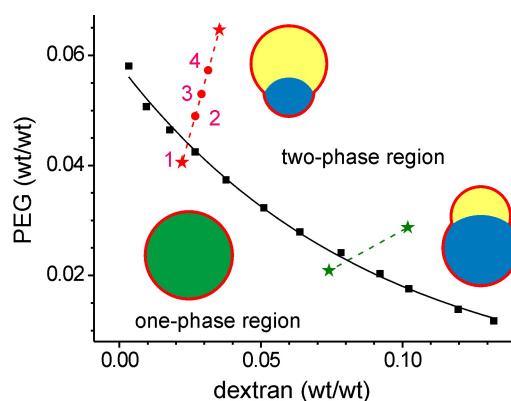


Figure 4.1.1 Vesicle trajectories in the phase diagram. The black squares present the binodal, which was determined using cloud-point titration at 23°C. The red dashed line connecting the red stars presents the trajectory of vesicle deflation in Sys I and II. The red dots show the polymer concentration enclosed in a vesicle. The green dashed line connecting the green stars presents the trajectory of vesicle deflation in Sys III and IV. The lines just guide the eyes. The insets schematically illustrate the vesicles loading with one-phase or two-phase solutions.

As the polymer concentration in vesicle interior is elevated along the deflating trajectories (see the dashed lines in Fig. 4.1.1), the vesicle may have different shapes. Figure 4.1.2 shows one examples.

In this two-phase system of PEG and dextran aqueous solution, the density of the dextran-rich phase is higher than the PEG-rich phase. For example, in the aqueous solution with 5.30% PEG and 2.90% dextran at 24°C, the density of the PEG-rich phase is 1.0098 g/cm³, and the density of the dextran-rich phase is 1.0458 g/cm³. The densities of the two coexisting phases are shown in Fig. 3.1.3. Thus, the dextran-rich phase is always located under the PEG-rich phase. In bulk solutions, the interface between the

two phases is flat. However, it is not the same in a vesicle because of the finite size of the droplet. The two phases are tens of microns in size with the volume of the order of picoliters. A curved interface is formed in vesicles instead of the flat interface in bulk; Fig. 4.1.2. In addition, the dextran-rich phase is not necessarily located under the PEG-rich phase as shown in image 3 and 4 in Fig. 4.1.2. It may simply be surrounded by the PEG-rich phase. However, the dextran-rich phase is always located at the bottom of the vesicle. Although the vesicles are small in size, as well as the coexisting phases, gravity still plays a role in the relative position of the two phases. Therefore, the vesicles with two-phase systems cannot be fully characterized only from the top-view images.

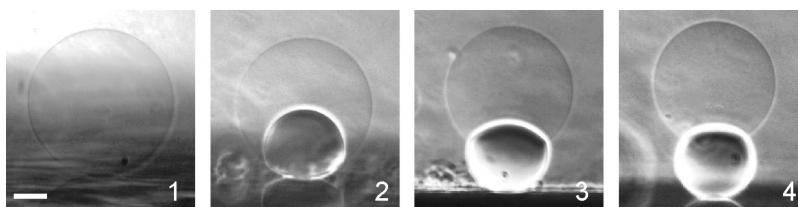


Figure 4.1.2 Morphologies of a deflated vesicle in Sys I exposed to different hypertonic mediums. The snapshots are phase contrast images (side view observation). They correspond to the concentrations indicated with 1 to 4 in Fig. 4.1.1. The osmolarity ratio r between the external medium and the initial internal polymer solution is 1.0, 1.3, 1.5 and 1.6, respectively. In the images 2 – 4, the lower dense part is the dextran-rich phase, and the upper light part is the PEG-rich phase. The scale bar is 20 μm .

By carefully choosing the external medium, we can get well defined geometries of vesicles loaded with the two-phase system. The density of the external medium has to be lower than the overall density of the vesicle so that the vesicles will sediment on the chamber bottom to be observed using inverted microscopes (the objective is located under the specimen, see also Fig. 2.4.3). The second criterion is that the density of the external medium must be lower than the dextran-rich phase but higher than the PEG-rich phase. In this way, the vesicles always “stand” on the surface of the bottom glass with the PEG-rich phase pointing upwards as shown in Fig. 4.1.2. The former criterion is a general rule for observing vesicles using inverted microscopes. The latter criterion is especially important for observing non-spherical vesicles which contain two phases. When the vesicles are observed using a horizontally-aligned inverted microscope (the inverted microscope is tilted 90 ° and the objective is on the left or right side of the specimen), they are found to have an axisymmetric shape, as well as the two phases, e.g. the vesicle shown in Fig. 4.1.2. Identifying the axisymmetric shape makes it possible to quantitatively characterize the vesicle’s properties during deflation, such as the apparent areas and the polymer concentrations.

4.2 Formation of membrane tubes

Microscopy observations of tube formation

During vesicle deflation, the volume of the vesicle becomes smaller, which can be directly seen in Fig. 4.1.2. However, no budding was observed during the deflation process. The excess membrane area, which is released as the volume decreases, forms tubular structures, which is also called tethers, in the vesicle. These tubular structures can be directly observed under fluorescence microscopy when the membrane contains fluorescent dye. Figure 4.2.1 shows one example for this membranous tubular network,

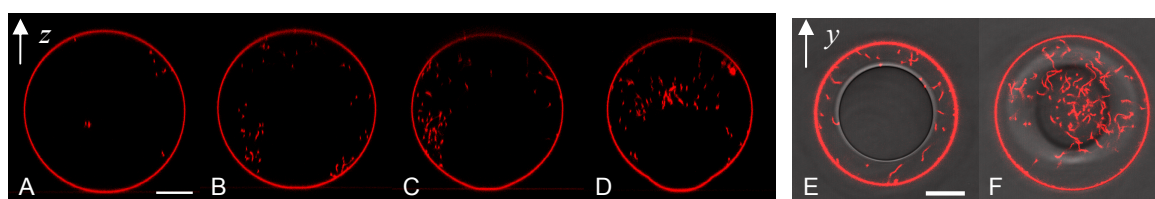


Figure 4.2.1 Tube formation for a vesicle with a sugar-membrane corresponding to Sys I. Red colour presents the labelled membrane. The horizontal axis is the x axis. (A) – (D): Vertical cross sections (xz plane) of a deflated vesicle. The osmolarity ratio r is 1.0, 1.14, 1.32 and 1.46, respectively. The images were taken in about 2 hours after each consecutive osmolarity change. The images are calibrated in z direction to eliminate the spherical aberration. (E) and (F): Horizontal cross sections (xy plane) of the overlay of fluorescent and bright field images of the snapshots. (E): At the equator of the dextran-rich phase. The central darker part is the dextran-rich phase. The lighter part is the PEG-rich phase. (F): At the equator of the PEG-rich phase. The dextran-rich phase is out of focus. The scale bars are 20 μm .

There is weak fluorescence signal inside the vesicle before the deflation (Fig. 4.2.1A), which arises from small defects (like internalized small vesicles or tubes) of the vesicle. When the vesicle is exposed to a hypertonic medium, more fluorescent signal is detected in the vesicle interior. The higher the osmolarity ratio r is, the more fluorescent signal is detected; Fig. 4.2.1B – D. The fluorescence in the vesicle interior is emitted from the tubes formed during vesicle deflation. The distribution of the tubes is not homogeneous in the vesicle interior. They prefer to stay in the PEG-rich phase rather than the dextran-rich phase, see Fig. 4.2.1E and F. No fluorescence is detected in the dextran-rich phase, namely the darker part in the centre of the image Fig. 4.2.1E. These tubes are fluctuating randomly in the PEG-rich phase. They appear as short flexible rods in the fluorescence image; Fig. 4.2.1F.

When the osmolarity ratio r becomes relatively high, the tubes align at the interface of the PEG-rich and dextran-rich phases to form a thin layer; Fig. 4.2.2A. The individual tubes are distinguishable in this layer. The tubes form a two dimensional

ordered structure to cover the interface through bending and looping. The ends of the tubes are located either in this layer or in the PEG-rich phase; Fig. 4.2.2B. The discontinuity of the fluorescence at the interface indicates that membrane at the interface exists in the form of tubes rather than folded sheets. The latter is another possibility for the fluorescence signal, but a sheet configuration would lead to continuous fluorescence.

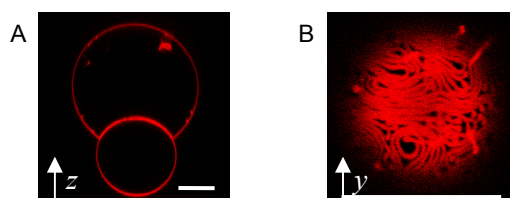


Figure 4.2.2 The membrane tubes aligning at the interface between the PEG-rich and dextran-rich phases in a deflated vesicle corresponding to Sys I. The vesicle in Fig. 4.2.1 was further deflated to the osmolarity ratio $r = 1.51$. The system was left to equilibrate for about 2 hours. (A): The vertical cross section (xz plane) of the vesicle. The lower small sphere (circle) encloses the dextran-rich phase, and the upper big one encloses the PEG-rich phase. The image was calibrated in z direction to eliminate the spherical aberration. (B): The horizontal section (xy plane) through the top of the interface in the vesicle interior. The scale bars are $20 \mu\text{m}$.

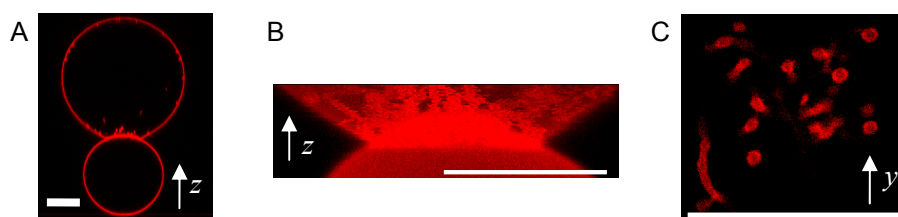


Figure 4.2.3 The over-crowded membrane tubes at the interface of the PEG-rich and dextran-rich phases. The vesicle is the same one as shown in Fig. 4.2.2. (A): The vertical cross section (xz plane) of the vesicle. The interface becomes smaller than the one shown in Fig. 4.2.2A after introducing a flow into the chamber. The lower small sphere (circle) encloses the dextran-rich phase, and the upper big one encloses the PEG-rich phase. The image was calibrated in z direction to eliminate the spherical aberration. (B): 3D projection on the xz plane in the vicinity of the interface. (C): The horizontal section of the tubular structure above the interface. This is one of the images that construct the image (B). The scale bars are $20 \mu\text{m}$.

It is rather difficult to obtain images of the cross sections of the fluctuating tubes because of the slow scanning speed of the microscope. When they are at the interface, they have a more ordered structure. However, the poor resolution in the z direction of the confocal microscope limits the direct observation of this tubular structure. If the interface becomes over-crowded, some (parts) of the tubes have to leave the interface for the PEG-rich phase; Fig. 4.2.3A. As a result, the tubes at the vicinity of the interface have relatively directional orientation, i.e. approximately perpendicular to the xy plane; Fig. 4.2.3B. Thus, it becomes possible to obtain images with cross sections of the tubes in the xy plane, see Fig. 4.2.3C. The cross sections of these tubes appear as circles with diameter about $1 \mu\text{m}$. Figure 4.2.3 provides direct evidence for the existence of the

membranous tubular network. The morphological change of the vesicle from the one shown in Fig. 4.2.2A to the one shown in Fig. 4.2.3A is related to the tube extraction. The details will be discussed in section 4.3.

Tubes do not only form in vesicles made of sugar-membrane, but also form in the ones made of PEG-membrane during deflation; see Fig. 4.2.4. The vesicle deflation is started with a vesicle containing the homogeneous polymer solution PS2; Fig. 4.2.4A. There is no visible fluorescence in the vesicle interior. After the phase separation completes, fluorescence is detected in the vesicle interior, which is indicated by the arrows in Fig. 4.2.4B. The fluorescence is emitted by the newly formed tubes. Figure 4.2.2A and B indicates that the tube formation occurs during the phase separating process.

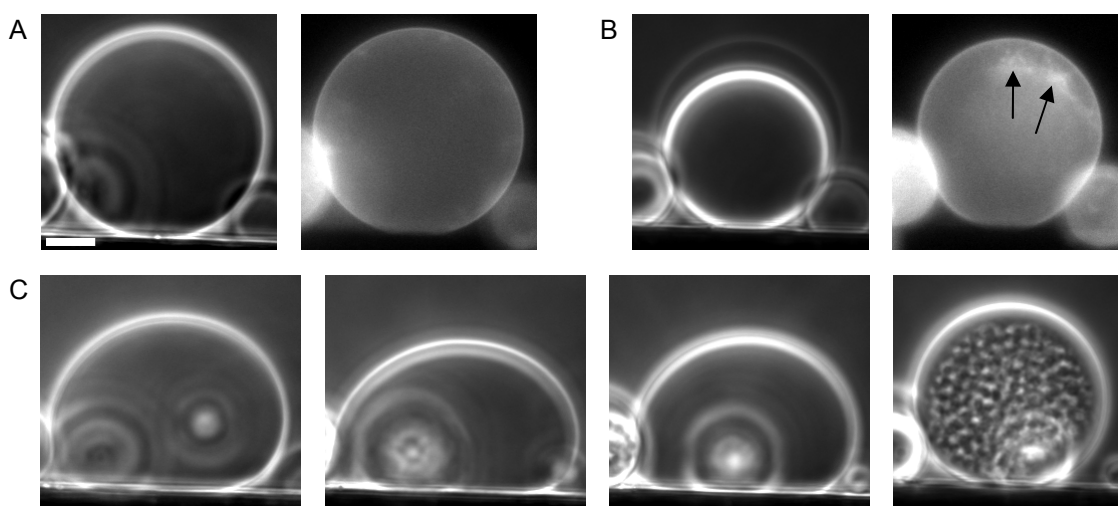


Figure 4.2.4 Tube formation for a vesicle with a PEG-membrane corresponding to Sys IV. These images present the side view observation of a vesicle sitting on the chamber bottom. The osmolarity of the external medium is increased 28%. (A): The vesicle before deflation. Left: phase contrast; Right: fluorescence. (B): The vesicle after the phase separation completes at time 56 min. Left: phase contrast. The dense part is the dextran-rich phase and the light part is the PEG-rich phase. Right: fluorescence. (C): Vesicle shape evolution during deflation. The phase contrast images were taken at time 3, 4 5 and 6 min after the addition of the hypertonic solution into the chamber. Phase separation started at time 6 min. The scale bar is 20 μm .

After the hypertonic solution is injected into the chamber, the vesicle deflates. If the vesicle surface area is constant, the smaller volume will result in sessile-shaped vesicle; see the first image in Fig. 4.2.4C. The sessile-shaped vesicle is the result of the balance between membrane tension and the gravity arising from the density difference between the vesicle interior and exterior. With time, more excess area is generated and the vesicle becomes flatter; see the second image in Fig. 4.2.4C. Afterwards, the vesicle starts to become rounder, and it becomes spherical again when lots of small PEG-rich droplets are observed in the vesicle interior; see the last image in Fig. 4.2.4C. The

morphology change of the vesicle from sessile shape to sphere indicates a sudden increase of membrane tension, which can overcome the gravity now. The increase of the membrane tension indicates the formation of the tubes which can coexist with spherical caps under mild tension and store the excess area. The excess area is exhausted and stored in the form of tubes after the phase separation completes; Fig 4.2.4B. The observation on the morphological changes of the vesicle indicates that the phase separation and the tube formation occur simultaneously.

The tube formation is initiated during a highly non-equilibrated state. The vesicle undergoes fast morphological and dynamical changes. To form tubes might be the most effective way for the vesicle to get rid of the excess area. On the other hand, it is also strongly influenced by the phase separation process. No tubes are observed in the deflated vesicles enclosing solutions, such as sucrose aqueous solution and PEG aqueous solution, which are not able to phase separate when their concentrations are elevated.

In our experiments, membrane tube formation is a common phenomenon during the deflation of vesicles containing PEG/dextran aqueous solution. Tubes are observed not only in the deflated vesicles made of sugar-membrane and PEG-membrane, but also in the deflated vesicle made of DOPS-membrane, see table 2.3.1. In most cases, the tubes exist in the vesicle interior as shown in Fig. 4.2.1 and Fig. 4.2.4. In very rare cases, tubes in the vesicle exterior can be observed. External tubes are seen more often for vesicles prepared in PS2 than for vesicles prepared in PS1. The external tubes may be induced by the motion of vesicles in the created flow due to the injection of the hypertonic solution.

It is difficult to determine statistically how often tubes form during vesicle deflation because the majority of the giant vesicles are not perfect. There are already defects in the vesicle interior, such as preformed tubes and small vesicles. According to the theoretical prediction that tubes can coexist with spherical caps under mild tension [Lipowsky 2005a], the fluctuation of the membrane on the vesicle surface can be utilized as a criterion for the tube formation, which leads to tense membrane according to the theoretical prediction [Lipowsky 2005a]. If the membrane fails to form tubes during the deflation, the membrane fluctuation can be directly observed under fluorescence microscopy. According to this criterion, tubes form in circa 95% of the deflated vesicles in all systems listed in Table 4.1.1. This statistics includes 188 vesicles in Sys I, 312 vesicles in Sys II, 163 vesicles in Sys III, and 435 vesicles in Sys IV.

The membrane tubes formed during the vesicle deflation are rather stable. In the absence of external disturbance, e.g. convection in the external medium, the tubes can exist for days. This is different from the behaviour of tubes formed by pulling. Without external pinning, tubes coalesce smoothly during tube pulling. [Evans 1996, Derényi 2002] In our system, there is no external force supplied during and after the tube formation. No coalescence is observed. The absence of external force in the tube formation process may be the reason for the stability of the tubes.

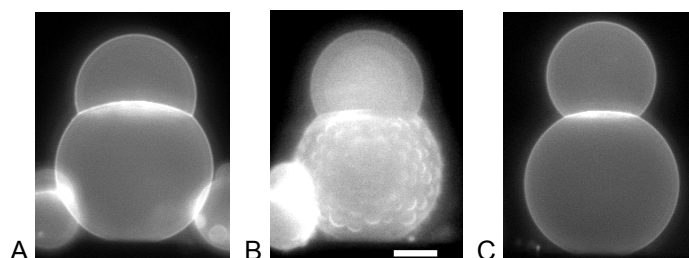


Figure 4.2.5 Fluorescence images (side view) of a vesicle during deflating. The big lower part is the dextran-rich phase. The small upper part is the PEG-rich phase. The higher fluorescence intensity at the interface in the left and right images is due to the tubes accumulating there. (A): Before deflation (corresponding to the fourth point in Sys III in Fig. 4.2.6). (B): Intermediate state of phase separation leading to a raspberry shape of the lower part of the vesicle. (C): After deflation (corresponding to the fifth point in Sys III in Fig. 4.2.6). The scale bar is 20 μm .

When a vesicle with two phases (e.g. Fig. 4.2.5A) is exposed to a hypertonic medium, the loss of water from the vesicle leads to phase separation in both the PEG-rich and the dextran-rich phases. Many small dextran-rich droplets form in the upper PEG-rich phase. They fall down due to their higher density and fuse with the lower continuous dextran-rich phase. At the same time, many small PEG-rich droplets form in the lower dextran-rich phase not only in the interior of the dextran-rich phase but also on its surface where in contact with the membrane is favoured. The PEG-rich droplets in the interior move up and fuse with the upper PEG-rich phase. However, the behaviour of the small PEG-rich droplets formed in contact with the membrane is quite different from that of those formed in the centre. They protrude out of the body of the dextran-rich phase because the PEG-rich droplets have lower interaction energy with the membrane than with the dextran-rich phase, see Fig. 4.2.5B. As a result, the lower part of the vesicle assumes a raspberry shape as intermediate state.

The small PEG-rich droplets (in contact with the membrane) move slowly upwards and fuse with the big PEG-rich phase. The released membrane is utilized to undergo the morphological change, instead of forming tubes again. As a result, the

contact area of the two phases becomes smaller. After the phase separation is completed, the vesicle has recovered its smooth surface again; Fig. 4.2.5C.

The raspberry-like surface only forms on the dextran-rich phase. In the PEG-rich phase, the dextran-rich droplets formed in the vicinity of the membrane are expelled away due to the higher interfacial energy with the membrane than the PEG-rich phase. For the same reason, no raspberry-shaped vesicle is observed in Sys II and IV, where the dextran-rich phase is surrounded by the PEG-rich phase. The dextran-rich phase is much smaller in the vesicles in Sys I than in Sys III. The relatively big contact area with the PEG-rich phase leads to the absence of the raspberry-shaped intermediate state.

The evolution of areas in deflated vesicles

Because of the axisymmetric shape of the two-phase vesicles, it is possible to measure the apparent area of the deflated vesicle for different osmolarity ratio r . The apparent area of the vesicle is the area estimated from the two dimensional vesicle contour. It can be obtained by fitting the vesicle contour with circles in the acquired images. The decrease of the vesicle apparent area implies an increase of the membrane area utilized to form tubes. Thus, we can find out how much membrane area is involved in the formation of tubes during deflation, and how it changes with increasing osmolarity. As shown in Fig. 4.2.6A, the vesicle apparent area can involve in three different ways as a function of the osmolarity ratio r .

In the first case, the apparent area of a deflated vesicle decreases continuously as the osmolarity of the external medium increases. This implies that more membrane area is stored in tubes when the vesicle volume becomes smaller. The deflated vesicles of Sys II and IV belong to this group. The vesicle is always spherical in the whole osmolarity range, as well as the dextran-rich phase which is enclosed by the PEG-rich phase.

In the second case, the apparent area of the vesicle decreases at first, and then remains approximately constant. Tubes stop forming when the osmolarity ratio $r > 1.2$. The vesicles in Sys I have such a behaviour. At low osmolarity regime, the vesicle is spherical; see image 2 in Fig. 4.1.2. At high osmolarity, the dextran-rich phase protrudes out of the PEG-rich phase, see images 3 and 4 in Fig. 4.1.2.

In the last case, the apparent area of the vesicle decreases at first. After it reaches a minimum, it starts to increase up to its original value. The decrease of the area implies

that the tubes form in the low osmolarity regime. However, the already existed tubes recede during further deflation at high osmolarity regime. This behaviour is observed in the deflated vesicle in Sys III. In this case, the PEG-rich phase protrudes out of the vesicle body and is always located on the top of the dextran-rich as shown in Fig. 4.2.5.

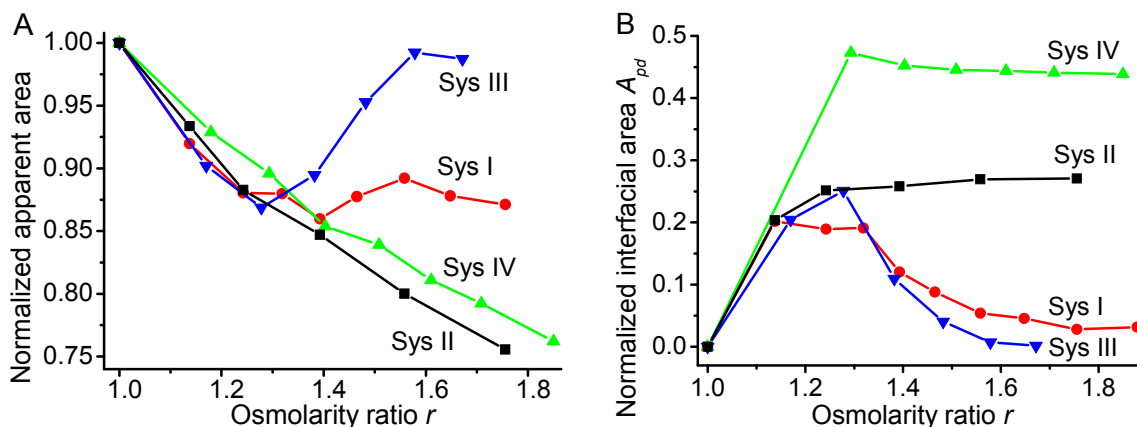


Figure 4.2.6 The area evolution with osmolarity ratio r . (A) The apparent area (A_v) of vesicles at different osmolarity ratios r . A_v is normalized by the initial area of the vesicle (at $r = 1.0$). (B) The evolution of interface area between the PEG-rich and dextran-rich phases (A_{pd}) with osmolarity ratio. A_{pd} is normalized by the total interface area, namely the sum of A_v and A_{pd} . A_{pd} is zero at $r = 1.0$ because the solutions are homogeneous. The lines just guide the eyes. All vesicles were diluted in the same external medium and deflated with the same hypertonic solution.

The evolution of the interface area between the PEG-rich and dextran-rich phases is rather different with the one of the vesicle apparent area; Fig. 4.2.6B. Two different situations are observed. In the first situation, the interface area increase at first, and then it reaches a plateau. The deflated vesicles of Sys II and IV belong to this group although the behaviours shown in Fig. 4.2.6B are rather different. In the whole osmolarity ratio range shown in Fig. 4.2.6, the dextran-rich phase is not in contact with the membrane for both systems. The interface area is also the surface area of the dextran-rich phase existing as a sphere. The different values in both systems are due to the different volume ratio of the dextran-rich and PEG-rich phases. The volume fraction of the dextran-rich phase in Sys IV is much bigger than the one in Sys II. Therefore, the curve presenting Sys IV is located above the curve presenting Sys II in Fig. 4.2.6B. Figure 3.1.4 shows the change of the volume fraction with polymer concentration in bulk for PS1 and PS2. The change of the volume fraction in vesicles is considered the same as the one in bulk.

Sys I and Sys III belong to the other situation. In this situation, the interface area increases at first, then it decrease again after reaching the maximum. In the low osmolarity range, the increasing of the interface area is dominated by the growth of the

new phase, i.e. bigger volume means bigger interface. In the high osmolarity range, the interface area decreases due to the increased contact area between the membrane and the dextran-rich phase. In this range, the membrane released during deflation does not form tubes any more. Instead, the excess membrane is utilized to perform morphological changes of the vesicle in order to decrease to the interface area. The membrane in the form of tubes can even be retracted back to the vesicle surface by forming raspberry-shaped vesicle in Sys III; Fig. 4.2.5. Therefore, the interface area decreases faster in the deflated vesicle in Sys III than in the deflated vesicle in Sys I.

Discussion

The formation of a membrane tube requires large changes in membrane curvature and leads to the increasing of bending energy. The corresponding energy cost depends on the mechanical property of the membrane, i.e., the bending rigidity, the membrane tension, as well as its interaction with the surroundings. The initiation of the tube extraction requires overcoming a large initial energy barrier. This energy barrier corresponds to the maximum in the external applied force as observed experimentally [Sun 2005, Huso 2007] and theoretically [Derényi 2002]. In tube pulling experiments, the force exerted, e.g. by the cantilever of AFM, reaches a maximum in the beginning of the tube pulling, then it decreases to a plateau with increasing the length of the tube. In the absence of external forces, the energy needed for the tube formation may be provided by the phase separation of the polymer solution, which is a spontaneous, exothermal process [Koningsveld 2001]. In addition, the liquid flow associated with the phase separation may also contribute to the tube formation. Phase separation and tube formation are coupled processes, as demonstrated in Fig. 4.2.4C.

Tube formation works on an all-or-nothing basis: the external force can pull out tubes only if it is strong enough to overcome the energy barrier [Derényi 2002]. It is the same in the vesicles with two-phase system. The tubes can only form when the energy released in the phase separation is big enough to overcome the energy barrier. When the membrane fails to form tube during the phase separation process, it can not form in the latter stage. However, tube may form when the vesicle is deflated again.

There are three possible locations for the tubes in the vesicle interior, namely the PEG-rich phase, the dextran-rich phase and the interface between these two phases. The tubes can be located in one or more of these locations. However, the final localization of

the tubes is the result of the minimization of the interface energy. The interface energy F of the vesicle with two-phase system is the superposition of four components:

$$F = F_{pd} + F_{pm} + F_{dm} + F_{em} \quad (4.2.1)$$

where F_{pd} , F_{pm} , F_{dm} and F_{em} are the energy of the interface between the PEG-rich and dextran-rich phases (pd), the PEG-rich phase and the membrane (pm), the dextran-rich phase and the membrane (dm), and the external solution and the membrane (em) respectively. Here, it is assumed that no long range interactions are present, which allows us to ignore the interaction between the solutions in the vesicle interior and exterior. The interface energy can be described by the interfacial tension and the corresponding area. Thus, Eq. 4.2.1 can be rewritten as:

$$F = \Sigma_{pd}A_{pd} + \Sigma_{pm}A_{pm} + \Sigma_{dm}A_{dm} + \Sigma_{em}A_{em} \quad (4.2.2)$$

where Σ_{pd} , Σ_{pm} , Σ_{dm} , and Σ_{em} are the interfacial tensions of the four interfaces, and A_{pd} , A_{pm} , A_{dm} and A_{em} are their corresponding areas, with the constrain that $A_{em} = A_{pm} + A_{dm}$. In addition, A_{em} is equal to the total membrane area including tubes.

In a vesicle with two phases, the compositions of the membrane, the coexisting phases and the external solution are fixed, leading to fixed interfacial tensions. The localization of the tubes does not affect the interface energy F_{em} because the membrane area A_{em} is constant. However, the tube localization may affect the interface energies F_{pd} , F_{pm} and F_{dm} , by altering the interface areas or the interfacial tensions in Eq. 4.2.2.

The tubes prefer to stay in the phase, which has a smaller interfacial tension with the membrane in order to minimize the interfacial energy. The location of the tubes can change the contact areas between the membrane and the two phases. In the vesicles made of sugar-membrane and PEG-membrane, the tubes stay in the PEG-rich phase because the interfacial tension Σ_{pm} is smaller than Σ_{dm} . It is worth to clarify that the sugar-membrane is named according to the compositions, i.e., this membrane contains G_{M1} ganglioside, whose headgroups consists of sugar moieties. One can not conclude from the name or the membrane composition that the sugar membrane has a lower interfacial tension with the dextran-rich phase than with the PEG-rich phase. In fact, the sugar-membrane has a lower interfacial tension with the PEG-rich phase; see Fig. 4.1.2. The contact angle of the PEG-rich phase on the membrane is smaller compared to the contact angle of the dextran-rich phase on the membrane, which indicates a smaller Σ_{pm} than Σ_{dm} .

When Σ_{pd} becomes big compared to the interfacial tensions Σ_{pm} , Σ_{dm} and their difference $|\Sigma_{pm} - \Sigma_{dm}|$, the tubes will be adsorbed onto the surface of the dextran-rich phases; see e.g. the vesicle in Fig 4.2.2. The relocation of the adsorbed tubes at the interface reduces the interfacial energy F_{pd} . Tube adsorption onto the interface is the result of the competition among Σ_{pd} , Σ_{dm} and Σ_{pm} , which are influenced by the composition of the membrane and the concentration of the polymer solution. In the vesicle made of PEG-membrane, the tube adsorption occurs at much higher osmolarity ratio, i.e. $r = 2.7$ for Sys II, which also means higher polymer concentration, due to the high affinity between the membrane and the PEG-rich phase. In comparison, the adsorption already occurs at $r = 1.51$ (Fig. 4.2.2) for Sys I with sugar-membrane.

The evolution of the vesicle apparent area in Fig. 4.2.6A implies that tube formation depends on the process of the vesicle deflation. It can be regulated by the interfacial tensions (Σ_{pd} , Σ_{pm} , and Σ_{dm}), the membrane tension, and the phase separation process of the polymer solution.

When a vesicle is deflated, the excess area can either form tubes or be absorbed in morphological change of the vesicle, e.g. by budding of the smaller phase. Which pathway is taken, depends on the competition between Σ_{pd} and $|\Sigma_{pm} - \Sigma_{dm}|$. When Σ_{pd} is small compared to $|\Sigma_{pm} - \Sigma_{dm}|$, the excess area will form tubes. Tube formation is a fast and effective way to dispose the excess area, which is generated rapidly during vesicle deflation. When Σ_{pd} is relatively big compared to $|\Sigma_{pm} - \Sigma_{dm}|$, the excess area will be utilized to undergo morphological change in order to reduce the interface area A_{pd} between the coexisting phases. Thus, the free energy of the whole system will be reduced.

In the deflated vesicles with the trajectories shown in Fig. 4.1.1, the polymer concentration in the vesicle interior increases with the osmolarity of the external medium, presented by the osmolarity ratio r . When the polymer solution is close to the mixing point, namely at polymer concentration close to but still above the binodal, Σ_{pd} is extremely low. It is smaller than $|\Sigma_{pm} - \Sigma_{dm}|$. Both Σ_{pd} and $|\Sigma_{pm} - \Sigma_{dm}|$ increase with increasing polymer concentration. However, Σ_{pd} increases faster than $|\Sigma_{pm} - \Sigma_{dm}|$. At certain point, Σ_{pd} becomes relatively big compared to $|\Sigma_{pm} - \Sigma_{dm}|$.

In principle, there must be two regimes in the vesicle apparent area evolution in deflated vesicles. These two regimes correspond to the two pathways of the excess

membrane area. In the first regime, namely at low polymer concentration or low osmolarity ratio r , the excess membrane forms tubes during deflation. As a result, the vesicle apparent area decreases with increasing osmolarity ratio r . In the second regime, namely at high osmolarity ratio r , the excess membrane area is utilized to perform morphological change, namely the protrusion of one phase from the vesicle body. Thus, the interface area A_{pd} is reduced significantly. In this regime, the vesicle apparent area stops decreasing. In the deflated vesicle of Sys III, the excess membrane even retracted back to the vesicle surface as the vesicle is further deflated (see Fig. 4.2.6A) due to the formation of the raspberry-shaped vesicle (see Fig. 4.2.5).

The formation of the raspberry-shaped vesicle requires more membrane area, and thus elevates the membrane tension. The elevated membrane tension breaks the balance between the coexisting tubes with the vesicle and leads to the withdrawal of the membrane from the tubes. The details will be discussed in the next section. Thus, the membrane tension is reduced. The lower fluorescence intensity at the interface in Fig. 4.2.5C than the one in Fig. 4.2.5A indicates the reduction of membrane tubes. The amount of the withdrawn membrane area from tubes depends on the membrane tension induced by the formation of the raspberry-shape vesicle.

The crossover of these two regimes is determined by the interfacial tension Σ_{pd} and $|\Sigma_{pm} - \Sigma_{dm}|$. In the deflated vesicle made of sugar-membrane in Sys I and III, both regimes are observed, see Fig. 4.2.6. However, only the first regime is observed in Fig. 4.2.6 for the deflated vesicle made of PEG-membrane in Sys II and Sys IV, due to the high affinity of the membrane to the PEG-rich phase. For the vesicles enclosing the same polymer solution, namely the same interfacial tension Σ_{pd} , the interfacial tension difference $|\Sigma_{pm} - \Sigma_{dm}|$ in the vesicle made of PEG-membrane is much higher than the one in the vesicle made of sugar-membrane. Therefore, the crossover of the two regimes is located at higher osmolarity ratio, which is not included in Fig. 4.2.6.

4.3 Retraction of membrane tubes

In the previous section, we showed that many tubes form when vesicles with aqueous two-phase system are deflated. When the membrane is under tension, the tubes can be recruited back to the vesicle surface. Figure 4.3.1 shows an example of the tube receding induced by applying tension to the vesicle via micropipette aspiration. The

strong fluorescence signal in the vesicle interior indicates that there are many tubes accumulating at the interface and spanning in the PEG-rich phase. When the pressure inside the micropipette decreases, the vesicle is aspirated into the micropipette. The membrane inside the pipette can be clearly seen in the fluorescence images. The pressure difference in and out of the pipette results in the increase of membrane tension, which can be calculated using Eq. 2.5.2. The effect of gravity is neglected in the calculation due to the insignificant density difference between the interior and exterior of the vesicle. At 25 °C, the density of the external medium is 1.01099 g/cm³, and the density of the polymer solution inside the vesicle is 1.01651 g/cm³, which is calculated according to the density of the polymer solution PS1 and the vesicle volume at $r = 1.0$ and $r = 1.4$ in Fig. 4.1.2. The change of the vesicle volume is assumed to be only due to the loss of water.

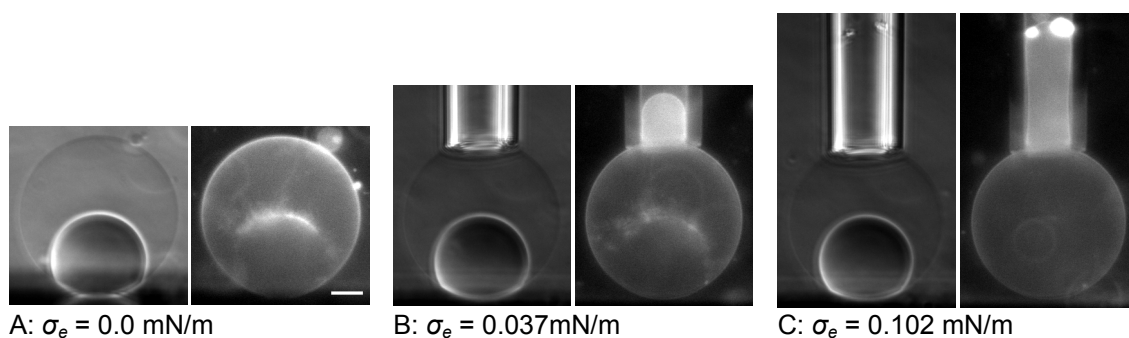


Figure 4.3.1 Microscope images (side view observation) of the vesicle under different tensions. σ_e is the membrane tension exerted by the pipette. Left panel: phase contrast. The dense part is the dextran-rich phase. The light part is the PEG-rich phase. Right panel: fluorescence. The big tube on the top of the vesicle in (B) and (C) is the glass pipette. The two bright spots in the pipette in (C) is due to fluorescence emitted by two pieces of dirt falling down along the pipette during the experiment. The vesicle of Sys I is pre-deflated in a hypotonic medium with osmolarity 30.5 mOsmol/kg. The conditions of this vesicle is equivalent to the one at $r = 1.4$ in Fig. 4.2.6 for Sys I. The system was left to equilibrate for approximately 3 minutes after each consecutive tension change. The scale bar is 20 μm .

As the membrane tension increases, there are less and less tubes in the vesicle interior. No fluorescent signal is detected in the vesicle interior at $\sigma_e = 0.102$ mN/m; Fig. 4.3.1C. At the same time, the membrane area inside the pipette increases significantly. The increased tension helps the vesicle to restore membrane from tubes. The membrane recruit process can be characterized through the vesicle apparent area including the part in and out of the pipette. Comparing to the thin and fluctuating tubes, the apparent area of the vesicle is very easy to estimate. This can be simply done by fitting the vesicle contour with spherical caps and cylindrical tube.

When the membrane is stretched, there are two regimes in the area expansion. The first one is the entropic regime, which corresponds to pulling out the membrane

fluctuation. The entropic regime is located at the low membrane tension region. In this regime, the fluctuation of the membrane is hindered and lead to the increase of the vesicle area when the membrane tension is elevated. The second regime is the stretching regime, which is located at the high membrane tension region. The increase of the membrane tension leads to the change of the area per lipid. The crossover of these two regimes, which is at about 0.5 mN/m, depends on the specific membrane composition. Since the membrane tension applied to the vesicle is very low in the vesicle pressurization experiments, e.g. the highest tension is 0.54 mN/m in the case shown in Fig. 4.3.1, the membrane dilation is mainly in the entropic regime. The stretching regime can not be easily accessed because the vesicle gets completely aspirated in the pipette at high applied tensions.

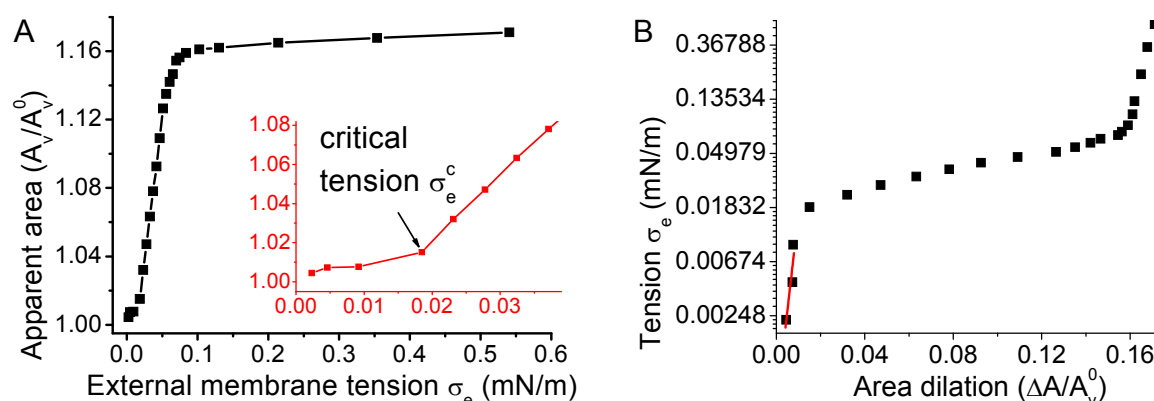


Figure 4.3.2 Area dilation as a function of the external membrane tension σ_e . The data were obtained by analyzing the images of the pressurized vesicle shown in Fig. 4.3.1. The area is normalized by the initial vesicle apparent area A_v^0 , see Fig. 4.3.1A. (A): Linear plot. The inset is a magnification of the region of area dilation under very low tension. (B): Semilogarithmic plot (same data as in (A)). The red line is the linear fit of the first three data points.

In contrast to the vesicles without tubes, there are three distinct regimes in the area dilation for vesicles with tubes; see Fig. 4.3.2A. There are two contributions to the area dilation. One contribution is from the well-known membrane fluctuation, which influences the area in the whole tension range. The other contribution is the increase of membrane area from tube receding. In the extremely low tension regime, the apparent area increases slowly with increasing tension; the inset in Fig. 4.3.2A. This regime corresponds to the smoothing out of the membrane fluctuation. Interestingly, at higher tensions, the logarithmic dependence of the tension on the apparent area has similar slope, which will be discussed below.

Since the area dilation in the first regime is only contributed by the membrane fluctuation, the area dilation with the membrane tension can be described by the

following equation [Evans 1990], if we assume that the main contribution in the area change is due to membrane bending.

$$\frac{\Delta A_v}{A_v^0} = \frac{A_v - A_v^0}{A_v^0} \approx \frac{k_B T}{8\pi\kappa} \ln \frac{\sigma_m}{\sigma_0} \quad (4.3.1)$$

where A_v^0 is the initial vesicle apparent area at $\sigma_m = \sigma_0$, ΔA_v is the area difference, T is the temperature, k_B is the Boltzmann constant. In this equation, the membrane tension σ_m is normalized by σ_0 . From the slope ($8\pi\kappa/k_B T$) of the linear fit in the semilogarithmic plot (see the red line in Fig. 4.3.2B), one can obtain the bending rigidity κ of the membrane. It is equal to $(5.7 \pm 1.9) \times 10^{-20}$ J (the average of the measurements on two vesicles). This is a rather rough estimation leading to relatively low value for the membrane bending stiffness. It is better to measure the membrane bending rigidity κ using another method. Note that the membrane fluctuation in the tubes is not taken into account, as well as the initial membrane tension σ_0 and its effect on the initial vesicle apparent area A_v^0 . The membrane fluctuation in the tubes leads to a faster change of the vesicle apparent area A_v , and thus a lower value for the bending rigidity κ . This error induced by the tubes can be partially counterbalanced by the error introduced from the membrane tension. It leads to a higher value for the bending rigidity κ to exclude the initial membrane tension σ_0 . Therefore, the external membrane tension σ_e is used in the linear fitting in Fig. 4.3.2B, instead of the membrane tension σ_m . The membrane tension σ_m is the superposition of the initial membrane tension σ_0 (before applying tension σ_e with the pipette) and the external membrane tension σ_e exerted by the pipette:

$$\sigma_m = \sigma_0 + \sigma_e \quad (4.3.2)$$

In the second regime with $0.01 < \Delta A/A_v^0 < 0.16$, the apparent area increases rapidly with tension. This regime is mainly corresponding to the membrane recruit process. The contribution of the membrane fluctuation is negligible compared to the tube receding. The membrane stored in the form of tubes is pulled back to the vesicle surface with increasing membrane tension. It is the dominant contribution to the area dilation. The apparent area of the vesicle increases linearly with tension. The apparent area increases about 15% in this regime. In other words, around 13% of the total membrane is stored as tubes, which is consistent with the vesicle deflation experiment in Sys I in Fig. 4.2.6A. Sometimes, the cylindrical part of the vesicle inside the pipette is observed to bud off to a small vesicle due to the high excess membrane area.

The third regime is located in the high tension region. The increasing of the vesicle apparent area is slowed down. The slope of the area dilation versus tension is smaller than in the first regime; Fig. 4.3.2A. The smaller slope indicates that both the membrane fluctuation and the tube receding contribute to the area dilation. In addition, the membrane may be entering the regime of stretching. There must be a small portion of very thin tubes still existing in the vesicle interior although no fluorescence can be detected. In this regime, the membrane fluctuation is comparable to the tube receding. When the membrane tension is further increased, the vesicle is completely sucked into the pipette due to the high excess membrane area. Therefore, it is impossible to reach the stretching regime.

One has to note that in most experiments the membrane inside the pipette was observed to oscillate slightly in the low tension regime. This oscillation can still be observed half an hour after a constant membrane tension is applied to the vesicle. The situation is different in different vesicles. In general, the membrane stops oscillating when the exerted membrane tension exceeds 0.05 mN/m. To exert such low tensions on a vesicle, the needed aspiration pressure (the pressure difference in and out of the pipette) is less than a few Pascal. Thus, the aspiration pressure can be easily perturbed by the surrounding, e.g. the convection of the air, which leads to the oscillation on the membrane inside the pipette. This oscillation results in high error in the measured the apparent area of the vesicle.

There are many experimental and theoretical studies concerning membrane tubes or tubular structures. Many of them are focused on tube extraction induced by external forces, but none of them concerns the tube receding process. A possible mechanism for the tube receding can be tube thinning, which means that the diameter of the tubes becomes smaller when the membrane tension is increased. We assume that all tubes have the same radius. In a tense vesicle coexisting with tubes, the stable radius of the tubes is equal to $(\kappa/2\sigma_m)^{0.5}$ [Lipowsky 2005a]. Here, κ is the bending rigidity of the membrane and σ_m is the membrane tension. When the membrane tension increases, the equilibrium between the tube radius and the tension is broken. The increased tension leads to lipid flow from the tubes to the vesicle surface in order to reduce the tube radius to match the membrane tension again. In addition, the lipid flow may result in shorter lengths of the tube.

However, the tubes seem not to respond to small elevation of the membrane tension. At a constant membrane tension, the radius of the tubes R_t may range from $(\kappa/2\sigma_m)^{0.5}$ (stable) to $(3\kappa/2\sigma_m)^{0.5}$ (unstable) [Lipowsky 2005a]. The tube becomes unstable if its radius exceeds $(3\kappa/2\sigma_m)^{0.5}$. In other words, tubes with radius R_t may become unstable for membrane tensions larger than $3\kappa/2R_t^2$. This threshold in the membrane tension is exhibited in the form of the critical external tension σ_e^c indicated by the arrow in the inset in Fig. 4.3.2A. Tube thinning occurs only when the exerted tension is higher than this critical tension, which also corresponds to the crossover between the first and the second regimes. Thus, one can estimate the initial membrane tension σ_0 (at which the tubes are initially stable) from the critical external membrane tension σ_e^c , which is equal to $2\sigma_0$, (at which the tubes with radius $(\kappa/2\sigma_m)^{0.5}$ become unstable). For the vesicle shown in Fig. 4.3.1, the critical external membrane tension σ_e^c is 0.0185 mN/m, and thus, the initial membrane tension σ_e is 0.0092 mN/m.

The critical external membrane tension σ_e^c differs slightly for every individual vesicle. It was measured to be 0.0186 mN/m and 0.0192 mN/m for two other vesicles. The critical tension for the membrane recruiting is related to the radius of the tubes. High tension is required if the radius of the tube is small. Therefore, it depends on the radius of the tubes to what extent the stored membrane can be recruited when tension is applied to a vesicle by means of the pipette. When the applied tension exceeds the critical tension, membrane recruit may occur. Three regimes (see Fig. 4.3.2) can be observed when the critical tension is very low as for the vesicle shown in Fig. 4.3.1. However, the highest tension that can be applied by the pipette is limited because the vesicle may be completely aspirated into the pipette at relatively high tension. When the tubes have very small radius, none or only part of the stored membrane can be recruited before the vesicle collapsed, and the tension regimes will be only one or two. Both cases are observed.

Knowing the initial membrane tension and the bending rigidity of the membrane, one can calculate the radius of the tubes. For the vesicle shown in Fig. 4.3.1 with the initial membrane tension $\sigma_0 = 0.0092$ mN/m and the bending rigidity $\kappa = 5.7 \times 10^{-20}$ J, the corresponding tube diameter is 110 nm (before applying tension by the pipette).

4.4 Possible implications for biological system

Tubular membrane structures of typical dimensions ranging from few microns in diameter (myelin structures) to a few tens of nanometers (also known as tethers or

nanotubes) exist widely in eukaryotes. One example is given by the smooth endoplasmic reticulum (ER), which is a tubular membranous network, see e.g. [Ducrose 1974, Alberts 1994] where the average tube diameter is on the order of 50-150 nm (in contrast, the rough ER consists of oriented stacks of flattened membrane as cisternae). The synthesis of fatty acids and phospholipids takes place in the smooth ER. The newly synthesized lipids as well as macromolecules as key enzymes and their products have to be stored in the smooth ER before they are transferred to their destinations. Folding into a tubular network is the most efficient way to store extra membrane, because such a network is characterized by a relatively small volume but significant area as compared to other geometrical surfaces. In addition, a tubular network provides the possibility for compartmentalizing various macromolecules at elevated concentration.

While the structure, purpose and functions of the smooth ER are well understood, the physical mechanism and driving forces involved in its formation and morphology remain elusive. Molecular motors are a possible participant for structuring parts of the endoplasm as they can pull out membrane tubes [Roux 2002, Koster 2003, Leduc 2004], but they require the presence of walking tracks provided by cytoskeletal filaments. Another possible participant in forcing the membrane to form protrusions is actin polymerization [Pantaloni 2001, Rustom 2004]. However, close colocalization between membrane tubes and the cytoskeleton has been observed only for limited regions of the endoplasm [Waterman-Storer 1998], and not particularly for the smooth endoplasmic reticulum, where the membrane has folded into relatively short tubes [Alberts 1994]. This suggests that the membrane restructuring in this area might have occurred according to other mechanism.

There is abundant work on tube or tube formation from cells and model membranes. Tubes have been extruded from cells or vesicles by applying an external force using either fluid drag [Hochmuth 1973, Waugh 1982, Schmidtke 2000, Dopheide 2002] gravitational forces on beads adhered to the membrane [Bo 1989], optical tweezers [Hochmuth 1996, Dimova 2002], magnetic tweezers [Heinrich 1996], or double micropipette system [Hochmuth 1982, Cuvelier 2005]. The thickness of the formed tubes was found to depend on the membrane tension and bending stiffness. The forces needed for pulling membrane tubes are in the picoNewton range. For example, forces as high as about 10 pN were found sufficient to pull out a tube from Golgi or ER membranes [Upadhyaya 2004]. In addition to single tube pulling, studies where several tubes were

pulled were also performed [Sun 2005, Huso 2007]. In all of the above-mentioned studies, external forces are required in tube formation.

A simpler mechanism can be suggested that may be involved in structuring the membrane in the smooth ER into a tubular network not involving externally applied force. Namely, the phase separation of solutions of water soluble macromolecules may provide the necessary prerequisite for membrane restructuring into tubular network. To a certain extent, the organization of the tubes at the PEG-dextran interface is observed in cells and referred to as “organized smooth endoplasmic reticulum” [Snapp 2003]. This organization has been attributed to be due to low affinity protein interactions. Similarly, the arrangement of the membrane tubules is witnessed in the presence of water soluble macromolecules; see Fig. 4.2.2.

In the smooth ER, the synthesis of new macromolecules and lipids causes drastic variations in concentration as well as requires accommodation of the newly acquired membrane area. In such a crowded environment, phase separation might occur and lead to a local composition difference. Phase separation may provide the energy needed for the formation of tubular structure.

During vesicle deflation, the acquired excess membrane formed tubes, whereby they resemble the tubular network of smooth ER. The tubes were found to coexist with the spherical vesicle under mild membrane tension, which has been predicted theoretically [Lipowsky 2005a]. They could be recruited back to the vesicle surface when the membrane was subjected to mild tensions. Producing the tubes is based on interplay between effects on the membrane spontaneous curvature, interfacial tension between the phases in the vesicle and the membrane, and the vesicle excess area. Being caused by macromolecular phase separation, as reported here, tube formation and retrieving might prove significantly to membrane storage and surface area regulation in cells. For example, drastic area and volume changes and subsequent surface adjustment in neurons may be influenced by local changes in concentration (for example cytoskeleton filament depolymerization leads to increase in monomer concentration). The latter can eventually alter the membrane-bulk interfacial tension, thus regulating the membrane reorganization. Thus, effects due to phase separation and membrane-related interfacial tensions should be considered when surface area homeostasis in cells is discussed (see for example membrane-tension hypothesis as reviewed in [Dai 1998]).

4.5 Summary

Phase separation occurs in giant vesicles enclosing PEG/dextran aqueous solution when they are exposed to hypertonic mediums. Accompanying to the polymer phase separation process, the excess membrane area, produced by the decrease of the vesicle, volume forms tubes, see Fig. 4.2.1. The energy released from the phase separation is utilized to overcome the energy barrier of the tube formation. These two processes are coupled, see Fig. 4.2.4C. Thus, the kinetics of the vesicle deflation, which influences the phase separation process, has obvious impact on tubes, e.g. the formation of the raspberry-shaped vesicle can result in the receding of tubes. These tubes are formed from a bilayer which is part of the membrane enclosing the vesicle body. The membrane in the form of tubes can be easily retracted back to the vesicle surface when the membrane tension increases, e.g. by means of micropipette, see Fig. 4.3.1. The membrane retraction from tubes requires a relatively high membrane tension. It occurs only if the membrane tension exceeds the critical tension as indicated in Fig. 4.3.2.

Tube formation can be regulated by the interfacial tension Σ_{pd} . When Σ_{pd} is small compared to $|\Sigma_{pm} - \Sigma_{dm}|$, the excess membrane forms tubes during vesicle deflation. When Σ_{pd} is big compared to $|\Sigma_{pm} - \Sigma_{dm}|$, the excess membrane is utilized to undergo morphological change in order to reduce the contact area between the two phases. When Σ_{pd} becomes bigger than Σ_{pm} and $|\Sigma_{pm} - \Sigma_{dm}|$, the tubes may be adsorbed at the interface between the PEG-rich and dextran-rich phases to form a two dimensional ordered tubular network, see Fig. 4.2.2.

Tubes, which can form and retract easily, might be relevant to membrane storage in cells. At least, tubes are an efficient way to store membrane. In Sys II, as much as 25% of the vesicle membrane can be stored in the form of tubes, see Fig. 4.2.6A. On the other hand, tubes might be relevant to surface area regulation. They can be receded under small tension perturbation, which can be caused either by an osmolarity changes in the surroundings, by a conformational change of the vesicle. Tubes can also help the cell survive under severe changes, e.g., dramatic osmolarity change in the surroundings.

Chapter 5

Morphologies of Vesicles with Internal Phase Separation

5.1 Classification of vesicle morphology

Membranes such as lipid bilayers are highly flexible and thus can easily change their shapes. The lipid membranes can be considered as elastic sheets, which can be stretched, sheared, and bent. The shear deformation relaxes by the lipid flow within the membrane due to its fluidity. The stretching of the membranes is limited because they start to rupture when the area increases by a few percentages. However, the membranes can be easily bent. The unique mechanical properties of the membrane lead to the diverse morphologies of vesicles in the low tension regime. Three types of models, namely the spontaneous-curvature model, the bilayer-coupling model and the Area-differential-elasticity (ADE) model, have been developed to describe the vesicle morphologies, as well as the shape transformation [Lipowsky 1991]. Theoretically calculated shapes were systematically compared with the experimentally observed shapes [Berndl 1990]. The bending energy is the shape-determining factor in vesicles with homogeneous membrane.

In inhomogeneous membranes, phase separation may occur depending on the temperature and the membrane composition, leading to the formation of lateral domains within the membrane. In general, the domain may have different spontaneous curvature from the membrane matrix. More important, the edge of the domain has energy that is proportional to its length. Therefore, the domain tries to attain a circular shape in order to minimize the edge energy. However, a flat circular shape does not represent the state of the lowest edge energy. As soon as the linear size of the domain exceeds a certain critical size [Lipowsky 1992], the domain must bud to further reduce the edge energy. [Jülicher 1993, Baumgart 2003] This is the so-called domain-induced budding, which is governed by line tension of the domain boundaries.

The aforementioned theories assume that the vesicle is essentially tensionless or the membrane tension is small enough to be neglected. At the high tension regime, the effects of membrane tension become relevant for the vesicle morphology. It is similar to the effect of the surface tension acting on a droplet. The membrane tension has the tendency to keep the vesicle spherical. Tension can arise from a number of factors such

as osmotic inflation, vesicle pressurization, and the formation of membrane tubes as introduced in Chapter 4.

There are abundant studies about the vesicle morphology both theoretically and experimentally. Most of them concern only the membrane. The interaction between the membrane and the solution in the vesicle interior is ignored. Actually this interaction is not important if the solution in the vesicle interior is homogeneous. However, it becomes relevant when there are two distinct phases in the vesicle interior, e.g. in the vesicle containing aqueous PEG/dextran solution. In this chapter, we will investigate this effect in detail.

Vesicles containing aqueous PEG/dextran solution have been prepared in the one-phase state. By exposing the vesicles to a hypertonic medium (deflation), phase separation is induced and the PEG-rich phase and the dextran-rich phase are formed in their interiors. The vesicles may have diverse shapes according to the interactions between the membrane and the two phases, the interfacial tension of the two phases, the excess area (the difference between the actual vesicle area and the area required to form a spherical vesicle of the same volume), the volume ratio of the two phases, and the membrane tension.

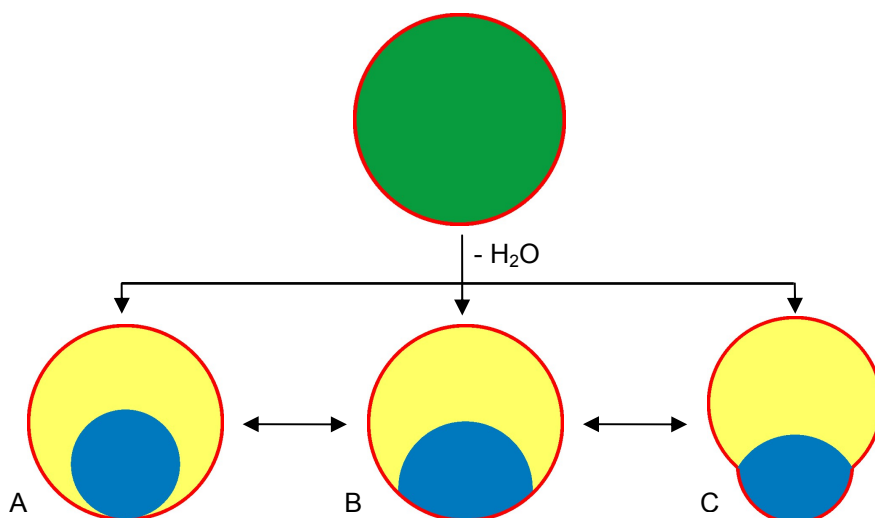


Figure 5.1.1 Morphologies observed in the deflated vesicles with two-phase system. Red presents the membrane, green presents the homogeneous polymer solution, yellow presents the PEG-rich phase, and blue presents the dextran-rich phase. A: Dewetted state. B: Wetted state. C: Budded state.

Three classes of vesicle morphologies have been observed upon osmotic dehydration as shown in Scheme 5.1.1. (A): Spherical vesicles with one phase (i.e. the PEG-rich phase) in contact with the lipid membrane, namely the dewetted state. The

name of this state is referred to the small dextran-rich phase which does not wet the membrane. (B): Spherical vesicles with both phases in contact with the lipid membrane, namely the wetted state; (C): Non-spherical vesicle in which the smaller phase (e.g. the dextran-rich phase) protrudes out of the body of the vesicle. This is called the budded state. During the deflation process, vesicles with more than one bud are observed. They are not in the stable state. The buds fuse into one after 1 or 2 hours according to the specific conditions. In rare cases, more buds may exist for tens of hours. Differing from the vesicle enclosing the homogeneous solution, not only the vesicle but also the two phases may have different configurations; Scheme 5.1.1A and B.

Due to the tether formation during the vesicle deflation process, the membrane is usually tensed. As a result, the vesicles are spheres or an assembly of spherical caps. The coexistence of the tethers and spherical caps indicates that the membrane is in the low tension regime. When the membrane fails to form tethers during the vesicle deflation process, the vesicles may attain sessile shape or dumbbell shape depending on the density difference between the vesicle interior and exterior. Furthermore, membrane fluctuations may be observed under the microscope. The membrane fluctuation indicates extremely low tension of the membrane. The vesicle morphology is similar to the vesicles containing homogeneous solution. Since the vesicles with tensionless membrane are the rare situation (less than 5%) under the experimental conditions described in chapter 2.4.1, we are not going to discuss them in this thesis.

In cases with spherical vesicles, the dextran-rich phase is always located at the bottom of the vesicle due to its higher density than the PEG-rich phase. In the vesicles at the budded state, the relative position of the dextran-rich phase in vesicles depends also on the density of the external medium. By carefully choosing the external medium, as discussed in chapter 4, we can obtain the vesicle with the configuration as shown in Scheme 5.1.1C. In the three states, the vesicles have axisymmetric shapes. Therefore, it is possible to quantitatively characterize the vesicle volume, the interfacial tensions and the contact angles under different conditions. This can help us understand the morphological evolution of the vesicles in a specific experiment.

These three states can transform between each other when one varies a certain control parameter. For example, by changing the polymer concentration, the transition from the dewetted state (Scheme 5.1.1A) to the wetted state (Scheme 5.1.2A) may occur.

This transition is called wetting transition and will be introduced in chapter 5.2. When the excess area of the vesicle increases, the vesicle may change from the wetted state to the budded state (Scheme 5.1.1C). This process is referred as budding. The details are shown in chapter 5.3.

5.2 Wetting transition in membrane compartment

Liquid droplets at interfaces may exhibit zero or nonzero contact angles corresponding to complete and partial wetting, respectively. As one varies a certain control parameter such as temperature or liquid composition, the system may undergo a transition from complete to partial wetting. Such transitions have been found and intensively studied for fluid-fluid interfaces in binary mixtures [Moldover 1980, Ross 1999, Bonn 2000] and for liquids at solid substrates [Klier 1995, Reinelt 2005]. Furthermore, liquid droplets at chemically patterned or topographically structured substrate surfaces can undergo morphological wetting transitions [Seemann 2005], which reflect the freedom of contact angles for pinned contact lines [Lipowsky 2005b]. Morphological wetting transition was introduced in the reference [Lenz 1998], and first studied experimentally in the reference [Gau 1999].

In this thesis, we provide the first experimental evidence that a transition between complete and partial wetting can also occur for an aqueous solution encapsulated within a lipid vesicle, i.e., for an aqueous solution in contact with a freely suspended lipid membrane. We recently reported this wetting transition in [Li 2008].

We encapsulate the aqueous solution PS1 (4.05% PEG and 2.22% dextran in weight fractions) within giant vesicles. 0.52% of the total dextran is labeled with fluorescein isothiocyanate. This solution is in the one-phase state at room temperature (see the phase diagram Fig. 3.1.1). Here we assume that the phase diagram is not significantly influenced by the presence of the small fraction of fluorescently labeled dextran. The vesicles are prepared in PS1 using the method of electroformation. The membrane consists of sugar-membrane (95.9% DOPC, 4.0% G_{MI} Ganglioside and 0.1% DPPE-Rhod with the membrane composition given in mole fractions).

Vesicles containing two phases are obtained by exposing them to a hypertonic medium as described in chapter 4. To eliminate the fluorescence signal outside the vesicles and to make them sediment to the bottom of the chamber, they were first diluted

in an isotonic solution containing 4.41 % PEG and 1.45 % dextran. The system was left to equilibrate for at least 2 hours after each consecutive injection.

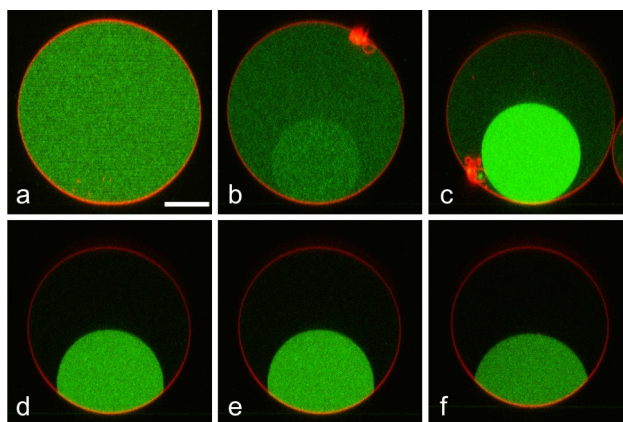


Figure 5.2.1 Confocal micrographs of a vesicle (vertical cross section), which contains a dextran-rich drop (green) undergoing wetting transition as the external osmolarity increases. From (a) to (f), the osmolarity ratio r is 1.0, 1.1, 1.4, 1.6, 1.8, and 2.0, respectively. The membrane (red) is labeled with DPPE-Rhod and the vesicle encapsulates fluorescent dextran (green). In (b)-(f), the part with more intensive green fluorescence presents the dextran-rich phase and the part with less fluorescence is the PEG-rich phase. The scale bar is $20\mu\text{m}$.

Figure 5.2.1 shows one example of such a vesicle (vertical cross section) with different polymer concentrations as observed by confocal microscopy. The first snapshot with $r = 1.0$ shows the vesicle before the phase separation occurs. As the osmolarity of the external medium increases, the polymer concentration is raised and phase separation occurs in the vesicle; Fig. 5.2.1b. The part with more intensive green fluorescence presents the dextran-rich phase and the part with less fluorescence is the PEG-rich phase. The former is heavier than the latter. Thus the spherical dextran-rich droplet is always located at the bottom of the vesicle; Fig. 5.2.1c. When the external osmolarity is further increased, $r > 1.4$, the dextran-rich phase starts to wet the membrane, see Fig. 5.2.1d, and the contact area between the dextran-rich phase and the membrane grows with increasing osmolarity ratio r ; Fig. 5.2.1d-f. The morphology change of the dextran-rich droplet indicates a wetting transition from complete wetting of the PEG-rich phase or complete dewetting of the dextran-rich phase in Fig. 5.2.1c to partial wetting in Fig. 5.2.1d-f.

In contrast to the dextran-rich droplet, the vesicle seems to remain spherical throughout the whole experiment. The volume of the vesicle decreases with increasing osmolarity. The excess area gained in this way forms a cluster of interconnected small vesicles and lipid aggregates. This cluster diffuses with the membrane and was not always located in the focal plane as in Fig. 5.2.1b and c.

By fitting the vesicle and the drop contours in the acquired images with spherical caps, one can obtain the vesicle volume and the contact angle, θ_d , between the dextran-rich phase and the membrane, see inset in Fig. 5.2.2, under different osmolarity conditions. Because the membrane is permeable only to water but not to the polymers, the number of polymer molecules inside the vesicle is fixed and the decrease of vesicle volume is due to the loss of water. Thus one can calculate the total polymer concentration in the vesicle for each osmolarity ratio r . The initial polymer concentration corresponding to $r = 1.0$, as in Fig. 5.2.1a, was considered to be the same as in the polymer solution, in which the vesicles were prepared.

The cosine of the contact angle θ_d , defines the wettability of the dextran-rich droplet on the membrane via

$$\cos(\theta_d) \equiv (\Sigma_{pm} - \Sigma_{dm})/\Sigma_{pd} \quad (5.2.1)$$

where Σ_{pm} , Σ_{dm} , and Σ_{pd} are the interfacial tensions at the interfaces between the PEG-rich phase and the membrane (pm), the dextran-rich phase and the membrane (dm), and the PEG-rich phase and the dextran-rich phase (pd). Here, the normal components of Σ_{pm} and Σ_{dm} have been neglected because the vesicle is approximately spherical. In addition, we have assumed that no long range interactions are present, which allows us to ignore the effect of the external medium. The wettability as a function of the total polymer concentration inside the vesicle is given in Fig. 5.2.2. A sharp change in the contact angle is observed for polymer concentration $\cong 8.5$ wt %, indicating a wetting transition. For contact angles larger than 170° , the error in the measured value for θ_d increases, as illustrated by the error bars in Fig. 5.2.2. This reflects the resolution limits of optical microscopy and slight deformations of the dextran-rich droplet (sessile shape) by gravity. Thus, directly from the contact angle behavior, one cannot conclude whether this wetting transition is of first or second order. No experimental techniques are aware, by which one could measure the contact angle in the present system with a higher precision. Vesicle simulations based on dissipative particle dynamics [Grafmüller 2007] may offer a possible way to reveal the order of this wetting transition.

We consider a possible mechanism involved in the observed wetting transition. When the polymer solution is close to the mixing point, namely at polymer concentration close to and above the binodal, Σ_{pd} is extremely low. It is smaller than $|\Sigma_{pm} - \Sigma_{dm}|$, which is why the dextran phase minimizes its contact with the membrane. The membrane is

fully wetted by the PEG-rich phase. Both Σ_{pd} and $|\Sigma_{pm} - \Sigma_{dm}|$ increase with increasing polymer concentration but Σ_{pd} increases faster than $|\Sigma_{pm} - \Sigma_{dm}|$. When $\Sigma_{pd} = |\Sigma_{pm} - \Sigma_{dm}|$, the wetting transition occurs, and the dextran-rich phase starts to wet the membrane. After this transition point, the wettability of the dextran-rich phase increases with the polymer concentration as shown in Fig. 5.2.2.

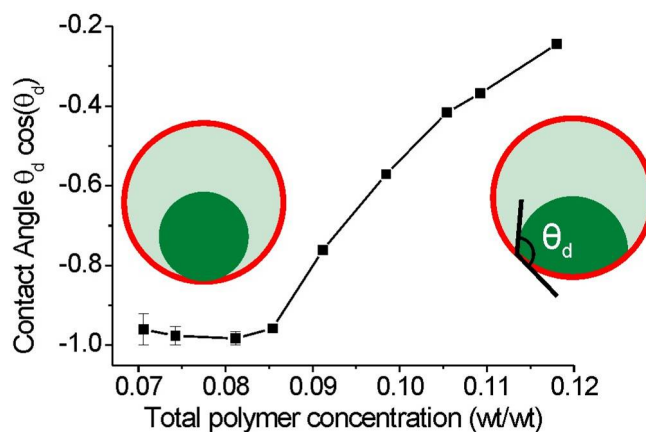


Figure 5.2.2 The cosine of the contact angle θ_d versus the total polymer concentration in the vesicle. The weight ratio between dextran and PEG is 0.55. The insets schematically illustrate the dewetted and wetted states.

In contrast to conventional surfaces (solid or bulk liquid), there is a constant water exchange through the lipid bilayer. In addition, this bilayer is rather flexible and, thus, can easily adapt its shape. In the experiments described here, this flexibility allows the membrane to deposit the excess area arising from the deflation of the vesicle in a small lipid aggregate and to keep the overall vesicle shape close to a sphere. We can then use the simplified description as given by Eq. 5.2.1 without addressing the delicate question of membrane tension, which can have several contributions arising from mechanical forces and constraints as well as from the different composition of the external and internal solution. The interfacial tensions in Eq. 5.2.1 will depend on the molecular structure of the lipid bilayer and on the interactions between the lipid head groups and the two polymer phases. Thus, these tensions can be varied by changing the membrane composition. Of particular interest would be to study wetting phenomena in vesicles containing domains of various compositions. The interfacial tensions in Eq. 5.2.1 will also be affected by the mechanical tension within the membrane, which can be manipulated by exerting an external pressure on the vesicle through a micropipette.

In our future work we want to consider additional factors, which might influence the wetting transition, such as the vesicle excess area and curvature. Having reported a

wetting transition on membranes for the first time opens the possibility to explore a number of biologically relevant systems. Wetting transitions in membrane-confined biological systems (vesicles or cells) could be used in order to locally regulate cellular processes such as protein synthesis, to restrict chemical reactions to particular segments of the membrane surface, or to stop such reactions by dewetting. In addition, the wetting transition is the first step for the budding event.

5.3 Wetting-induced budding

The flexibility of the fluid bilayer membrane allows it to undergo morphological changes easily. The bilayer can be stretched by external constraints or forces and exhibit different tension regimes. In the high tension regime below the rupture tension, the vesicles behave much like liquid droplets whose spherical shape is due to the surface tension. In the low tension regime, membranes and vesicles undergo new types of shape transformations that have not found for liquid droplets. One particular interest is the budding event. The term “budding” is often used loosely to describe the multistep process, in which a single spherical (or prolate) parent vesicle undergoes a sequence of shape changes resulting in the formation of a distinct daughter vesicle still linked to the parent via a narrow neck. [Miao 1994]

Two types of budding transition have been intensively studied in giant vesicles. The first one is referred to the budding transition in homogeneous membranes [Döbereiner 1993]. The budding transition is driven by the minimization of the bending energy [Miao 1994]. The other one is the domain-induced budding in the inhomogeneous membrane, which is driven by the minimization of the edge energy. It was theoretically predicted more than ten years ago [Lipowsky 1992, Jülicher 1993], and was experimentally confirmed by fluorescence microscopy of giant vesicles [Baumgart 2003]. In both types of transitions, budding can occur inwards or outwards depending on the area difference in the inner and outer monolayer [Miao 1994, Yanagisawa 2008].

Budding is a frequently encountered event in cells since it presents the first step in the vesicular transport, which is cycled by vesicle budding and fusion. Transport vesicles ferry molecules between different compartments. The vesicles are loaded with a cargo of molecules from the lumen of one compartment as they pinch off from its membrane. They discharge their cargo into the lumen of another compartment by fusing with its membrane. Two types of budding processes can be distinguished in cells: (i)

Endocytosis of the plasma membrane, i.e., budding of the plasma membrane towards the interior of the cell, which allows the eukaryotic cells to take up macromolecular aggregates on the cell surface; (ii) Budding of the membranes bounding internal compartments such as the endoplasmic reticulum, the stack of the Golgi cisternae, and the trans Golgi network, which can regulate the delivery of the newly synthesized proteins and carbohydrates to the exterior along the biosynthetic-secretory pathway.

Molecular crowding widely exists in the interior of cells. Phase separation might occur and lead to a local composition difference, e.g. in the lumen of the Golgi apparatus, which is full of proteins and polysaccharides. The interaction between the membrane and the phases varies according to their compositions. The membrane always likes to engulf the phase which has a higher affinity to it. The transport vesicles that bud from a compartment must take the appropriate molecules in order to perform their function properly. The phase separation can help the transport vesicle to load the appropriate molecules which are enriched in one phase. Phase separation might be the mechanism for the selective vesicular transport from lumen to lumen. Furthermore, the interaction between the membrane and the phases can be modulated by the membrane receptors, which have specific interaction with one of the components in the phases.

Vesicles containing the polymer solution have been prepared in the one-phase state. By exposing the vesicles to a hypertonic medium (deflation), phase separation was induced in their interior. Differing with the vesicle which has constant area, the volume of each coexisting phase is constant, but the interfacial area can be changed. Thus, the surface energy, which is much bigger than the bending energy and the edge energy, may become dominant in the vesicle morphology. Budding of one phase from the other phase may occur in order to reduce the surface energy between the coexisting phases, as well as the surface energy of the whole system. The budding transition of the vesicles with two-phase system may provide the insight into the physical basis of the vesicular transport of macromolecules, e.g. proteins, from lumen to lumen.

Budding transition

Giant vesicles were formed by electroformation in PS1 and PS2 (see Table 2.3.2). The vesicles with two phases were obtained through deflation, see chapter 4 for details. The system was left to equilibrate for hours after each consecutive deflation. Figure 5.3.1 shows a typical trajectory of deflated vesicles. All three states, which are schematically

shown in Scheme 5.1.1, can be observed in this deflated vesicle. Two regimes are observed in the vesicle morphological evolution.

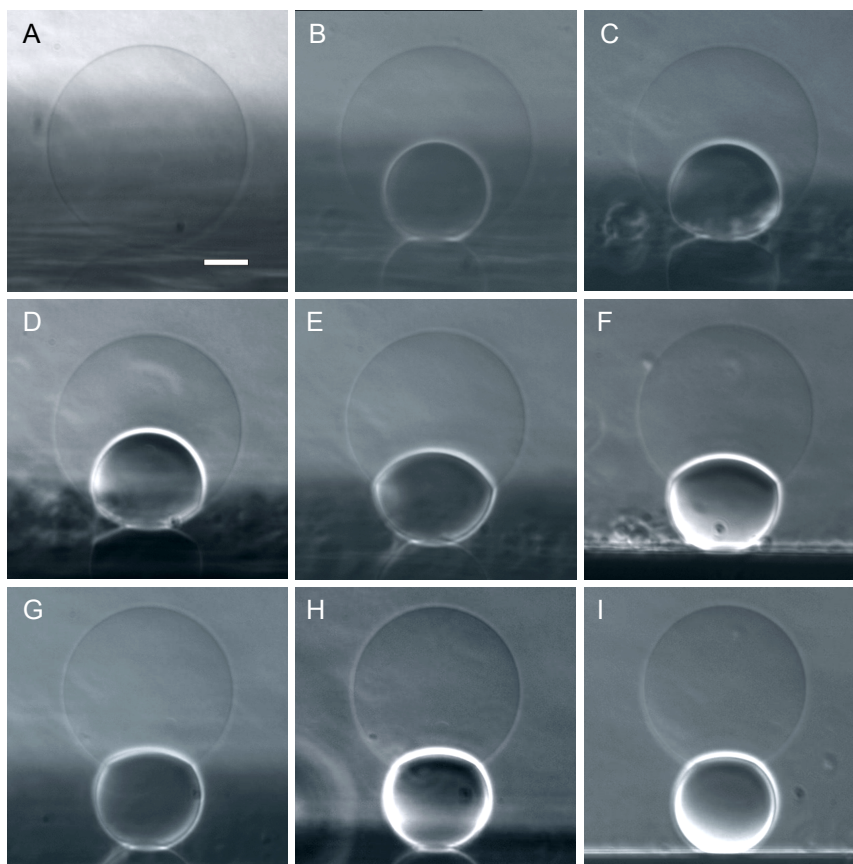


Figure 5.3.1 The vesicle morphology evolution during deflation. The snapshots are the phase contrast micrographs of a vesicle (side view observation), which contains a dextran-rich drop undergoing budding transition as the external osmolarity increases. (A): The vesicle containing the homogeneous solution at osmolarity ratio $r = 1.0$. (B): The dewetted state at $r = 1.14$. (C): The wetted state at $r = 1.24$. (D) – (I): The budding process of the dextran-rich phase. From (D) to (I), the osmolarity ratio r is 1.32, 1.39, 1.46, 1.56, 1.65, and 1.76, respectively. In (B) – (I), the small dense part is the dextran-rich phase, and the big light part is the PEG-rich phase. The system was left to equilibrate for about 2 hours after each consecutive osmolarity change. The vesicle made of sugar-membrane (see Table 2.3.1) was prepared in PS1 (Sys I). The vesicle was deflated by the addition of the HS into the observation chamber. The scale bar is 20 μm .

Figure 5.3.1A shows the vesicle before the phase separation occurs. As the osmolarity of the external medium increases, the polymer concentration is raised and phase separation occurs; Fig. 5.3.1B. In this state, both the vesicle and the dextran-rich phase are spherical. The membrane is completely wetted by the PEG-rich phase. Because the dextran-rich phase has a higher density than the PEG-rich phase (see also Fig. 3.1.3), it is always located at the bottom of the vesicle. When the external osmolarity is further increased, $r = 1.24$, the dextran-rich phase starts to wet the membrane, see Fig. 5.3.1C. The transition between the dewetted state (Fig. 5.3.1B) and the wetted state (Fig. 5.3.1C)

with respect to the dextran-rich phase is the complete-to-partial wetting transition. The details have been introduced in chapter 5.2.

After the dextran-rich phase wets the membrane, the protrusion of the dextran-rich phase becomes possible if more excess area is created by the deflation process. This process involves the morphological evolution of the vesicle and it is shown in Fig. 5.3.1D – I. When the osmolarity ratio is increased to $r = 1.32$, the dextran-rich phase slightly protrudes out of the vesicle body. The vesicle shape can be represented as an assembly of spherical caps instead of a sphere as in Fig. 5.3.1A – C. As the osmolarity ratio r increased further, a bigger part of the dextran-rich phase buds out of the PEG-rich phase. The contact area between the dextran-rich phase and the membrane increases. In contrast, the interfacial area between the dextran-rich and PEG-rich phases decreases. The morphological transition of the vesicle from the wetted state (Fig. 5.3.1C) to the budded state (Fig. 5.3.2D) is called budding transition. The budding event only occurs along the contour of the droplets in tense vesicles. If enough excess area is available, the budding will lead to the transformation of the vesicle into two daughter vesicles: one containing only the dextran-rich phase; and the other containing only the PEG-rich phase. No daughter vesicle(s) containing both phases is observed in budded tense vesicles.

Since the membrane is flexible, it may bend at the three-phase line when the vesicle starts to bud. The three-phase line appears as a circle if the vesicle is viewed from above. The three phases, namely the external medium, the PEG-rich phase and the dextran-rich phase, are in contact with each other forming the so-called contact angles as shown in the insets in Fig. 5.3.2. Note that the membrane actually separates the external medium from the dextran-rich and PEG-rich phases located in the vesicle interior. The sum of the three contact angles, namely θ_m (the contact angle of the external medium bound by the membrane), θ_p (the contact angle of the PEG-rich phase) and θ_d (the contact angle of the dextran-rich phase) is 360° . The morphology of the vesicle can be described by the three contact angles. On the other hand, the area-to-volume ratio is another parameter which may influence the final shape of the vesicle. The area-to-volume ratio can be characterized by the reduced volume ν which is the volume ratio between the vesicle volume and the volume of a sphere with the same area. It is defined as:

$$\nu = \frac{3V_v / 4\pi}{(A_v / 4\pi)^{3/2}} \quad (5.3.1)$$

Where V_v is the vesicle volume and A_v is the vesicle area. Here, only the apparent area along the vesicle contour is taken into account. The case $v = 1$ corresponds to a vesicle with spherical shape.

The axial symmetry of the vesicle makes it possible to obtain the contact angles, the vesicle area and volume by fitting the vesicle and the droplet contours with spherical caps in the acquired images, e.g., the images in Fig. 5.3.1 which show the side view of the vesicle. Thus, one can obtain the relation between the contact angles and the reduced volume under different osmolarity conditions which is shown in Fig. 5.3.2 (the red data sets). At the dewetted state, θ_m and θ_d are 180° , and θ_p is 0° , at the point $v = 1$.

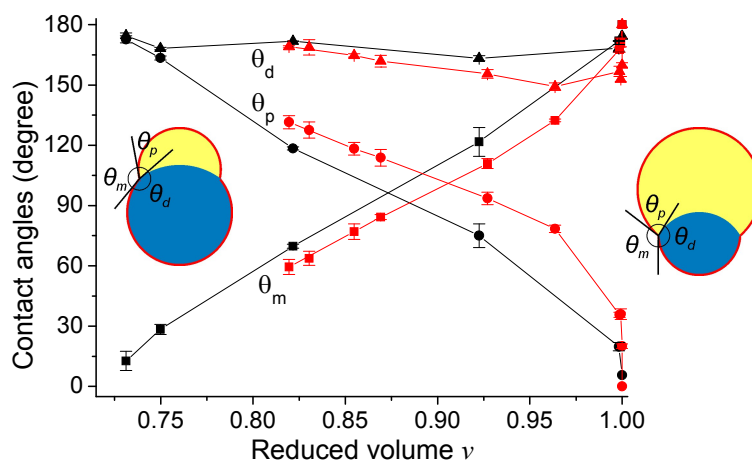


Figure 5.3.2 The contact angles θ_m , θ_p and θ_d versus reduced volume v during stepwise vesicle deflation. Note that small reduced volume means high osmolarity ratio and high polymer concentration. The insets schematically illustrate the budded states and the contact angles. Yellow presents the PEG-rich phase, blue presents the dextran-rich phase, and red presents the membrane. The red data sets are from a deflated vesicle with a big PEG-rich phase (see the right inset). The data were obtained from the images in Fig. 5.3.1B-I. The error bars indicate the difference between the maximum and minimum in three measurements on the same image. The vesicle made of sugar-membrane was prepared in PS1 (Sys I). The system was left to equilibrate for about 2 hours after each consecutive osmolarity change. The black data sets are from a deflated vesicle with a big dextran-rich phase (see the left inset). The vesicle was made of sugar-membrane and prepared in PS2 (Sys III). The system was left to equilibrate for about 4 hours after each consecutive osmolarity change. The remaining conditions are the same as for the vesicle with a big PEG-rich phase.

There are two regimes in the contact angles change with the reduced volume. In the regime with v close to one, where the vesicle is close to spherical (see images in Fig. 5.3.1B, C and D), all contact angles change rapidly with the reduced volume. In the regime with $v < 0.99$, the contact angles change linearly with reduced volume. However, θ_d does not change as much as θ_m and θ_p do in the whole range. One should note that the volume ratio of the two phases changes during the vesicle deflation.

Since the budding event occurs along the contour of the two phases, it is constrained by the volume ratio of the dextran-rich phase and the PEG-rich phase. The volume ratio may influence the contact angles and the reduced volume. For instance, the minimum reduced volume is 0.76 in case of volume ratio 1:4, and 0.72 in case of volume ratio 1:2. The minimum reduced volume is at the state where the budding is completed resulting in two daughter vesicles enclosing only one phase. These two daughter vesicles are interconnected by a microscopic neck. The contact angles of a deflated vesicle with a bigger dextran-rich phase are also shown in Fig. 5.3.2 (the black data sets). The tendency of the contact angle changes is similar as the one in vesicles with bigger PEG-rich phase. However, the contact angles are quite different at the same reduced volume due to the volume ratio difference of the two phases.

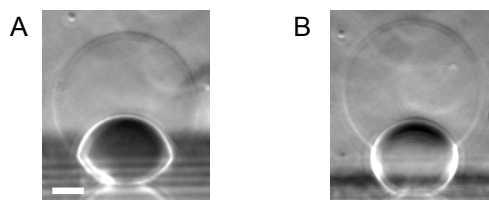


Figure 5.3.3 The effect of excess area on the vesicle morphology. A: A vesicle with less excess area B: The same vesicle with more excess area. The images (A) and (B) are the side view of the vesicle. The vesicle was aspirated into a micropipette, and then released. Image (A) shows the vesicle before aspiration. Image (B) was taken after the vesicle was released from the pipette. The exerted tension led to the recruitment of membrane from the tethers back to the vesicle surface (see chapter 4.3). The dense part is the dextran-rich phase and the light part is the PEG-rich part. The vesicle was made of sugar-membrane and prepared in PS1 (Sys I), and exposed to a hypertonic solution to obtain the vesicle with two phases. The scale bar is 20 μm

In both cases shown in Fig. 5.3.2, the vesicles are spherical before they are deflated ($\theta_m = 180^\circ$). When budding occurs, the membrane bends toward the vesicle interior. As a result, θ_m starts to decrease towards 0° when the vesicle buds into two daughter vesicles. At the same time, θ_p increases towards 180° from 0° (if the dewetted state exists in the vesicle deflating trajectory). The behaviour of θ_d is quite different. Chapter 5.2 shows that as the polymer concentration increases, the wettability of the dextran-rich phase on the membrane increases in the wetted state. In other words, θ_m decreases with increasing osmolarity ratio r . θ_d has the same tendency when the vesicle is approximately spherical. However, θ_d starts to increase when the reduced volume become smaller. This means that the excess area also plays an important role on the vesicle morphology in the budded state. One will expect increasing θ_d when the excess area increases. Figure 5.3.3 shows such an example.

As introduced in chapter 4, part of the membrane is stored in the form of tethers during the vesicle deflation (note that the excess area as described by the reduced volume ν does not include the membrane area stored as tethers). The stored membrane can be easily recruited back to the vesicle surface when the membrane tension increases, i.e., by apply a pressure on the vesicle through micropipette. The recruited membrane is used to perform budding spontaneously after the vesicle is released from the pipette; Fig. 5.3.3B. This probably implies that one of the states in Fig.5.3.3 is not in equilibrium. θ_m becomes bigger after the pressurization, and the dextran-rich phase protrudes further from the PEG-rich phase. The volume of the vesicle does not change after the pressurization, which implies that there is no change in the droplets polymer concentration and respectively constant interfacial tensions before and after the pressurization. The morphological change is due to the change of the membrane area on the vesicle surface, which is reflected by the area-to-volume ratio.

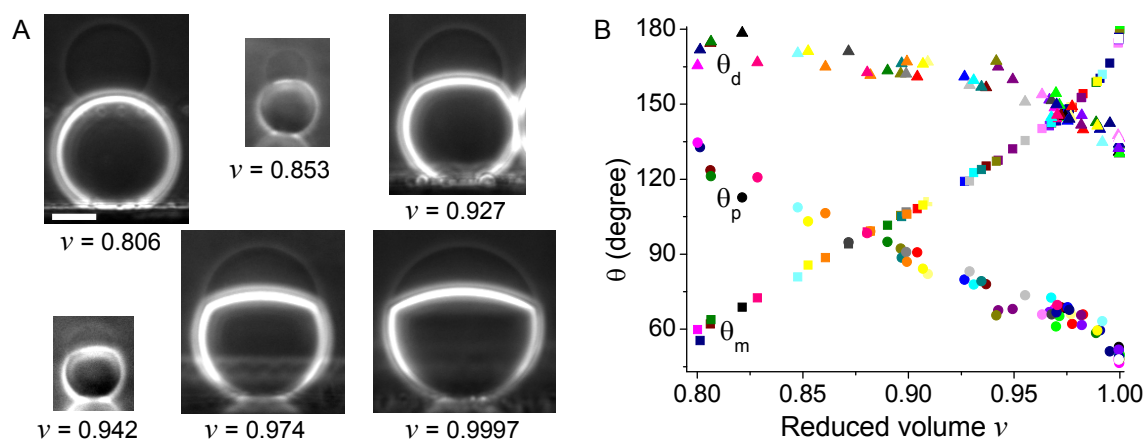


Figure 5.3.4 The vesicle morphologies in a hypertonic solution. (A): Phase contrast images (side view observation) of different vesicles. The big dense part is the dextran-rich phase and the small light part is the PEG-rich part. All images have the same magnification. The scale bar is 20 μm . (B): Contact angles θ_m , θ_p , and θ_d at different reduced volumes ν obtained from 64 vesicles. Contact angles θ_m , θ_p , and θ_d are presented by squares, dots and triangles, respectively. The contact angles obtained from different vesicles are presented with different colours. The vesicles made of sugar-membrane were prepared in PS2 (Sys III). The vesicles were deflated through the addition of the HS into the external solution in the observation chamber. The osmolarity is increased 48%. The system was left to equilibrate for 21 hours.

Budding event has been observed in vesicles with different sizes in the range from 200 μm to a few micrometers. However, the vesicles have diverse shapes even if they are prepared in the same batch and deflated through the same procedures. Several examples are shown in Fig. 5.3.4A. Both phases wet the membrane in these vesicles, but the degree of the budding are different due to their differences in the area-to-volume ratio,

which is characterized by the reduced volume, although the volume ratio of the coexisting phases is approximately the same in the vesicles shown in Fig. 5.3.4A.

By fitting the vesicle and drop contours in the acquired images, one can obtain the contact angles in each vesicle. The results are shown in Fig. 5.3.4B. Since the deflation process is not followed for each vesicle after the addition of the hypertonic solution, it is not clear if budding and fission of small vesicles to the vesicles occur due to the convection introduced by the addition of the hypertonic solution. The budding and fission of small vesicles will lead to a change in the total polymer concentration in the analyzed vesicles. The volume ratio of the PEG-rich phase and dextran-rich phase, which can be directly measured, can be used as an indicator of the polymer concentration in each specific vesicle. Therefore, the data shown in Fig. 5.3.4B are from vesicles with the volume ratios of the PEG-rich phase and the dextran-rich phase in the limited range from 0.722 and 0.777 with the average value 0.750. These vesicles are considered to contain solutions with similar polymer concentration.

The change of the contact angles as a function of the reduced volume in Fig. 5.3.4B has the same tendency as the one in Fig. 5.3.2 (the black data sets). The data shown in Fig. 5.3.4B are from different vesicles but containing solutions with the same total polymer concentration. In other words, the compositions of the coexisting phases in the vesicle interior are the same although they belong to different vesicles. From thermodynamical point of view, the three interfacial tensions, which present the energy densities at the interfaces, have the same values in the different vesicles because the energy density depends only on the compositions. However, the three contact angles are quite different in the vesicles with different reduced volumes. It is impossible to always have the interfacial tensions balanced at the three-phase line when their directions change, but not their values. This implies that there must be other contributions to the force balance on the three-phase line besides the interfacial tension arising from the surface energy. Another proof is the morphological change in the vesicle with changes in excess area as shown in Fig. 5.3.3.

Force balance at three-phase contact line

In the vesicles shown in Fig. 5.3.1, 3 and 4, the dextran-rich phase, the PEG-rich phase and the external medium, by which the vesicle is surrounded, meet at the so-called three-phase line. At equilibrium, the net force on any place of the three-phase line

vanishes. In other words, the tensions of the three interfaces, namely Σ_{pd} (PEG-rich phase – dextran-rich phase), σ_{pm} (PEG-rich phase – external medium) and σ_{dm} (dextran-rich phase – external medium) are mechanically balanced on the three-phase line; Fig. 5.3.5A. The force balance at the three-phase line can be described by the Neumann's equations (Eq. 1.5.2) together with the contact angles θ_m , θ_d and θ_p with the sum of 360° . Neumann's equations are a dependent set of equations for the tensions. They determine the ratio of the tensions rather than the tensions themselves in terms of the contact angles.

By fitting the vesicle and the drop contours in the acquired images in Fig. 5.3.1 with spherical caps, the contact angles θ_d , θ_p , and θ_m , have been obtained under different osmolarity conditions, see the red data sets in Fig. 5.3.2, as well as the vesicle volumes. Because the membrane is permeable only to water but not to the polymers, the number of polymer molecules inside the vesicle is fixed and the decrease of vesicle volume is due to the loss of water. Thus, one can calculate the total polymer concentration in the vesicle for each osmolarity ratio r . The initial polymer concentration, corresponding to $r = 1.0$ as in Fig. 5.3.1A, is considered to be the same as in the polymer solution, in which the vesicles were prepared. After knowing the polymer concentrations enclosed in the vesicle, one can prepare bulk solutions with the same polymer concentrations, and measure the tensions at the interface between the coexisting dextran-rich and PEG-rich phases. Therefore, the Neumann's equation can be solved.

Figure 5.3.5B shows the tensions σ_{pm} and σ_{dm} at the three-phase line obtained by solving the Neumann's equations, as well as the interfacial tension Σ_{pd} , which is measured in bulk polymer solution. The interfacial tension Σ_{pd} increases with increasing total polymer concentration. The measured values of Σ_{pd} are consistent with the experimental result in similar systems (same polymers and solvent, but different molecular weights and concentrations) [Forciniti 1990]. However, the behavior of the tensions σ_{pm} and σ_{dm} are significantly different from that of Σ_{pd} . They do not change monotonically with the total polymer concentration as Σ_{pd} does. In the beginning, both σ_{pm} and σ_{dm} are higher than Σ_{pd} . As the total polymer concentration increases, or in other words, as the vesicle is further deflated, both tensions decrease. After they reach their minima, they start to increase again. Their difference $|\sigma_{pm} - \sigma_{dm}|$ is always smaller than Σ_{pd} in the whole range. The abnormal behaviors of the tensions σ_{pm} and σ_{dm} imply the

existence of other contribution(s) to the force balance at the three-phase line besides the thermal dynamic interfacial energy.

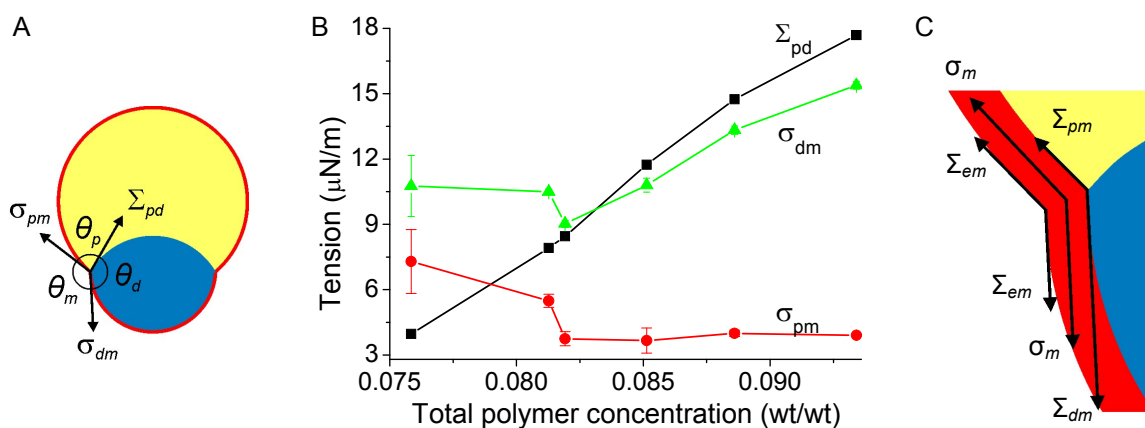


Figure 5.3.5 The force balance at the three-phase line. (A): Schematic illustration of the tensions at the three-phase line and the contact angles. Red presents the membrane, yellow presents the PEG-rich phase, blue presents the dextran-rich phase, and white presents the external medium. (B): The three tensions in the vesicle with different total polymer concentrations. The data from left to right are corresponding to the image D – I in Fig. 5.3.1. Higher concentration means higher osmolarity ratio r . The error bars show the errors introduced by the contact angles. (C): Decomposition of the tensions σ_{pm} and σ_{dm} at the three-phase line. The cartoon is only a schematic illustration. The tensions are not in scale.

The PEG-rich phase is in direct contact with the dextran-rich phase in the vesicle interior. The thermodynamic surface energy density (characterized by the surface energy density J/m^2) is equivalent with the mechanical description (characterized by the surface tension N/m) at this interface. In contrast to the interfacial tension Σ_{pd} , the tensions σ_{dm} and σ_{pm} , which are schematically illustrated in Fig. 5.3.5C, have several contributions. The membrane separates the external medium from direct contact with the two phases enclosed in the vesicle interior. Thus, three interfaces form at the membrane surface and can be characterized by the interfacial tensions Σ_{pm} (PEG-rich phase – membrane), Σ_{dm} (dextran-rich phase – membrane) and Σ_{em} (external medium – membrane). In addition, the elasticity of the membrane allows it to bend and/or to be stretched in response to the stimuli, such as the interfacial tension Σ_{pd} . The membrane can be easily bent, but hard to be stretched. The flexibility of the membrane allows the tension σ_{dm} and σ_{pm} to change their directions. However, the bending energy of the membrane is much smaller than the stretching energy. The contribution of the bending energy to the vesicle morphology can be neglected if the stretching energy is considered. The stretching of the membrane leads to the increase of the membrane tension.

Another possible contribution to the tensions σ_{dm} and σ_{pm} are the interactions between the internal phases and the external phase. The thickness of the hydrophobic core region in the bilayer formed by DOPC is 2.7 nm [Lee 2003]. The final thickness of the bilayer is about 4 ~ 5 nm depending on the headgroups (note that we have used lipids with modified headgroups in this work). The molecules in the vesicle interior and exterior are kept far enough by the membrane from interacting with each other. The cutoff distance is usually 1.4 nm for the long-range interactions in simulations [Oostenbrink 2004], which means that the interaction between two molecules or particles are negligible when the distance between them is larger than 1.4 nm. Therefore, the interactions between the vesicle interior and exterior can be ignored. The tensions σ_{dm} and σ_{pm} are coupled quantities arising from the mechanical stretching of the membrane and the thermodynamic interfacial energy between the membrane and the phases; Fig. 5.3.5C.

After knowing the origins of the tensions, one can explain the abnormal behaviour of σ_{dm} and σ_{pm} in Fig. 5.3.5B. The decrease in the low concentration or osmolarity region is mainly caused by the decrease in the membrane tension σ_m . This can be proved by the vesicle pressurization through micropipette which allows the manipulation of the membrane tension externally.

Vesicle aspiration

The elasticity of the membrane allows it to be stretched and thus, produce a lateral tension. This tension is a component in the σ_{dm} and σ_{pm} . When the lateral tension changes, it may cause morphological change in the budded vesicles with two phases in order to keep the force balance at the three-phase line. Figure 5.3.6A shows such an example. Before the pressurization, most of the dextran-rich phase has protruded far out of the PEG-rich phase; Fig. 5.3.6A(1). When the pressure inside the micropipette decreases, the vesicle is aspirated into the micropipette. The pressure difference in and out of the pipette results in an increase in the membrane tension which can be calculated using Eq. 2.5.2. The effect of gravity is neglected in the calculation due to the insignificant density difference between the interior and exterior of the vesicle. As the membrane tension increases, the vesicle is lifted up from the bottom of the chamber, see Fig. 5.3.6A(2), and the protruded dextran-rich phase is forced back into the PEG-rich phase (as reflected by the contact angle θ_p). At the same time, the vesicle part aspirated

inside the pipette increases only a little bit. At relatively high membrane tension, the vesicle part out of the pipette becomes approximately spherical ($\theta_m \approx 180^\circ$); Fig. 5.3.6A(5) and (6).

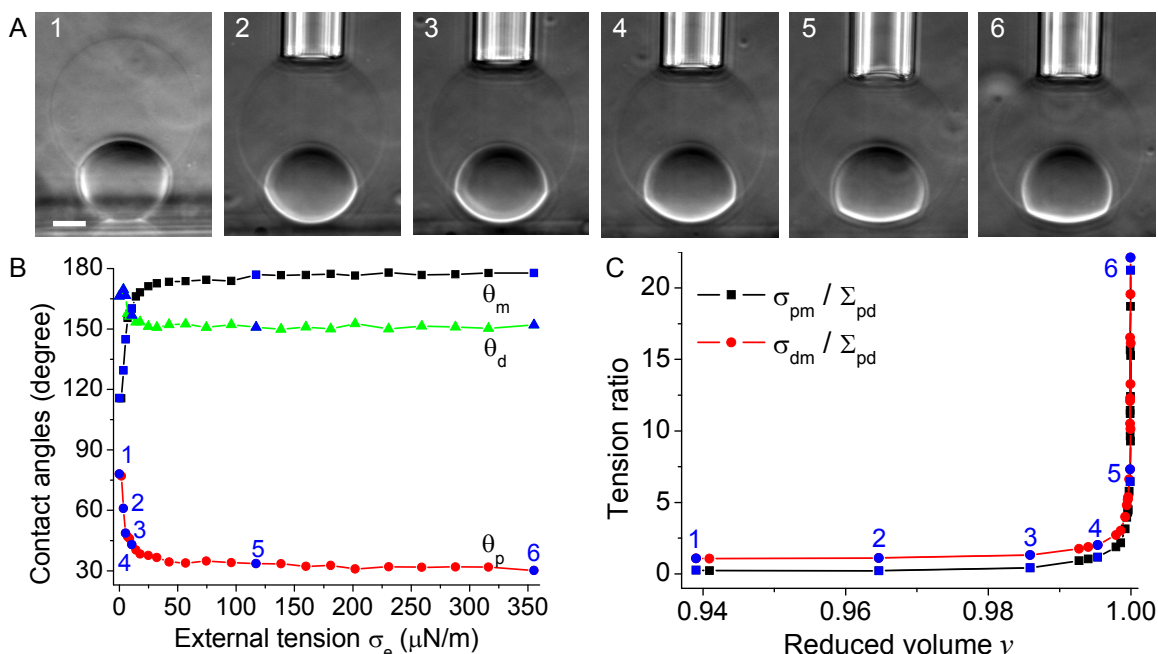


Figure 5.3.6 The withdrawal of the budded dextran-rich phase in an aspirated vesicle. (A) Phase contrast images (side view observation) of the vesicle under different tensions. The small dense part is the dextran-rich phase, and the big light part is the PEG-rich phase. The scale bar is 20 μm . (B) The contact angles changing with the applied tension σ_e . (C) The tension σ_{pm} and σ_{dm} versus the reduced volume. They are in the unit of Σ_{pd} . The data from left to right in (B) and (C) are obtained from the same set of images. The blue associated symbols numbered from (1) to (6) in (B) and (C) present the data obtained from images (1) to (6) in (A), respectively. The vesicles made of sugar-membrane were prepared in PS1 (Sys I). They were first diluted in the IS. Then the osmolarity of the external medium was increased by 32% by the addition of the HS. The system was left to equilibrate for about one day.

The increase of the membrane tension σ_m leads to the increase of the tension σ_{dm} and σ_{pm} , but it does not influence the interfacial tension Σ_{pd} . Σ_{pd} may change if the phase equilibrium is broken during the vesicle pressurization. Three parameters may influence the phase behaviour of the polymer solution in the vesicle interior, namely the temperature, the total polymer concentration, and the pressure. The vesicle pressurization is performed at constant temperature (24 $^\circ\text{C}$). The total polymer concentration in the solution enclosed in the vesicle interior may change due to the water exchange across the membrane under external stimuli because the membrane is only permeable to water molecules but not to polymer molecules. The volume of the vesicle remains constant during the pressurization, which indicates that there is no net water flow across the membrane, and thus, indicates constant total polymer concentration. The increases of the

membrane tension will lead to a higher pressure in the vesicle interior, e.g., the pressure increases 25 Pa when the membrane tension increases 500 $\mu\text{N/m}$ in a vesicle with radius 40 μm . The increment of the pressure is too small to affect the phase equilibrium of the polymer solution.

Therefore, the force balance at the three-phase line is broken by the increased tensions σ_{dm} and σ_{pm} . The flexibility of the membrane allows the three tensions (Σ_{pd} , σ_{dm} and σ_{pm}) to change their directions through membrane bending in order to achieve the force balance at the three-phase line again. The change of the contact angles with the external tension, which is the tension exerted through the pipette, is shown in Fig. 5.3.6B.

For low external tension, the contact angles θ_m , θ_d and θ_p change significantly with external tension. The external tension induces a notable morphological change. For higher external tension, the changes of the contact angles become less pronounced. When the external tension is higher than 100 $\mu\text{N/m}$, no effect is observed. In this regime, θ_m approaches 180°. The vesicle part out of the pipette is approximately spherical. At the same time, the corresponding θ_p decreases insignificantly with external tension. The changes in θ_m and θ_p are counter-balanced, resulting in constant contact angle θ_d with external tension. In this regime, the value of θ_d presents the intrinsic contact angle, which means that the cosine of θ_d describes the wettability of the dextran-rich phase on the membrane.

Knowing the contact angles and using the Neumann's equations, one can determine the ratio of the tensions, which can be described in the unit of the interfacial tension Σ_{pd} because it does not change during the vesicle pressurization. From the vesicle geometry obtained from the image analysis, one can also obtain the area and volume of the vesicle under different external tension, as well as the reduced volume. Fig. 5.3.6C shows the tensions σ_{dm} and σ_{pm} as a function of the reduced volume. Since the part of the vesicle in the pipette is very small ($< 4\%$ in volume) for the vesicle shown in Fig. 5.3.6, it is not included in the reduced volume calculation. More important, the reduced volume calculated in this way is equivalent to the one of vesicles without micropipette.

The interfacial tension Σ_{pd} pulls the membrane towards the vesicle interior. Its normal component is counterbalanced by the normal parts of σ_{dm} and σ_{pm} . As the reduced volume increases, the contact angle θ_d decreases and leads to the increase of the normal component of Σ_{pd} . Thus, σ_{dm} and σ_{pm} have to increase in order to balance Σ_{pd} ; Fig. 5.3.6C.

Their increments stem from the increased membrane tension induced by the pressure difference in and out of the micropipette. On the other hand, the increased reduced volume leads to increase in the contact angle θ_m , and consequently smaller normal components of σ_{dm} and σ_{pm} . Therefore, high tensions σ_{dm} and σ_{pm} are required to balance Σ_{pd} when the reduced volume is close to one; Fig. 5.3.6C.

Discussion

The free energy of the vesicles with two phases includes three components: the bending energy of the membrane, the stretching energy of the membrane, and the surface energy. The bending energy is very small compared to the stretching energy. In tense giant vesicles such as those shown in this thesis, its contribution to the free energy can be neglected. The stretching can be characterized by the membrane tension. The surface energy has contributions from the four interfaces, namely the interface between the dextran-rich phase and the PEG-rich phase, the interfaces between the membrane and the phases in the vesicle interior and exterior. They are characterized by their interfacial tensions: Σ_{pd} , Σ_{dm} , Σ_{pm} and Σ_{em} . The equilibrated morphology of the vesicles with two phases is determined by the surface energy and the stretching energy.

In a two-phase vesicle with fixed volume and area, the surface energy between the membrane and the external medium does not change with the vesicle morphology due to the constant membrane area. The separation of the dextran-rich phase from the PEG-rich phase through budding event can significantly reduce the surface energy of their interface by reducing the area of the interface. In addition, the stretching energy of the membrane decreases with the membrane tension, which has been confirmed by the vesicle pressurization; see Fig. 5.3.6C. Therefore, the budding of the small phase from the vesicle body is energetically favoured.

However, the budding of one phase from the vesicle body does not always occur in the vesicles with two phases. No budding event is observed in the vesicles made of PEG-membrane (95.9% DOPC, 4.0% DOPE-PEG200 and 0.1% DPPE-Rhod in mole fractions) during the vesicle deflation under the same conditions as in the vesicle shown in Fig. 5.3.1. The membrane is only wetted by the PEG-rich phase due to their low interaction. Budding of the dextran-rich phase is only observed in vesicles where both phases are in contact with the membrane. In such vesicles, Σ_{pd} is bigger than $|\Sigma_{pm} - \Sigma_{dm}|$. The energy cost by the increased contact area between the membrane and the dextran-

rich phase is smaller than the energy lost by the decreased interface area between the dextran-rich and the PEG-rich phases. Therefore, the precondition for the budding transition is that Σ_{pd} must be bigger than $|\Sigma_{pm} - \Sigma_{dm}|$. In morphological terms, the membrane has to be wetted by both phases. In such vesicles, budding of one phase occurs spontaneously if more membrane is available, see Fig. 5.3.3. We did not consider the effect of the line tension of the three-phase line.

The budding of the vesicles with two phases is mainly governed by the surface energy in the budded state and modulated by the membrane tension. The membrane can automatically adjust its tension to restore the force balance at the three-phase line after the morphological change. The membrane tension can be increased to tens of mN/m before it ruptures. Therefore, the membrane tension is able to balance the pulling of the interfacial tension Σ_{pd} which is extremely low (in the order of $\mu\text{N/m}$ or even lower); Fig. 5.3.5B. Due to the existence of the membrane tension, the mechanical balance is not equivalent to the thermodynamic balance at the three-phase line. The cosine of the contact angles θ_d can not be utilized to describe the wettability of the dextran-rich phase on the membrane during the budding process.

The shape of the vesicle at the budded state can be characterized using the area-to-volume ratio with the constraint on the volume ratio of the two phases. The vesicles may have diverse shapes according to their differences in the area-to-volume ratio even if they are prepared in the same batch and deflated with the same conditions; Fig. 5.3.5. The area-to-volume ratio in deflated vesicles highly depends on the kinetic of the tether formation. The details were introduced in Chapter 4.

Chapter 6

Conclusion and Outlook

In this work, the phase separation of dextran/PEG aqueous solution loaded in giant vesicles has been studied through dehydration, i.e., by exposing vesicles to hypertonic solutions. The loss of water leads to a polymer concentration quench in the vesicle interior, and thus, induces phase separation, which may take place through either spinodal decomposition or nucleation and growth. When the concentration quench ends up sufficiently for inside the two-phase region, the phase separation takes place through spinodal decomposition. Otherwise it occurs through nucleation. The depth of the concentration quench can be controlled by the osmotic pressure changes in the external medium. The new phase may form at the membrane or/and in the vesicle interior depending on the interactions between the membrane and the coexisting phases. There are three stages in the dynamics: the formation and coarsening of the spinodal network of droplets or the nucleation and growing of droplets, the gravity (or buoyancy)-driven flow of the newly formed phase, and the formation of the sharp mesoscopic interface. The dynamics of the phase separation is discussed in details in Chapter 3.2.

As described in Chapter 4, the phase separation process within the vesicle leads to the formation of membrane tubes (or tethers), an unexpected process that has been observed in this study for the first time, see Fig. 4.2.1 and Fig. 4.2.4. Tube formation has been found to be a common phenomenon in deflated vesicles loaded with two-phase system such as dextran/PEG aqueous solution. The energy released from the phase separation is utilized to overcome the energy barrier for the tube formation. These two processes are coupled. The kinetics of the vesicle deflation, which influences the phase separation process, has obvious impact on tubes, e.g. the formation of the raspberry-shaped vesicle (see Fig. 4.2.5B) can cause receding of the tubes. By applying a tension by means of micropipette, the membrane stored in the form of tubes can be withdrawn back to the vesicle surface (see Fig. 4.3.1), which means that the tubes are formed from a bilayer, which is part of the membrane enclosing the vesicle body.

The tube formation can be regulated by the interfacial tension Σ_{pd} , Σ_{dm} and Σ_{pm} . When Σ_{pd} is small compared to $|\Sigma_{pm} - \Sigma_{dm}|$, the excess membrane forms tubes during

vesicle deflation. When Σ_{pd} is big compared to $|\Sigma_{pm} - \Sigma_{dm}|$, the excess membrane is utilized to undergo a morphological change in order to reduce the contact area between the two phases. When Σ_{pd} is bigger than Σ_{pm} and $|\Sigma_{pm} - \Sigma_{dm}|$, the tubes may be adsorbed at the interface between the PEG-rich and dextran-rich phases to form a two dimensional ordered tubular network, see Fig. 4.2.2. In addition, the membrane tension plays an important role on tubes. High membrane tension may forbid tubes to form, and even lead to the receding of existing tubes.

Tubes might be relevant to membrane storage in cells. At least, they are an efficient way to store membrane. As much as 25% of the vesicle membrane can be stored in the form of tubes in the deflated vesicles, see Fig. 4.2.6A. The smooth ER, where the lipids are synthesized, is a tubular membranous network. The membrane tubes can recede under small tension perturbation which can be caused either by osmotic swelling, by morphological changes (e.g. the formation of a raspberry-shaped vesicle), or by applying an external pressure. Therefore, membrane tubes, which can form and recede easily, might be relevant to surface area regulation in cells. Many cells, including growing neurons, undergo rapid volume and surface area change. The increased volume needs more membrane area in order to release the tension. This requires a rapid exchange of membrane between the surface and the internal stores. Tubes might be the internal storage points, from which the membrane can be recruited easily.

As described in Chapter 5, the two liquid phases formed within the vesicles may exhibit partial to complete wetting of the membrane. The interactions between the membrane and the two coexisting phases, which can be described by their interfacial tensions, can affect the morphologies of the two phases enclosed in the vesicle. When the interfacial tension Σ_{pd} is smaller than $|\Sigma_{pm} - \Sigma_{dm}|$, the membrane is only wetted by the phase with a smaller interfacial tension, i.e., the PEG-rich phase in the systems discussed in this work. When Σ_{pd} is bigger than $|\Sigma_{pm} - \Sigma_{dm}|$, the membrane is wetted by both phases. By increasing the polymer concentration enclosed in the vesicles, the transition from complete dewetting of the dextran-rich phase or complete wetting of the PEG-rich phase to partial wetting may occur. Having reported a wetting transition on membranes for the first time, opens the possibility to explore a number of biologically relevant systems. Wetting transitions in membrane-confined biological systems (vesicles or cells) can be used to locally regulate cellular processes such as protein synthesis, to restrict

chemical reactions to particular segments of the membrane surface, or to stop such reactions by dewetting. The wetting transition of the dextran-rich phase on the membrane is discussed in detail in Chapter 5.2, see Fig. 5.2.1.

One of the two phases may protrude out of the vesicle body (budding) when the membrane is in contact with both phases, which is called wetting-induced budding. In such vesicles, the interfacial tension Σ_{pd} is bigger than $|\Sigma_{pm} - \Sigma_{dm}|$. The energy gained by the increased contact area of the membrane with the dextran-rich phase is smaller than the energy lost by decreasing the interface area between the two liquid phases. Budding of one phase can minimize the surface energy of the vesicle, and thus, occurs spontaneously if more excess membrane area is available.

In vesicles with both phases wetting the membrane, the thermodynamic description of the surface energy is not equivalent to the mechanical description of the force balance at the three-phase line due to the existence of the membrane tension. The equilibrium morphology of vesicles with two phases is governed by the surface energy and modulated by the stretching energy. The surface energy is a superposition of the energy from the four interfaces, which can be characterized by their interfacial tensions: Σ_{pd} , Σ_{dm} , Σ_{pm} and Σ_{em} . The separation of the dextran-rich phase from the PEG-rich phase through budding event can significantly reduce the surface energy of their interface by reducing the area of the interface. The morphological change of the vesicle breaks the force balance at the three-phase contact line. However, the membrane can automatically adjust its tension to restore the force balance at the three-phase contact line, which is possible due to the elasticity of the membrane. The membrane tension can be increased to tens of mN/m before it ruptures. The membrane tension is capable to balance the pulling of the interfacial tension Σ_{pd} , which is of the order of $\mu\text{N/m}$ or even lower. In fact, the stretching energy of the membrane is also reduced via budding event by reduced membrane tension, which was demonstrated by the micropipette aspiration experiments; see Fig. 5.3.6. Therefore, the wetting-induced budding is energetically favoured.

The shape of the vesicle at the budded state can be characterized using the area-to-volume ratio with the constraint of the volume ratio of the two phases. The vesicles may have diverse shapes according to their differences in the area-to-volume ratio even if they are prepared in the same batch and deflated with the same conditions. The vesicle apparent area highly depends on the process of the deflation due to the tube formation.

The membrane receding from tubes requires a relatively high membrane tension as indicated by the critical external membrane tension applied by the pipette in Fig. 4.3.2. This critical tension limits the utilization of the membrane stored in the form of tubes. The pulling of the low interfacial tension Σ_{pd} at the three-phase contact line can not induce a sufficiently high membrane tension to recruit the membrane to the vesicle surface from the tubes. The budding event is discussed in detail in Chapter 5.3.

Budding is a frequently encountered event in cells. For example, it presents the first step in the vesicular transport, which is cycled by vesicle budding and fusion. The phase separation, which results in the sorting of macromolecules by forming two distinct phases, can help the transport vesicle to load the appropriate molecules, which are enriched in one phase. Phase separation might be the mechanism for the selective vesicular transport from lumen to lumen in cells. Furthermore, the interaction between the membrane and the phases can be modulated by the membrane receptors, which have specific interaction with one of the components in the phases.

In future studies, of particular interest will be the behaviour of deflated vesicles containing two liquid phases and bounded by membranes that contain domains of various compositions. The formation of membrane tubes may be affected by the composition of the membrane domains, which have different bending rigidity. Furthermore, the wetting transition and the budding transition may be affected by the existence of the different domains. In addition, vesicles with two phases can be used to study the motion of the solution in the vesicle interior induced by the moving of the membrane, e.g. in an alternating electric field [Staykova 2008] or hydrodynamic flows [Abkarian 2008].

The interactions between the membrane and the two liquid phases play an important role on the dynamics of the phase separation. The growth of the new phase may take place in the vesicle interior and/or in contact with the membrane. It will be interesting to study the phase separation occurring only at the membrane, which can be achieved by controlling the membrane composition or/and the depth of the concentration quench.

List of Abbreviations

ADE	Area-difference elasticity
ATPS	Aqueous two-phase system
CP	Critical point
dextran-FITC	Fluorescein isothiocyanate-dextran
DIC	Differential interference contrast
DOPC	1,2-dioleoyl- <i>sn</i> -glycero-3-phosphocholine
DOPE-PEG2000	1,2-dioleoyl- <i>sn</i> -glycero-3-phosphoethanolamine-N-[methoxy-(polyethylene glycol)-2000]
DOPE-rhod	1,2-dioleoyl- <i>sn</i> -glycero-3-phosphoethanolamine-N-(lissamine rhodamine B sulfonyl)
DOPS	1,2-dioleoyl- <i>sn</i> -glycero-3-[phospho-L-serine]] (sodium salt)
DOPS-membrane	27.94% DOPS, 71.98% DOPC and 0.07% DOPE-rhod in mole ratio
DSPE-PEG-CF	1,2-distearoyl- <i>sn</i> -glycero-3-phosphoethanolamine-N-[poly(ethylene glycol)2000-N'-carboxyfluorescein]
DPPC	1,2-Dipalmitoyl- <i>sn</i> -Glycero-3-Phosphocholine
DPPE-Rhod	1,2-dipalmitoyl- <i>sn</i> -glycero-3-phosphoethanolamine-N-(lissamine rhodamine B sulfonyl)
Dvl	Dishevelled protein
ER	Endoplasmic reticulum
GPC	Gel permeation chromatography
G _{MI} Ganglioside	galbeta1-3galnacbeta1-4(neuacalpha2-3)galbeta1-4glcbeta1-1'-cer
HS	Hypertonic aqueous solution consisting of 3.27% sucrose, 3.92% PEG, 2.14% dextran.
IS	Isotonic aqueous solution consisting of 4.41% PEG and 1.45% dextran
ITO	Indium tin oxide
LCST	Lower critical solution temperature
PEG	Poly (ethylene glycol)
PEG-membrane	4.00% DOPE-PEG2000, 95.93% DOPC and 0.07% DPPE-rhod in mole ratio
PS	Polymer solution
PS1	Polymer aqueous solution with 2.22% dextran and 4.05% PEG

PS2	Polymer aqueous solution with 7.44% dextran and 2.10% PEG
sugar-membrane	4.00% G _{M1} ganglioside, 95.93% DOPC and 0.07% DPPE-rhod in mole ratio
UCST	Upper critical solution temperature

List of Symbols

A	Area, apparent area
A_{dm}	The area of the interface between the dextran-rich phase and the membrane
A_{em}	The area of the interface between the external medium and the membrane
A_{pd}	The area of the interface between the PEG-rich and the dextran-rich phases
A_{pm}	The area of the interface between the PEG-rich phase and the membrane
A_v	Initial vesicle apparent area
A_v^0	Vesicle apparent area
ΔA	Area difference
Δa_0	Equilibrium differential area
α, β, γ	phases
F	Interface energy
F_{dm}	The energy of the interface between the dextran-rich phase and the membrane
F_{em}	The energy of the interface between the external medium and the membrane
F_{pd}	The energy of the interface between the PEG-rich and the dextran-rich phases
F_{pm}	The energy of the interface between the PEG-rich phase and the membrane
g	Gravitational acceleration
h	Position
h_0	Initial position
κ	Bending rigidity of the membrane
L	Length
ω	Angular velocity
p	Packing parameter
P	Pressure, Osmotic pressure
r	Osmolarity ratio between the external medium and the initial internal polymer solution of the vesicle
R	Radius
R_m	Radius of the micropipette at the entrance
R_t	Radius of the tether
R_v	Radius of the vesicle

ρ	density
ρ_d	The density of the dextran-rich phase
ρ_p	The density of the PEG-rich phase
ρ_p	The density of water
Σ	Surface energy density, interfacial tension
Σ_{dm}	Interfacial tension between the dextran-rich phase and the membrane
Σ_{em}	Interfacial tension between the external medium and the membrane
Σ_{pd}	Interfacial tension between the PEG-rich and dextran-rich phases
Σ_{pm}	Interfacial tension between the PEG-rich phase and the membrane
σ	Tension, that includes the part of the membrane tension
σ_0	Initial membrane tension
σ_{dm}	The tension between the external medium and the dextran-rich phase.
σ_e	Membrane tension exerted by means of the pipette
σ_e^c	Critical external membrane tension
σ_m	Membrane tension
σ_{pm}	The tension between the external medium and the PEG-rich phase.
θ	Contact angle
θ_d	Contact angle of the dextran-rich phase
θ_m	Contact angle of the external medium
θ_p	Contact angle of the PEG-rich phase
T	Temperature
v	Reduced volume
V	Volume
V_v	Vesicle volume

List of Figures

- Figure 1.1.1 The crowded state of the cytoplasm in eukaryotic and *E. coli* cells.
- Figure 1.1.2 Colocalisation of F-actin and HA-Dvl-2-ER protein in single-copy cell line.
- Figure 1.2.1 Typical phase diagram of temperature versus volume fraction.
- Figure 1.2.2 The (temperature versus weight fraction of polymer w_2) phase diagram for the polystyrene-cyclohexane system for samples of indicated molecular weight
- Figure 1.3.1 molecular structure of 1,2-dioleoyl-*sn*-glycero-3-phosphocholine (DOPC)
- Figure 1.3.2 Structure of amphiphilic aggregates.
- Figure 1.3.3 Schematic phase diagram of vesicle shapes.
- Figure 1.4.1 Optical microscope images of giant vesicles (horizontal cross section).
- Figure 1.4.2 DIC images of dynamic aqueous phase budding within an ATPS giant vesicle (horizontal cross section).
- Figure 1.4.3 ATPS-containing giant vesicle before (A) and after (B) budding was induced by osmotic stress.
- Figure 1.5.1 Wetting of a liquid drop (red) on a solid substrate (gray).
- Figure 1.5.2 Wetting of a liquid drop (red) on a soft interface.
- Figure 2.2.1 Structures of PEG and dextran.
- Figure 2.2.2 Geometry of a spinning drop of a light PEG-rich phase p in the dense dextran-rich phase d .
- Figure 2.3.1 The molecular structures of DOPE-PEG2000 and G_{MI} ganglioside.
- Figure 2.4.1 Schematic illustration of the chamber used for the side-view microscope filled with the external medium and vesicles.
- Figure 2.4.2 Schematic illustration of the chamber used for confocal microscope.
- Figure 2.4.3 Schematic configurations of phase contrast microscopy and differential interference contrast microscopy in an inverted microscope.
- Figure 2.4.4 Schematic configuration of fluorescence microscopy.
- Figure 2.4.5 Schematic configuration of a simple confocal microscope setup.
- Figure 2.5.1 The vertical cross section of the micropipette system setup
- Figure 3.1.1 Binodals of dextran (500 kg/mol) and PEG (8 kg/mol) aqueous solution at 23 °C (black squares), 40 °C (red dots) and 60 °C (green triangles).
- Figure 3.1.2 Coexistence curve and tie lines of dextran (500 kg/mol) and PEG (8 kg/mol) aqueous solution at 23 °C.

- Figure 3.1.3 The density (left) and the osmolarity (right) at 24.2 °C of the coexisting phases at different overall concentrations.
- Figure 3.1.4 Volume fraction of the dextran-rich phase at different total polymer concentrations at 23 °C.
- Figure 3.1.5 Volume fraction of the dextran-rich phase in bulk polymer solution at 4°C.
- Figure 3.2.1 DIC images of the phase separating process induced by dehydration.
- Figure 3.2.2 The bicontinuous structure in the phase separating solution in the vesicle interior.
- Figure 3.2.3 The effect of the polymer composition on the phase separating process induced by dehydration.
- Figure 3.2.4 The effect of membrane composition on the phase separating process induced by dehydration.
- Figure 4.1.1 Vesicle trajectories in the phase diagram.
- Figure 4.1.2 Morphologies of a deflated vesicle in Sys I exposed to different hypertonic mediums.
- Figure 4.2.1 formation for a vesicle with a sugar-membrane corresponding to Sys I.
- Figure 4.2.2 membrane tubes aligning at the interface between the PEG-rich and dextran-rich phases in a deflated vesicle corresponding to Sys I.
- Figure 4.2.3 The over-crowded membrane tubes at the interface of the PEG-rich and dextran-rich phases.
- Figure 4.2.4 Tube formation for a vesicle with a PEG-membrane corresponding to Sys IV.
- Figure 4.2.5 Fluorescence images (side view) of a vesicle during deflating.
- Figure 4.2.6 Figure 4.2.6 The area evolution with osmolarity ratio r .
- Figure 4.3.1 Microscope images (side view observation) of the vesicle under different tensions.
- Figure 4.3.2 Area dilation as a function of the external membrane tension.
- Figure 5.1.1 Morphologies observed in the deflated vesicles with two-phase system.
- Figure 5.2.1 Confocal micrographs of a vesicle (vertical cross section), which contains a dextran-rich drop (green) undergoing wetting transition as the external osmolarity increases.
- Figure 5.2.2 The cosine of the contact angle θ_d versus the total polymer concentration in the vesicle.
- Figure 5.3.1 The vesicle morphology evolution during deflation.
- Figure 5.3.2 The contact angles θ_m , θ_p and θ_d versus reduced volume v during stepwise vesicle deflation.
- Figure 5.3.3 The effect of excess area on the vesicle morphology.

- Figure 5.3.4 The vesicle morphologies in a hypertonic solution.
- Figure 5.3.5 The force balance at the three-phase line.
- Figure 5.3.6 The withdrawal of the budded dextran-rich phase in pressurized vesicle.

List of Tables

Table 2.3.1 The membrane compositions.

Table 2.3.2 Weight concentrations and polymer weight ratios in the polymer solutions used in this work.

Table 4.1.1 The systems used in vesicle deflation.

Bibliography

Aarts DGAL, Schmidt M, Lekkerkerker HNW (2004) Direct visual observation of thermal capillary waves. *Science* 304:847-850.

Aarts DGAL, Dullens RPA, Lekkerkerker HNW (2005) Interfacial dynamics in demixing systems with ultralow interfacial tension. *New J Phys* 7:40.

Abkarian M, Viallat A (2008) Vesicles and red blood cells in shear flow. *Soft Matter* 4:653 – 657.

Alberts B, Bray D, Lewis J *et al.* (1994) Molecular biology of the cell, 3rd edition, Garland Publishing, Inc., New York & London.

Al-Habori M (1995) Microcompartmentation, metabolic channelling and carbohydrate metabolism. *Int J Biochem Cell Biol* 27:123-132.

Evans E, Rawicz W (1990) Entropy-driven tension and bending elasticity in condensed-fluid membranes. *Phys Rev Lett* 64:2094-2097.

Baumgart T, Hess ST, Webb WW (2003) Imaging coexisting fluid domains in biomembrane models coupling curvature and line tension. *Nature* 425:821 – 824.

Berndl K, Käs J, Lipowsky R, Sackmann E, Seifert U (1990) Shape transformations of giant vesicles: extreme sensitivity to bilayer asymmetry. *Europhys Lett* 13:659-664.

Bo L, Waugh RE (1989) Determination of bilayer membrane bending stiffness by tether formation from giant, thin-walled vesicles. *Biophys J* 55:509-519.

Bonn D, Bertrand E, Meunier J, Blossey R (2000) Dynamics of wetting layer formation. *Phys Rev Lett* 84:4661-4664.

Boyce JF, Schürch S (1984) The measurement of surface and interfacial tension by the axisymmetric drop technique. *Coll Surf* 9:307-317.

Brochard-Wyart F, Borghi N, Cuvelier D, Nassoy P (2006) Hydrodynamic narrowing of tubes extruded from cells. *Proc Natl Acad Sci USA* 103:7660-7663.

Cahn JW (1977) Critical point wetting. *J chem phys* 66:3667-3672.

Cans AS, Andes-Koback M, Keating CD (2008) Positioning lipid membrane domains in giant vesicles by micro-organization of aqueous cytoplasm mimic. *J Am Chem Soc* 130:7400-7406.

Cesi V, Katzbauer B, Narodoslowsky M, Moser A (1996) Thermophysical properties of polymers in aqueous two-phase systems. *Intern J Thermophysics* 17:127-135.

Croll T, Munro PD, Winzor DJ, Trau M, Nielsen LK (2003) Quantitative prediction of phase diagrams for polymer partitioning in aqueous two-phase systems. *J Poly Phys* 41:137-443.

Cuvelier D, Derenyi I, Bassereau P, Nassoy P (2005) Coalescence of membrane tethers: experiments, theory, and applications. *Biophys J* 88:2714–2726.

Dai J, Sheetz MP, Wan X, Morris CE (1998) Membrane tension in swelling and shrinking molluscan neurons. *J Neurosci* 18:6681-6692.

Daniel B, Ross D (2001) Wetting transition. *Rep. Prog. Phys.* 64:1085-1163.

Davidson MW, Abramowitz M, Optical microscopy.

Derényi D, Jülicher F, Prost J 2002 Formation and interaction of membrane tubes. *Phys Rev Lett* 88:238101.

de Gennes PG (1985) Wetting: statics and dynamics. *Rev Mod Phys* 57:827-863.

Diamond AD, Hsu JT (1989) Phase diagrams for dextran-PEG aqueous two-phase systems at 22°C. *Biotechnology Techniques* 3:119-124.

Dimova R, Aranda S, Bezlyepkina N, Nikolov V, Riske KA, Lipowsky R (2006) A practical guide to giant vesicles. Probing the membrane nanoregime via optical microscopy. *J. Phys.: Condens. Matter* 18:S1151-S1176.

Dimova R, Seifert U, Pouligny B, Förster S and Döbereiner H-G (2002) Hyperviscous diblock copolymer vesicles. *Eur Phys J B* 7:241-50.

Döbereiner HG, Käs J, Mopple D *et al.* (1993) Budding and fission of vesicles. *Biophys J* 65:1396-1403.

Dominak LM, Keating CD (2007) Polymer encapsulation within giant lipid vesicles. *Langmuir* 23:7148-7154.

Dopheide SM, Maxwell MJ, Jackson SP (2002) Shear-dependent tether formation during platelet translocation on von Willebrand factor. *Blood* 99:159-167.

Ducros C (1974) Ultrastructural study of the organization of axonal agranular reticulum in Octopus nerve. *J Neurocytology* 3:513-523.

Durian DJ, Franck C (1987) Wetting phenomena of binary liquid mixtures on chemically altered substrates. *Phys Rev Lett* 59:555-558.

Ebner C, Saam WF (1977) New phase-transition phenomena in thin argon films. *Phys Rev Lett* 38:1486-1489.

Edelman MW, van der Linden E, Tromp RH (2003) Phase separation of aqueous mixtures of poly(ethylene oxide) and dextran. *Macromolecules* 36:7783-7790.

Edmond E, Ogston AG (1968) An approach to the study of phase separation in ternary aqueous systems. *Biochem J* 109:569-576.

Ellis RJ (2001a) Macromolecular crowding: an important but neglected aspect of the intracellular environment. *Curr Opin Struct Biol* 11:114-119.

- Ellis RJ (2001b) Macromolecular crowding: obvious but underappreciated. *Trends Biochem Sci* 26:597-604.
- Evans E, Rawicz W (1990) Entropy-driven and bending elasticity in condensed fluid membrane. *Phys Rev Lett* 64:2094-2097.
- Evans E, Bowman H, Leung A *et al.* (1996) Biomembrane templates for nanoscale conduits and networks. *Science* 273:933-935.
- Forciniti D, Hall CK, Kula MR (1990) Interfacial tension of polyethyleneglycol-dextran-water systems: influence of temperature and polymer molecular weight. *J Biotechnol* 16:279-296.
- Galina H, Gordon P, Irvine P, Kleintjens LA (1982) Pulse-induced critical scattering and the characterisation of polymer samples. *Pure & Appl Chem* 54:365-377.
- Gau H, Herminghaus S, Lenz P, Lipowsky R (1999) Liquid morphologies on structured surfaces: from microchannels to microchips. *Science* 283:46-49.
- Grafmüller A, Shillcock J, Lipowsky R (2007) Pathway of membrane fusion with two tension-dependent energy barriers. *Phys Rev Lett* 98:218101.
- Heinrich V, Waugh RE (1996) A piconewton force transducer and its application to measurement of the bending stiffness of phospholipid membranes. *Ann Biomed Eng* 24:595-605.
- Hill AVS (1991) in *Molecular Evolution of the Major Histocompatibility Complex*, ed. Klein J, Klein D, Springer, Heidelberg, pp 403-420.
- Helfrich MR, Mangeney-Slavin LK, Long MS, Djoko KY, Keating CD (2002) Aqueous phase separation in giant vesicles. *J Am Chem Soc* 124:13374-13375.
- Hochmuth RM, Marcus WD (2002) Membrane tethers formed from blood cells with available area and determination of their adhesion energy. *Biophys J* 82:2964-2969.
- Hochmuth RM, Mohandas N, Blackshear PL (1973) Measurement of the elastic modulus for red cell membrane using a fluid mechanical technique. *Biophys J* 13:747-762.
- Hochmuth RM, Shao J-Y, Dai J, Sheetz MP (1996) Deformation and flow of membrane into tethers extracted from neuronal growth cones. *Biophys J* 70:358-369.
- Hochmuth RM, Wiles HC, Evans EA, McTown JT (1982) Extensional flow of erythrocyte membrane from cell body to elastic tether II. Experiment. *Biophys J* 39:83-89.
- Hopkinson I, Myatt M (2002) Phase separation in ternary polymer solutions induced by solvent loss. *Macromolecules* 25:5153-5160.
- Hosu BG, Sun M, Marga F, Grandbois M, Forgacs G (2007) Eukaryotic membrane tethers revisited using magnetic tweezers. *Phys Biol* 4:67-78.
- Jülicher F, Lipowsky R (1993) Domain-induced budding of vesicles. *Phys Rev Lett* 70:2964-2967.

- Käs J, Sachmann E (1995) Shape transitions and shape stability of giant phospholipid vesicles in pure water induced by area-to volume changes. *Biophys J* 60:825-844.
- Klier J, Stefanyi P, Wyatt AFG (1995) Contact angle of Liquid ^4He on a Cs surface. *Phys Rev Lett* 75:3709-3712.
- Koningsveld R, Staverman AJ (1968) Liquid-liquid phase separation in multicomponent polymer solutions. II. The critical state. *J Pol Sci A-2*, 6:325-347.
- Koningsveld R, Stockmayer WH, Nies E (2001) *Polymer phase diagrams a text book* Oxford University Press, Inc., New York.
- Koster G, VanDuijn M, Hofs B and Dogterom M (2003) Membrane tube formation from giant vesicles by dynamic association of motor proteins. *Proc Natl Acad Sci USA* 100:15583-15588.
- Kroll DM, Lipowsky R (1983) University classes for the critical wetting transition in two dimensions. *Phys Rev B* 28:5273-5280.
- Kwok R, Evans E (1981) Thermoelasticity of large lecithin bilayer vesicles. *Biophys J* 35:637-652.
- Lasic DD (1993) *Liposomes: from physics to applications*. Elsevier, Amsterdam, London, New York, Tokyo.
- Leduc C *et al.*, (2004) Cooperative extraction of membrane nanotubes by molecular motors. *Proc Natl Acad Sci USA* 101:17096-17101.
- Lee AG (2003) Lipid-protein interactions in biological membranes: a structural perspective. *Biochim Biophys Acta* 1612:1-40.
- Lenz P, Lipowsky R (1998) Morphological transitions of wetting layers on structured surfaces. *Phys Rev Lett* 80:1920-1923.
- Li Y, Lipowsky R, Dimova R (2008) Transition from complete to partial wetting within membrane compartments. *J Am Chem Soc* 130:12252-12253.
- Lipowsky R, Kroll DM, Zia RKP (1983) Effective field theory for interface delocalization transitions. *Phys Rev B* 27:4499-4502.
- Lipowsky R (1984a) Upper critical dimension for wetting in systems with long-range forces. *Phys Rev Lett* 52:1429-1432.
- Lipowsky R, Kroll DM (1984b) Critical wetting in systems with long-range forces. *Phys Rev Lett* 52:2303.
- Lipowsky R, Fisher ME (1987) Scaling regimes and functional renormalization for wetting transitions. *Phys Rev B* 36:2126-2141.
- Lipowsky R (1991) The conformation of membranes. *Nature* 349:475-481.

- Lipowsky R (1992) Budding of membranes induced by intramembrane domains. *J Phys II France* 2:1825-1840.
- Lipowsky R (1998) Vesicles and biomembranes. *Encyclo Appl Phys* 23:199-222.
- Lipowsky R (1999) From membrane to membrane machines. In *Statistical Mechanics of Biocomplexity*, ed. by Reguera D, Rubi JM, Vilar JMB, *Lecture Notes in Physics* 527:1-23.
- Lipowsky R, Lenz P, Swain PS (2000) Wetting and dewetting of structured and imprinted surfaces. *Colloids and Surfaces A: Physicochemical and Engineering Aspects* 161:3-22.
- Lipowsky R (2002) Domains and rafts in membranes—hidden dimensions of self-organization. *J Biol Phys* 28:195-210.
- Lipowsky R, Brinkmann M, Dimova R *et al.* (2005a) Droplets, bubbles, and vesicles at chemically structured surfaces. *J Phys: Condens Matter* 17:537-558.
- Lipowsky R, Brinkmann M, Dimova R (2005b) *et al.* Wetting, budding, and fusion—morphological transitions of soft surfaces. *J Phys: Condens Matter* 17: S2885-S2902.
- Liu C, Asherie N, Lomakin A, Pande J *et al.* (1996) Phase separation in aqueous solutions of lens γ -crystallins: Special role of γ_s . *Proc Natl Acad Sci USA* 93:377-382.
- Logan CY, Nusse R (2004) The Wnt signalling pathway in development and disease. *Annu Rev Cell Dev Biol* 20:781-810.
- Long MS, Jones CD, Helfrich MR, Mangeney-Slavin LK, Keating CD (2005) Dynamic microcompartmentation in synthetic cells. *Proc Natl Acad Sci USA* 102:5920-5925.
- Long MS, Cans AS, Keating CD (2008) Budding and asymmetric protein microcompartmentation in giant vesicles containing two aqueous phases. *J Am Chem Soc* 130:756-762.
- Marsh D, Bartucci R, Sportelli L (2003) Lipid membranes with grafted polymers: physicochemical aspects. *Biochim Biophys Acta* 1615:33-59.
- Miao L, Seifert U, Wortis M, Döbereiner HG (1994) Budding transition of fluid-bilayer vesicles: the effect of area-difference elasticity. 49:5389-5407.
- Minton AP, Wilf J (1981) Effect of macromolecular crowding upon the structure and function of an enzyme: glyceraldehyde-3-phosphate dehydrogenase. *Biochem* 20:4821-4826.
- Moldover MR, Cahn JW (1980) An interface phase transition: complete to partial wetting. *Science* 207:1073-1075.
- Mui BLS, Döbereiner HG, Madden TD, Cullis PR (1995) Influence of transbilayer area asymmetry on the morphology of large unilamellar vesicles. *Biophys J* 69:930-941.

- Neuhaus J-M, Sitcher L, Meins F, Jr, Boller T (1991) A short C-terminal sequence is necessary and sufficient for the targeting of chitinases to the plant vacuole. *Proc Natl Acad Sci USA* 88:10362-10366.
- Oostenbrink C, Villa A, Mark AE *et al.* (2004) A biomolecular force field based on the free enthalpy of hydration and solvation: the GROMOS force-field parameter sets 53A5 and 53A6. *J Comput Chem* 25:1656-1676.
- Ovádi J, Saks V (2004) On the origin of intracellular compartmentation and organized metabolic systems. *Mol Cell Biochem* 256/257:5-12.
- Paine PL (1984) Diffusive and non-diffusive proteins in vivo. *J Cell Biol* 99:188s-195s.
- Rämsch C, Kleinlanghorst LB, Knieps EA, Thömmes J, Kula M-R (1999) Aqueous two-phase systems containing urea: influence on phase separation and stabilization of protein conformation by phase components. *Biotechnol Prog* 15:493-499.
- Reinelt D, Iov V, Leiderer P, Klier J (2005) Liquid ^4He on Cs: drying, depinning, and the non-wetting 'thin-film'. *J Phys: Condens Matter* 17:S403-S414.
- Rolley E, Guthmann C (1997) Optical measurement of contact angle of liquid helium on cesium. *J Low Temp Phys* 108:1-9.
- Ross D, Rutledge JE, Taborek P (1996) Triple point dewetting transitions of helium mixtures on cesium. *Phys Rev Lett* 76:2350-2353.
- Ross D, Taborek P, Rutledge JE (1998) Wetting behaviour of H_2 on cesium. *Phys Rev B* 58:R4274-R4276.
- Ross D, Bonn D, Meunier J (1999) Observation of short-range critical wetting. *Nature* 400:737-739.
- Ross D, Bonn D, Meunier J (2001) Wetting of methanol on the n-alkanes: observation of short-range critical wetting. *J Chem Phys* 114:2784-2792.
- Roux A, Cappello G, Cartaud J, Prost J, Goud B, Bassereau P (2002) A minimal system allowing tabulation with molecular motors pulling on giant liposomes. *Proc Natl Acad Sci USA* 99:5394-5399.
- Rowlinson, JS, Widom B (2002) Molecular theory of capillarity. Dover Publ Inc.
- Rutledge JE, Ross D, Taborek P (1998) Direct optical imaging of superfluid ^4He droplets on a cesium surface. *J Low Temp Phys* 113:811-816.
- Rustom A, Saffrich R, Markovic I, Walther P, Gerdes HH (2004) Nanotubular highways for intercellular organelle transport. *Science* 303:1007-1010.
- Ryan TA, Myers J, Holowea D, Baird B, Webb WW (1988) Molecular crowding on the cell surface. *Science* 23:61-64.
- Ryden J, Albertsson P-Å (1971) Interfacial tension of dextran-polyethylene glycol-water two-phase systems. *J Coll Interf Sci* 37:219-222.

Panataloni D, Le Clainche C, Carlier M-F (2001) Mechanism of actin-based motility. *Science* 292:1502-1506.

Saeki S, Kuwahara N, Konno S, Kaneko M (1973) Upper and lower critical solution temperatures in polystyrene solutions. *Macromolecules* 6:246-250.

Schmidtke DW, Diamond SL (2000) Direct observation of membrane tethers formed during neutrophil attachment to platelets or P-selectin under physiological flow. *J Cell Biol* 149:719-729.

Schürch S, Gerson DF, Mciver DJL (1981) Determination of cell/medium interfacial tension from contact angles in aqueous polymer systems. *Biochim Biophys Acta*, 640:557-571.

Schwarz-Romond T, Merrifield C, Nichols BJ, Bienz M (2005) The Wnt signaling effector Dishevelled forms dynamic protein assemblies rather than stable associations with cytoplasmic vesicles. *J Cell Sci* 118:5269-5277.

Sear RP (2007) Dishevelled: a protein that functions in living cells by phase separating. *Soft Matt* 3:680-684.

Seemann R, Brinkmann M, Kramer EJ *et al.* (2005) Wetting morphologies at microstructured surfaces. *Proc Natl Acad Sc. USA* 102:1848-1852.

Seifert U, Berndl K, Lipowsky R (1991) Shape transformations of vesicles: phase diagram for spontaneous-curvature and bilayer-coupling models. *Phys Rev A* 44:1182-1202.

Smalley MJ, Signoret N, Robertson D, Tilley A *et al.* (2005) Dishevelled (Dvl-2) activates canonical Wnt signalling in the absence of cytoplasmic puncta. *J Cell Sci* 118:5279-5289.

Snapp EL *et al.* (2003) Formation of stacked ER cisternae by low affinity protein interactions. *J Cell Biol* 163:257-269.

Staykova M, Lipowsky R, Dimova R (2008) Membrane flow patterns in multi-component giant vesicles induced by alternating electric fields. *Soft Matt* in press DOI: 10.1039/b811876k.

Sun M, Graham JS, Hegedüs B *et al* 2005 Multiple membrane tethers probed by atomic force microscopy. *Bioph J* 89:4320-4329.

Upadhyaya A, Sheetz MP (2004) Tension in tubulovesicular networks of Golgi and endoplasmic reticulum membranes. *Biophys J* 86:2923-2928.

Waterman-Storer CM, Salmon ED (1998) Endoplasmic reticulum membrane tubules are distributed by microtubules in living cells using three distinct mechanisms. *Curr Biol* 8:798-806.

Waugh R (1982) Surface viscosity measurements from large bilayer vesicle tether formation II. Experiments. *Biophys J* 38:29–37.

Wu Y-T, Zhu Z-Q (1999) Modelling of interfacial tension of aqueous two-phase systems. *Chem Eng Sci* 54:433-440.

Yanagisawa M, Imai M, Taniguchi T (2008) Shape deformation of ternary vesicles coupled with phase separation *Phys Rev Lett* 100:148102.

Zimmerman SB, Trach SO (1991) Estimation of macromolecule concentrations and excluded volume effects for the cytoplasm of *Escherichia coli*. 222:599-620.

Acknowledgements

Finally, I would like to thank all the many people who have in any way contributed to this work, and have lent me their support, guidance or friendship.

I would like to thank Prof. Reinhard Lipowsky, for giving me the possibility to work on my PhD in the Theory & Bio-Systems department, and for the guidance and patient discussions. I would also like to thank Dr. Rumiana Dimova for many long and patient discussions throughout the work.

Thanks to the theoretician Andrea Grafmüller, who has done the vesicle shape analysis and has spent quite some time on trying to make the experimentalist to understand what exactly she has done with the vesicles. Thanks to Rubèn Serral Gracià for developing the software to analyze the contour of the vesicles.

Many thanks to Carmen Remde who showed me how to make vesicles, Natalya Bezlyepkina who was always there when I had problems with the confocal microscope, Said Aranda for teaching me how to use the micropipette setup, and Patia Vlahovska for showing me how to assemble the chamber used in the horizontally aligned microscope. Many thanks to the groupies in the membrane lab for many helpful discussions, but also for some very good times and nice evenings.

Thank you to all the present and former members of the theory group, and the surrounding institutes, for the company, patience and the many helpful discussions. In particular, I thank Jörg Menche for solving my language problems and constant friendship since 'Freiburg'.

A final thank you goes to my family and friends for the moral support and the cheering up.